ปฏิกิริยาออกซิเดชั่นด้วยแสงของเอธิลีนบนตัวเร่งปฏิกิริยา

ไทเทเนียมไดออกไซด์ที่เติมทอง

นายพีรพนธ์ บัวแก้ว

วิทยานิพนธ์นี้เป็นส่วนหนึ่งของการศึกษาตามหลักสูตรปริญญาวิศวกรรมศาสตรมหาบัณฑิต
สาขาวิชาวิศวกรรมเคมี ภาควิชาวิศวกรรมเคมี
คณะวิศวกรรมศาสตร์ จุฬาลงกรณ์มหาวิทยาลัย
ปีการศึกษา 2548
ISBN 974-17-4396-3

PHOTOOXIDATION OF ETHYLENE OVER GOLD DEPOSITED TITANIUM DIOXIDE

Mr. Peerapon Buakaew

A Thesis Submitted in Partial Fulfillment of the Requirements
for the Degree of Master of Engineering Program in Chemical Engineering
Department of Chemical Engineering
Faculty of Engineering
Chulalongkorn University
Academic Year 2005
ISBN 974-17-4396-3

Thesis Title	PHOTOOXIDATION OF ETHYLENE OVER GOLD DEPOSITED TITANIUM DIOXIDE
By	Mr. Peerapon Buakaew
Field of Study	Chemical Engineering
Thesis Advisor	Akawat Sirisuk, Ph.D.

Accepted by the Faculty of Engineering, Chulalongkorn University in Partial Fulfillment of the Requirements for the Master's Degree

....Dean of the Faculty of Engineering

(Professor Direk Lavansiri, Ph.D.)

THESIS COMMITTEE

.....Chairman

(Professor Piyasan Praserthdham, Dr.Ing.)

..... Thesis Advisor

(Akawat Sirisuk, Ph.D.)

..... Member

(Assistant Professor Joongjai Panpranot, Ph.D.)

.....Member

(Assistant Professor Muenduen Phisalaphong, Ph.D.)

.....Member

(Okorn Mekasuvandamrong, Ph.D.)

พีรพนธ์ บัวแก้ว: ปฏิกิริยาออกซิเดชั่นด้วยแสงของเอธิลีนบนตัวเร่งปฏิกิริยาไทเทเนียมไดออกไซด์ที่เติมทอง (PHOTOOXIDATION OF ETHYLENE OVER GOLD DEPOSITED TITANIUM DIOXIDE) อ. ที่ปรึกษา: ดร.อัครวัต ศิริสุข, xx หน้า, ISBN: 974-17-4396-3

ไทเทเนียมไดออกไซด์แต่ละชนิดมีค่าความว่องไวในการเร่งปฏิกิริยาโดยใช้แสงของปฏิกิริยาออกซิเดชั่นด้วยแสงของเอธิลีนไม่เท่ากัน ไทเทเนียมไดออกไซด์ที่สังเคราะห์ด้วยวิธีโซล-เจลแบบที่ 1 (ใช้กรดไนตริก) จะให้ค่าการสลายตัวของเอธิลีนมากที่สุด รองลงมาคือ วิธีโซล-เจล แบบที่ 2 (ใช้เอธานอล), วิธีโซลโวเทอร์มอล และ แบบเจอาร์ซี-ทีไอโอวัน ตามลำดับ เมื่อเติมทองลงไป พบว่าไทเทเนียมไดออกไซด์ที่สังเคราะห์ด้วยวิธีโซล-เจลแบบที่ 1, วิธีโซล-เจล แบบที่ 2 รวมทั้งวิธีโซลโวเทอร์มอล จะให้ค่าการสลายตัวของเอธิลีนลดลงตามค่าความเป็นกรด-เบสที่เพิ่มมากขึ้น เนื่องจากปริมาณจุดบกพร่องบนพื้นผิว (Ti^{3+}) ที่ลดลงอันเป็นผลของอนุภาคทองขนาดนาโนเมตรโดยยืนยันได้จากผลของ Electron Spin Resonance (ESR) และการลดลงของอนุภาคทองขนาดนาโนเมตรที่มีความว่องไวในการทำปฏิกิริยา ซึ่งยืนยันจากผลของ Transmission Electron Microscope (TEM) อย่างไรก็ตาม, ไทเทเนียมไดออกไซด์แบบเจอาร์ซี-ทีไอโอวันจะให้ค่าการสลายตัวของเอธิลีนเพิ่มขึ้นเมื่อมีการเติมทองลงไป โดยจะให้ค่าการสลายตัวของเอธิลีนสูงที่สุดที่ค่าความเป็นกรด-เบสเท่ากับ 9 ซึ่งที่สภาวะนี้อนุภาคของทองจะมีขนาดโดยเฉลี่ยน้อยกว่า 5 นาโนเมตรและมีความว่องไวในการเร่งการเกิดปฏิกิริยาที่พื้นผิวของไทเทเนียมไดออกไซด์ด้วย

ภาควิชา.... ...วิศวกรรมเคมี..... ลายมือชื่อนิสิต.....

สาขาวิชา.....วิศวกรรมเคมี..... ลายมือชื่ออาจารย์ที่ปรึกษา.....

ปีการศึกษา.... .2548.....

#4770484321: MAJOR CHEMICAL ENGINEERING
KEY WORD: TITANIUM DIOXIDE / SOL-GEL METHOD / SOLVOTHERMAL METHOD / DEPOSITION-PRECIPITATION METHOD / GOLD/ PHOTOOXIDATION OF ETHYLENE
PEERAPON BUAKAEW: PHOTOOXIDATION OF ETHYLENE OVER GOLD DEPOSITED TITANIUM DIOXIDE. THESIS ADVISOR: AKAWAT SIRISUK, Ph.D. xx pp. ISBN 974-17-4396-3

Each type of titanium dioxide has different photocatalytic activity on photooxidation of ethylene. Titanium dioxide synthesized via sol-gel method type I (prepared in nitric acid and water) yielded the most conversion of ethylene and less for that synthesized via sol-gel method type II (prepared in ethanol and water), solvothermal method and JRC-TIO1, respectively. When gold was deposited, for titanium dioxide synthesized via sol-gel method type I and type II including solvothermal method, conversion of ethylene decreases with increasing of pH values due to decreasing of amount of Ti^{3+} affected from gold nanoparticles confirmed by Electron Spin Resonance results (ESR) and decreasing of active gold nanoparticles confirmed by Transmission Electron Microscope results (TEM). However, JRC-TIO1 titanium dioxide yielded more conversion of ethylene when it was deposited with gold nanoparticles. The highest conversion could be obtained at pH value of 9 at which the average particle size of gold nanoparticles were less than 5 nm and gave high activity for the reaction at the surface of titanium dioxide.

Department.....Chemical Engineering..... Student's signature.....Peerapon Buakaew.....
Field of study....Chemical Engineering..... Advisor's signature.....
Academic year...2005.....

ACKNOWLEDGEMENTS

The author would like to express his greatest gratitude to his advisor, Dr. Akawat Sirisuk, for his invaluable guidance throughout this study. Moreover, I would also grateful to thank Professor Piyasan Praserthdam, as the chairman, Assistant Professor Joongjai Panpranot and Assistant Professor Muenduen Phisalaphong, members of the thesis committee for their kind cooperation.

Many thanks for kind suggestions and useful help to Dr. Okorn Mekasuvandamrong, Mr. Kongkiat Suriyae, Miss Ratchadaporn Ninpetch and many best friends in Chemical Engineering Department who have provided the encouragement and co-operation throughout this study

Finally, he also would like to dedicate this thesis to his parents who have always been the source of his support and encouragement.

CONTENTS

page

LIST OF TABLES

TABLE **page**

LIST OF FIGURES

FIGURE **page**

FIGURE **page**

CHAPTER I

INTRODUCTION

Titanium dioxide (TiO_2), also known as titania, is commonly used in many industries such as paint, printing ink, plastics, paper, synthetic fibers, rubber, condensers, painting colors and crayons, ceramics, electronic components along with food and cosmetics. Other applications of titanium dioxide include gas sensor (Xu *et al.*, 1993; Dutta *et al.*, 1999) and heterogeneous catalyst, especially photocatalyst (Sopyan *et al.*, 1996). For application as heterogeneous photocatalyst, titanium dioxide is usually employed to decompose organic compounds in water detoxification and gaseous pollutant removal (Kamat, 1993; Hoffmann *et al.*, 1995; Augugliaro *et al.*, 1999; Arabatsiz *et al.*, 2003; Balasubramanian *et al.*, 2004; Nakano *et al.*, 2004).

Titanium dioxide has been used extensively in photocatalysis because of its high photocatalytic activity, stability, and suitable band-gap energy (Linsebigler *et al.*, 1995). Moreover, these properties are dictated to a large extent by its crystalline phase, morphology, and particle size. In recent years, many researchers have synthesized a variety of nanosized titanium dioxide materials via many methods such as a sol-gel method (Kang *et al.*, 2001; Su *et al.*, 2004), a hydrothermal method (Kolenko *et al.*, 2004), and solvothermal method (Kang *et al.*, 2001).

Titanium dioxide has three crystalline phases: anatase, rutile and brookite (Hoffmann *et al.*, 1995; Linsebigler *et al.*, 1995) but anatase phase is generally more chemically and optically active. Crystalline structures of titanium dioxide can be controlled by heat treatment (Kontos *et al.*, 2005) and sometimes by addition of dopants (Calza *et al.*, 1997; Mills and wang, 1997; Nam and Han, 2003).

Particle size plays an important role in catalysis because it directly has an impact on the specific surface area, chemical stability and chemical reactivity of the catalyst. Smaller particle size has more active surface sites and surface charge carrier transfer rate in photocatalysis. Titanium dioxide that possesses nanocrystallite size and high surface area has attracted interest due to the unusual photocatalytic

properties. However, nanosized titanium dioxide has a strong tendency to agglomerate to larger particles, leading to a decrease of thermal stability and exerting an influence on its applications.

There are always structural defects on the surface and inside the titanium dioxide particles (Torimoto *et al.*, 1996). These defects are related with the amount of the photoexcited electrons. Surface defects are advantageous for high photoactivity because they are used as active sites on which the electron donors or acceptors are adsorbed. In contrary, the bulk defects lower the photoactivity because they provide sites for the recombination of the photogenerated electrons. According to the electron spin resonance (EPR) spectroscopic study, the photoexcited electrons are trapped at the Ti^{3+} sites on the surface or Ti^{4+} sites within the bulk and the holes are trapped at lattice oxygen ions (Howe *et al.*, 1985; Howe *et al.*, 1987; Nakaoka *et al.*, 1997). Therefore, the bulk defects should be reduced to yield high photoactivity. The reduction of bulk defects can be achieved by high temperature calcination, however the anatase phase is metastable and transforms to rutile phase when the temperature is over about 500 ^{o}C. Moreover, the surface area is reduced dramatically during the high temperature calcinations.

Among the many methods to synthesize nanosized titanium dioxide, a sol-gel method is the one usually used because it produces titanium dioxide with high surface area resulting in high photocalytic activities (Dagan and Tomkiewicz, 1994; Zaharescu *et al.*, 1997; Sonawane *et al.*, 2002). However, the agglomeration of the particles can occur easily because of the large specific surface area and leads to the degradation of the properties. This method involves hydrolysis of metal alkoxide to form a sol, gelling, aging, drying and thermal stabilization, respectively. Each step can be controlled and modified in order to obtain specific material, narrow pore size distribution and narrow particle size distribution (Montoya *et al.*, 1992). Nevertheless, the as-synthesized titanium dioxide contains some amorphous phase and the surface areas decrease dramatically when being calcined to become crystalline (Iwamoto *et al.*, 2001). Moreover, several aqueous-based methods using metal salts as precursor material such as hydrolysis method and homogenous precipitation method have many problems, including low concentration of the reaction species needed and long reaction time required.

Hydrothermal methods have been widely used for the synthesis of many ceramic materials. Inoue *et al.*, (1991) used organic media in place of water for hydrothermal method. They explored the synthesis of inorganic materials in glycol at temperature higher than the boiling point of glycol, a so-called "Glycothermal method" and many groups of researchers have employed other organic solvents for synthesis of metal oxide (Bibby *et al.*, 1985; Inoue *et al.*, 1992; Kominami *et al.*, 1999; Wang *et al.*, 2002; Kim *et al.*, 2003). This method is called "Solvothermal method". By this method, the crystals of metal oxide are formed via several mechanisms at high temperature and pressure. This method is useful in controlling grain size, particle morphology, crystalline phase and surface chemistry by regulating sol composition, reaction temperature, pressure, property of solvent, additives, and time.

Supported gold nanoparticles have been found to be catalytically active for a number of different reactions, for example, oxidation of carbon monoxide (Haruta *et al.*, 1989; Haruta *et al.*, 1997; Kang and Wan, 1997), hydrochlorination of acetylene (Nkosi *et al.*, 1991), oxidation of hydrocarbons (Hayashi *et al.*, 1998; Ueda *et al.*, 1998; G□sior *et al.*, 2004), hydrogenation of carbon dioxide (Sakurai *et al.*, 1995; Sakurai *et al.*, 1996), reduction of nitric oxide (Ueda *et al.*, 1997; Demicheli *et al.*, 1993) and so on. Besides being catalytically active, gold nanoparticles have been used as gas sensors (Haruta, 1997), catalyst in unheated CO_2 lasers (Farkas *et al.*, 1983) and CO safety gas masks (Haruta, 1997). However, the requirement for particle size of gold nanoparticles to be catalytically active is that the size not larger than 5 nm (Bond and Thompson, 1999).

In the field of photocatalysis with titanium dioxide, gold nanoparticles have been used in the form of dopant where gold ions, *e.g.*, Au^{+} and Au^{3+} or maybe metallic gold atoms, *e.g.*, Au^{0} are arranged in the lattice of titanium dioxide or in the form of particles supported on titanium dioxide surface. In the form of dopant, the preparation method that is usually employed is a sol-gel method and it has been found that gold could retard the phase transition of titanium dioxide from anatase phase to rutile phase and accelerate the transformation from brookite phase to anatase phase (Debeila *et al.*, 2005). Moreover, it has been found that the presence of gold or gold

ion in the lattice of titanium dioxide could raise the amount of Ti^{3+}, resulting in the improvement of photocatalytic activity of titanium dioxide, too (Li *et al.*, 2002).

In the form of particles supported on titanium dioxide surface, the method frequently used is a deposition-precipitation method and a coprecipitation method (Haruta *et al.*, 1989). These two methods can produce the particle size of gold smaller than 5 nm, which is needed in order to be photocatalytically active. However, deposition-precipitation has the advantage over coprecipitation in that all gold particles remain on the surface of the titanium dioxide and none is buried within it. In addition, it gives a narrower particle size distribution (Bond and Thompson, 1999).

In this work, we studied the effects of gold nanoparticles on the photocatalytic activity of four types of titanium dioxide. The titanium dioxide catalysts were synthesized via a solvothermal method, a sol-gel method type I (prepared in nitric acid and water), a sol-gel method type II (prepared in ethanol and water) and the last one was JRC-TIO1, a commercially available catalyst. The method employed to deposit gold nanoparticles on the surface of each type was a deposition-precipitation method under similar conditions. In addition, we studied the effect of pH used while aging on photocatalytic activity of gold supported on titanium dioxide.

Objective of the thesis

1. Study the effect of gold nanoparticles on the photocatalytic activity of titanium dioxide.
2. Study the effect of pH used during gold deposition of titanium dioxide.

The thesis is arranged as following:

Chapter II presents literature reviews of the previous works related to this research.

Chapter III explains the basic information about titanium dioxide and gold nanoparticles such as the general properties, the preparation methods and the basic theory about photocatalytic reaction.

Chapter IV shows the experimental equipment and systems, and the preparation methods of titanium dioxide by solvothermal and sol-gel method (type I and type II), and gold deposition on titanium dioxide by deposition-precipitation method.

Chapter V presents the experimental results and discussion.

In the last chapter the overall conclusions and recommendation for the future studies of this research are given.

Finally, the calculations used for the preparation of gold doped titanium dioxide and crystallite size are included in the appendices at the end of this thesis.

CHAPTER II

LITERATURE REVIEWS

This chapter presents literature reviews of the previous works related to this research.

2.1 Hydrothermal method

Yanagisawa and coworkers (1997) had synthesized anatase titania at temperature below than 350 ^{o}C by hydrothermal hot-pressing of amorphous titania consisting of spherical particles prepared by hydrolysis of titanium tetraethoxide. Water contained in the starting powder was released to produce hydrothermal conditions by heating. Hydrothermal treatment at 100 ^{o}C accelerated crystallization of amosphous titania to anatase. Remarkable decrease in surface area with an increase in reaction temperature from 100 ^{o}C to 150 ^{o}C indicated that a large amount of amorphous portion remained in the products prepared at 100 ^{o}C.

2.2 Solvothermal method

Ionue and coworkers (1992) studied reaction of aluminium alkoxides with various glycols and the layered structure of the products. Alumina was synthesized by hydrothermal reaction of aluminium isopropoxide in various glycols, instead of water for hydrothermal synthesis, such as 1,4 butanediol (1,4–BG), 1,3 propanediol (1,3-PG) and 1,6 hexanediol (1,6-HG). The products were amorphous or boehmite, depending on type of glycol. When different precursors were employed to synthesize alumina in 1,4-BG, the products possessed identical structure. Crystallite size increased with increasing carbon number of glycols and the products contained same glycol moieties. The glycol moieties were incorporated between the layers of boehmite resulting in enlargement of the basal spacing that increased with increasing carbon number of the glycol. A small amount of water could be present in the glycol sample and was possibly formed during thermal decomposition of glycol.

Kominami and coworkers (1997) employed titanium (IV) tetra-tert-butoxide (TTB) to synthesize titania by thermal decomposition reaction in organic solvent at 573 K. Precursor was completely decomposed at this condition and gave rise to anatase without contamination of other phase. When toluene was used as solvent, TTB was decomposed at a lower temperature of 473 K to give anatase having large surface area. Since the BET surface area of a sample synthesized at 523 K was larger than that calculated from its crystalline size, assuming the density of anatase to be 3.84 g/cm^3, the product synthesized at lower temperature were believed to be contaminated with the amorphous-like hydrated phase.

2.3 Sol-gel method

Jung and coworkers (2004) studied the photoluminescence characteristics of anatase titania particles prepared by the sol–gel method. Using X-ray diffractometry, anatase phase was observed at calcination temperatures between 400^oC and 500^oC. Rutile phase was detected at the calcination temperature of 600^oC. Moreover, the photoluminescence intensity of pure titania particles measured at 77 K gradually increased as the calcination temperature increased. The increase in the photoluminescence intensity indicated that the intersystem crossing of excitons was facilitated while the radiationless decay or the deactivation process for excitons was suppressed. In addition, the photoluminescence was increased due to the reduction of the internal defects that were responsible for the radiationless recombination of photoexcited electron/hole pairs. The calcination temperature also shifted the maximum peak position of the photoluminescence spectra of titania. A blue shift of the photoluminescence spectrum occurs as a consequence of the enlargement of the band gap of titania as calcination temperature increased. Based on the above results, they concluded that calcination of titania at higher temperature generated more active surface sites that easily reacted with oxygen molecules as well as improved the crystallinity of anatase phase. Consequently, heat treatment of anatase titania particles high temperature gave rise to higher photoactivity as long as no significant rutile phase was formed.

Su and coworkers (2004) investigated the microstructural and chemical properties of TiO_2, obtained by a sol–gel procedure. Titania was prepared by hydrolysis and condensation of titanium (IV) n-butoxide in isopropyl alcohol and was calcined at temperature varying from 400°C to 700^{o}C for two hours. At 400^{o}C, only anatase phase was observed. When calcination temperature was increased to 700^{o}C, the rutile phase became the prevalent phase of TiO_2. The crystal size of TiO_2 increased from 4 to 35 nm as the temperature was increased from 400^{o}C to 700^{o}C while the BET surface area decreased from 122 to11.5 m^2/g.

2.3 Gold doped titanium dioxide

Sakthivel and coworkers (2004) studied effects of metal doping on titania. Metal (Pt, Au, Pd)-doped semiconductor systems were prepared by impregnation method. Both physical and chemical properties of catalysts together with their photocatalytic activities towards photocatalytic degradation of acid green 16 were investigated. Surface area of TiO_2 decreased with increasing metal content mainly due to blocking of fine capillaries of TiO_2 surface by metal film. The metal-doped TiO_2 systems possessed a light absorption threshold that extended into the visible region. Photonic efficiency increased with increasing metal loading up to an optimum level because of reduced recombination of electron and hole. Beyond the optimum metal doping, the dopants behaved as centers for electron/hole recombination. Defect sites on the TiO_2 surface, identified as Ti^{3+}, were necessary for adsorption and photoactivation of oxygen.

Debeila and coworkers (2005) studied the microstructure and phase transformation behavior of sol-gel derived Au-TiO_2. Titanium (IV) isopropoxide and propanol were used as precursor and solvent, respectively. The gel obtained was divided into two batches. In the first batch, the solvent was removed at 150 °C for four hours and the solid obtained was denoted as Dry-TiO_2. The remainder of the gel was transferred to a solution of $HAuCl_4$ at pH 3.5 at room temperature, resulting in Au-complex/TiO_2 and denoted as Dry-Au-TiO_2. For Dry-TiO_2, the brookite-to-anatase transformation occurred at a temperature below 600 °C. Brookite-to-rutile and anatase–to-rutile transformation occurred at a temperature above 600 °C. Brookite

disappeared at 600 °C and transformed into rutile without the formation of anatase. For Dry-Au–TiO_2, the brookite transformed to anatase and then to rutile. Brookite disappeared at 500 °C. Gold enhanced the transformation from brookite to anatase phase but retarded the transformation from anatase to rutile phase. Substitution of Ti^{4+} ions by gold or gold ions was not observed in TiO_2 and gold was found mostly on the surface of TiO_2 as metallic gold.

CHAPTER III

THEORY

3.1 Titanium (IV) dioxide (Sornnarong, 2000 and Fujishima et al., 1999)

3.1.1 Physical and chemical properties

Titanium (IV) dioxide may take on any of the following three crystal structures: anatase, which tends to be more stable at low temperature; brookite, which is usually found only in minerals; and rutile, which tends to be more stable at higher temperature and thus is sometimes found in igneous rock.

Anatase generally shows a higher photocatalytic activity than the other types of titanium dioxide. Comparison of some physical properties of anatase, brookite and rutile is shown in Table 3.1

Table 3.1 Comparison of some physical properties of anatase, brookite and rutile. (Othmer, 1991 and Fujishima et al., 1999).

Properties	Anatase	Brookite	Rutile
Crystal structure	Tetragonal	Orthorhombic	Tetragonal
Optical	Uniaxial, negative	Biaxial, positive	Uniaxial, negative
Density, g/cm^3	3.9	4.0	4.23
Hardness, Mohr scale	5 ½ - 6	5 ½ - 6	7 – 7 ½
Unit cell	$D_4a^{19}.4TiO_2$	$D_2h^{15}.8TiO_2$	$D_4h^{12}.3TiO_2$
Dimension, nm			
a	0.3758	0.9166	0.4584
b	-	0.5436	-
c	0.9514	0.5135	2.953
Refractive index	2.52	-	2.75
Permittivity	31	-	114
Melting point, ^oC	Changes to rutile at high temperature	-	1,858

The reason that anatase is more photoactive than rutile may lie in the differences in their so-called energy band structures. The band gap energy of a

semiconductor is the minimum energy of light required to make the material electrically conductive or, in other words, to get the electrons excited enough to get moving. The band gap energy of anatase is 3.2 eV, which corresponds to UV light with wavelength of 388 nanometers, while the band gap energy for rutile is 3.0 eV, corresponding to violet light that has a wavelength of 413 nanometers. The level of the conduction band for anatase is 0.2 eV higher than that for rutile. In more technical terminology, the band gap energy for a semiconductor indicates the minimum energy of light necessary to produce electrons in the conduction band (CB) and give rise to electrical conductivity (photoconductivity) and "holes," which are actually the absence of electrons, in the valence band (VB). These holes can react with water to produce the highly reactive hydroxyl radical (OH^-). Both holes and hydroxyl radicals can oxidize most organic materials.

The VB energies for both anatase and rutile are very low in the energy. Consequently, the VB holes (and the hydroxyl radicals) have great oxidizing power. The CB energy for rutile is close to the potential required to electrolytically reduce water to hydrogen gas, but that for anatase is higher in the energy, meaning that it has higher reducing power. Therefore, anatase can drive the very important reaction involving the electrolytic reduction of molecular oxygen (O_2) to superoxide (O_2^-).

Although anatase and rutile are both tetragonal, they are not isomorphous. Anatase exists in near-regular octahedral structure and rutile forms slender prismatic crystal. Rutile is the thermally stable form and is one of the two most important ores of titanium.

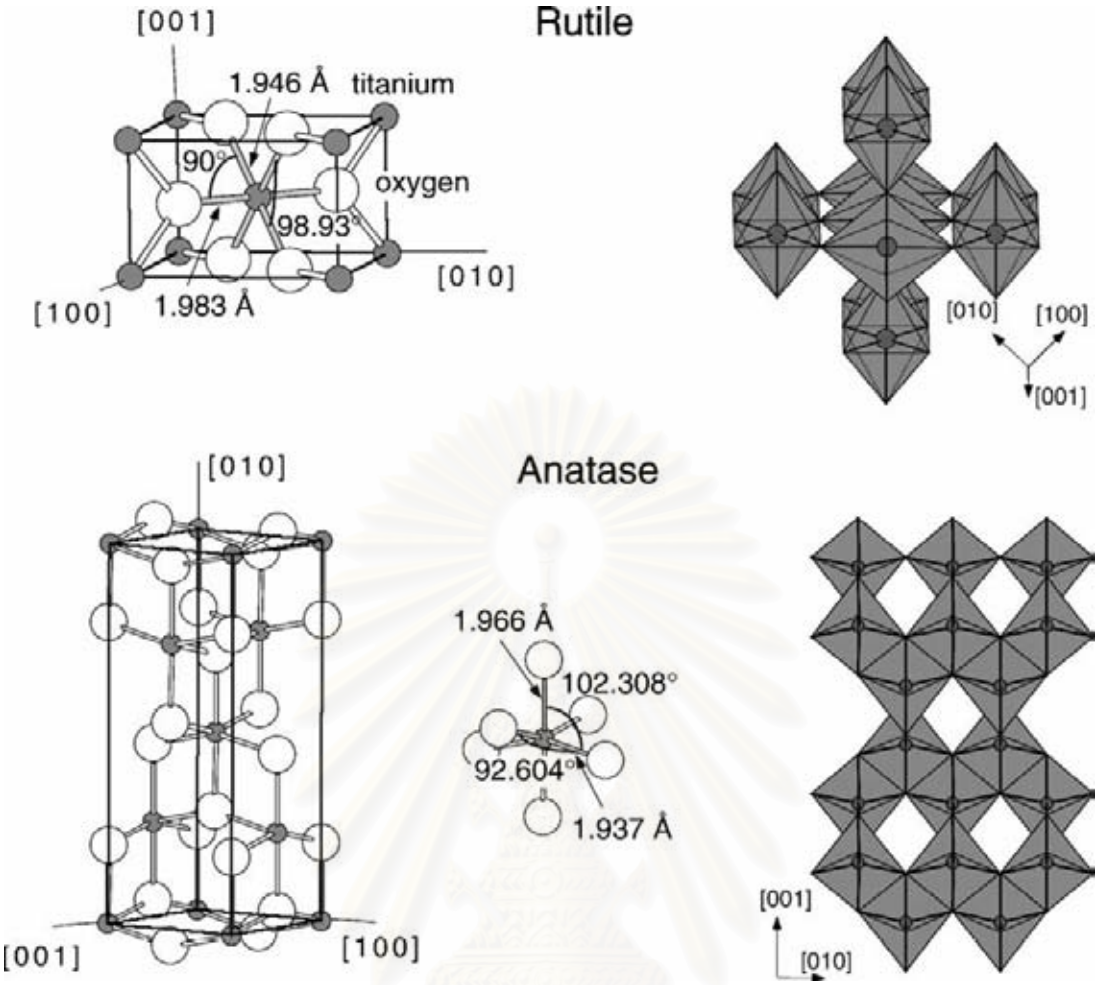

Figure 3.1 Crystal Structure of TiO_2 (Diebold, 2003)

The three forms of titanium (IV) oxide have been prepared in laboratories but only rutile, the thermally stable form, has been obtained in the form of transparent large single crystal. The transformation from anatase to rutile is accompanied by the evolution of ca. 12.6 kJ/mol (3.01 kcal/mol), but the rate of transformation is greatly affected by temperature and by the presence of other substance, which may either catalyze or inhibit the reaction. The lowest temperature at which transformation from anatase to rutile takes place at a measurable rate is around 700˚C, but this is not a transition temperature. The change is not reversible since ΔG for the change from anatase to rutile is always negative.

Brookite has been produced by heating amorphous titanium (IV) oxide, which is prepared from an alkyl titanate or sodium titanate, with sodium or potassium hydroxide in an autoclave at 200 to 600°C for several days.

The important commercial forms of titanium (IV) oxide are anatase and rutile, and they can readily be distinguished by X-ray diffraction spectrometry. Since anatase and rutile are tetragonal, both of them are anisotropic. Their physical properties, e.g. refractive index, vary according to the direction relative to the crystal axes. In most applications of these substances, the distinction between crystallographic directions is lost because of the random orientation of large numbers of small particles, and only average values of the properties are significant.

Measurement of physical properties, in which the crystallographic directions are taken into account, may be made for both natural and synthetic rutile, natural anatase crystals and natural brookite crystals. Measurements of the refractive index of titanium (IV) oxide must be made by using a crystal that is suitably orientated with respect to the crystallographic axis as a prism in a spectrometer. Crystals of suitable size of all three modifications occur naturally and have been studied. However, rutile is the only form that can be obtained in large artificial crystals from melts. The refractive index of rutile is 2.75. The dielectric constant of rutile varies with direction in the crystal and deviation from the stoichiometric formula (TiO_2) An average value for rutile in powder from is 114. The dielectric constant of anatase powder is 48.

Titanium (IV) oxide is thermally stable (mp 1855 °C) and very resistant to chemical attack. When it is heated strongly under vacuum, there is a slight loss of oxygen corresponding to a change in composition to $TiO_{1.97}$. The product is dark blue but reverts to the original white color when it is heated in air.

3.2 Gold

3.2.1 Physical and chemical properties of bulk gold

(http://www.gold.org/discover/sci_indu/properties/)

Gold (symbol Au) has an atomic number of 79. The atomic mass of the gold atom is 196.967 and the atomic radius is 0.1442nm. Interestingly this is smaller than would be predicted by theory. The arrangement of outer electrons around the gold nucleus is based on 14 4*f* shell electrons, 10 5*d* shell electrons and a single 6*s* shell electron (i.e., [Xe] $4f^{14}$ $5d^{10}$ $6s^1$).

The arrangement of these electrons is related to characteristic yellow color of gold. The color of a metal is based on transitions of electrons between energy bands. The conditions for the intense absorption of light at the wavelengths necessary to produce the typical gold color are fulfilled by a transition from the *d* band to unoccupied positions in the conduction band. The addition of alloying elements has a profound effect on color of a gold based alloy. Adding nickel or palladium, for example, has a whitening effect.

While the number of protons in a gold nucleus is fixed at 79, the number of neutrons can vary from one atom to another giving a number of isotopes of gold. However, there is only one stable non-radioactive isotope accounting for all naturally found gold.

The crystal structure for metallic gold is face center cubic (FCC). This crystal structure contributes to very high ductility of gold since FCC lattices are particularly suitable for allowing the movement of dislocations in the lattice. Such dislocation movement is essential for achieving high ductility.

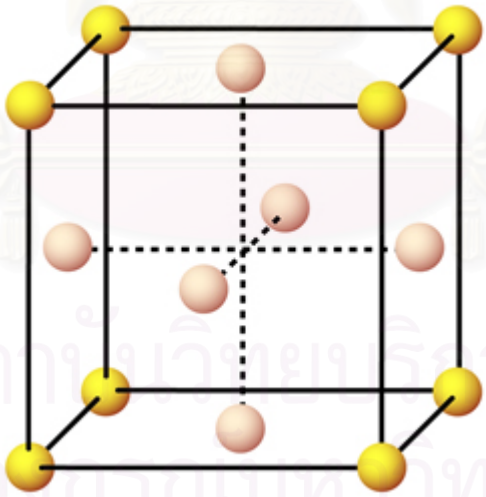

Figure 3.2 Crystal structure of metallic gold

The density of gold (19.3 g/cm^3) depends on both its atomic mass and the crystal structure. This makes gold rather heavy compared to some other common materials. For example, aluminium has a density of 2.7 g/cm^3 and even density of steel is only 7.87 g/cm^3.

The melting point of pure gold is 1064 °C, although when alloyed with other elements such as silver or copper, the gold alloy will melt over a range of temperatures. The boiling point of gold, when gold transforms from the liquid to gaseous state, is 2860°C.

The ability of gold to efficiently transfer heat and electricity is bettered only by copper and silver, making it indispensable in electronics for semiconductors and connectors in computer technology. The electrical resistivity of gold is 0.022 micro-ohm•m at 20 °C. The thermal conductivity is 310 W/m.K at the same temperature. The corrosion resistance of gold is perhaps one of its most useful properties. In practice, it is corroded only by a mixture of nitric and hydrochloric acid (aqua regia). In everyday use gold does not tarnish. Gold only dissolves in cyanide.

Table 3.2 Properties of gold.

Property	
Atomic weight	196.97
Atomic number	79
Number of naturally occurring isotopes	1
Melting point (^{o}C)	1064
Crystal structure	FCC
Density (g/cm^{3})	19.3
Thermal conductivity (W/m.K)	310
Electrical resistivity micro-ohm m at 20°C	0.022
Young's modulus, E (GPa)	79
Hardness Hv	25
Tensile stress (MPa)	124
0.2% proof stress (MPa)	30
Poison's ratio	0.42

3.3 Preparation methods

3.3.1 Hydrothermal method

The method involves heating the reactants in water/steam at high pressure and temperature. The water performs two roles, as a pressure-transmitting medium and as a solvent, in which the solubility of the reactants depends on pressure and temperature. In addition, some or all of the reactants are partially soluble in the water under pressure and this enables reactions to take place in, or with the aid of, liquid and/or vapor phases. Under these conditions, reactions that, in the absence of water, would occur only at much high temperature are possible. The method is therefore particularly suitable for the synthesis of phases that are unstable at high temperature. The technique is also useful for growth of single crystals. By arranging for an appropiate temperature gradient to be present in the reaction vessel, dissolution of the starting material may occur at the hot end and reprecipitation at the cold end.

The equipment designed for hydrothermal method is basically a tube, usually made of steel, closed at one end. The other end has a screw cap with a gasket of soft copper to provide a seal. Alternatively, the ‘reactor’ may be connected directly to and independent pressure source, such as a hydraulic ram. This is known as the ‘cold seal’ method. The reaction mixture and an appropriate amount of water are placed inside the reactor, which then sealed and placed inside an oven at the required temperature, usually in the range between 100 and 500 ^{o}C. Pressure is controlled either externally or by the degree of filling in a sealed reactor. By making use of the pressure-temperature phase diagram, as shown in figure 3.3 (a), curve AB is the saturated steam curve and separates water (above) from steam (below). At temperature above 374 ^{o}C (point B), the water is in the supercritical condition and there is no distinction between liquid and vapor states.

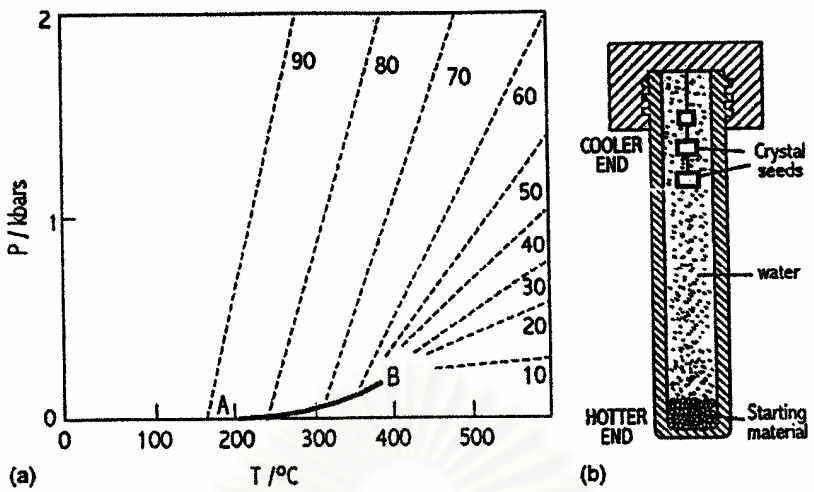

Figure 3.3 (a) Pressure-temperature relations for water at constant volume, dashed curves represent pressures developed inside a close vessel; numbers represent the percentages degree of filling of the vessel by water at ordinary P, T. (b) Schematic hydrothermal bomb used for crystal growth.

3.3.2 Glycothermal and solvothermal method

Glycothermal and solvothermal method have been developed for synthesis of metal oxide and binary metal oxide by using glycol and solvent as the reaction medium, respectively. The use of glycol or solvent instead of water in the hydrothermal method produces the different form of intermediate phase. Instability of such intermediates provides a large driving force for the formation of product under mild condition.

3.3.3 Precipitaion method

Precipitation method involves the growth of crystals from a solvent of different composition. The solvent may be one of the constituents of the desired crystals, e.g., crystallization of salt hydrate crystals using water as solvent, or the solvent may be entirely separate liquid element or compound in which the crystals of interest are partially soluble, e.g., SiO_2 and various high melting silicates may be precipitated from low melting borate or halide melts. In these cases, the solvent melts

are sometimes referred to as fluxes since they effectively reduce the melting point of the crystals by a considerable amount.

This method has recently been used to grow crystals of titanium (IV) oxide using titanium tetrachloride as starting material. Titanium (IV) oxide which, after washing and drying at 110 ^{o}C, is calcined at 800 ^{o}C to remove combined water and chloride, according to the stoichiometric relation as following:

$$TiCl_4 + 4NH_4OH \rightarrow Ti(OH)_4 + 4NH_4Cl$$

This method involves precipitation of titanium tetrachloride as hydrated titanium (IV) oxide, conversion of the precipitate to double oxalate, recrystallization and subsequent calcinations.

3.3.4 Sol-gel method (Fu *et al.*, 1996; Su *et al.*, 2004)

This process occurs in liquid solution of organometallic precursors such as tetraethyl orthosilicate, zirconium propoxide and titanium isopropoxide, which, by means of hydrolysis and condensation reaction, lead to the formation of sol.

$$M\text{-}O\text{-}R + H_2O \Rightarrow M\text{-}OH + R\text{-}OH \quad \text{(hydrolysis)} \quad (3.1)$$

$$M\text{-}O\text{-}H + HO\text{-}M \Rightarrow M\text{-}O\text{-}M + H_2O \quad \text{(water condensation)} \quad (3.2)$$

$$M\text{-}O\text{-}R + HO\text{-}M \Rightarrow M\text{-}O\text{-}M + R\text{-}OH \quad \text{(alcoholcondensation)} \quad (3.3)$$

A typical example of a sol-gel method is the addition of metal alkoxides to water. The alkoxides are hydrolyzed giving the oxide as a colloidal product.

The sol is made of solid particles of a diameter of few hundred nanometers suspending in a liquid phase. After that, the particles condense into gel, in which solid macromolecules are immersed in a liquid phase. Drying the gel at low temperature (25-100˚C), produces porous solid matrices or xerogels. To obtain a final product, the gel is heated. This heat treatment serves several purposes, *i.e.*, to remove solvent, to

decompose anions such as alkoxides or carbonates to give oxides, to rearrange of the structure of the solid, and to allow crystallization to occur.

Using the sol-gel method, one can easily control a stoichiometry of solid solution and a homogeneous distribution of nanoparticles and metal oxides. In addition, the advantages are that the metal oxides are prepared easily at room temperature and high purity can be obtained.

3.4 Photocatalytic process (Fujishima et al., 1999)

The primary photocatalytic process occurs upon irradiation of a semiconductor catalyst. A semiconductor is characterized by an electric band structure in which the highest occupied energy band, called valence band, and the lowest empty band, called conduction band, are separated by a band gap. The magnitude of the fixed energy gap between the electrochemically populated valence band and the largely vacant condition band governs the extent of thermal population of the conduction band in its intrinsic state. The band gap also defines the wavelength sensitivity of the semiconductor to irradiation (Fox and Dulay, 1993). When a photon of energy higher or equal to the band gap energy is absorbed by a semiconductor particle, an electron from the valence band is promoted to the conduction band with simultaneous generation of an electronic vacancy or "hole" (h^+) in the valence band.

Figure 3.4 shows the photocatalytic process occurring on an illuminated semiconductor particle.

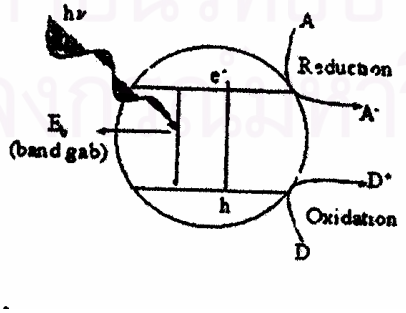

Figure 3.4 The photocatalytic process occurring on an illuminated semiconductor particle (Fujishima, 1999).

In most materials that are electrically conductive, i.e., metals, two types of carriers, electron (e-) and holes (h+), immediately recombine on the surface or the bulk of particle in a few nanoseconds and the energy is dissipated as heat (equation 3.4). On semiconductor such as titanium dioxide, however , they survive for period of time to allow these carriers be trapped in surface states where they can react with donor (D) or acceptor (A) species adsorbed or close to the surface of the particle (equations 3.5, 3.6 and 3.7) (Litter(1999)).

Recombination $h^+ + e^- \rightarrow heat$ (3.4)

Photoexcitation $Semiconductor + h\upsilon \rightarrow e^- + h^+$ (3.5)

$h^+ + D \rightarrow D^+$ (3.6)

$e^- + A \rightarrow A^-$ (3.7)

In aqueous solution, hydroxyl radicals (OH^-) production is favorable because of the abundance of hydroxyl groups and water molecules on the surface of catalyst. However, in the gas phase, organic substrates can act as adsorbed traps for the photogenerated hole since in the gas phase, water molecules are not the predominant species in contact with the catalyst. Although in the presence of water vapor, OH groups are presented on the catalyst surface and their contribution to photooxidation cannot be discarded (Alberici et al., 1997).

When adsorbed water molecules are oxidized by holes, hydroxyl radicals which have strong oxidizing power are formed (equations 3.8 and 3.9).

$h^+ + H_2O \rightarrow \bullet OH + H^+$ (3.8)

$h^+ + OH^- \rightarrow \bullet OH$ (3.9)

The hydroxyl radicals can then react with organic components, initially producing free radicals (unstable molecules that have one unpaired electron). When oxygen molecule is present, it prefers to react with these free radicals producing organic peroxyl radicals which, in addition to containing an unpaired electron, also now contain two oxygen molecules. These radicals can then take part in chain

reactions. In a short time, organic compounds are completely degraded, i.e., converted to carbon dioxide and water.

Meanwhile, these electrons are used to reduce oxygen in air because oxygen is easier to reduce than water.This reduction results in the superoxide radical anion (O_2^-) (equation (3.10)).

$$e^- + O_2 \rightarrow O_2^- \qquad (3.10)$$

The superoxide anion attaches itself to the peroxyl radicals mentioned above. The resulting unstable product now contains at least four oxygen atoms and can be decomposed to produce carbon dioxide molecule.

3.5 Ostwald ripening (http://xray.bmc.uu.se)

Many small crystals form in a system initially but slowly disappear except for a few that grow larger, at the expense of the small crystals. The smaller crystals act as "nutrients" for the bigger crystals. As the larger crystals grow, the area around them is depleted of smaller crystals.

Ostwald ripening is a spontaneous process that occurs because larger crystals are more energetically favored than smaller crystals. While the formation of many small crystals is *kinetically* favored, (i.e. they nucleate more easily) large crystals are *thermodynamically* favored. Thus, from a standpoint of kinetics, it is easier to nucleate many small crystals. However, small crystals have a larger surface area to volume ratio than large crystals. Molecules on the surface are energetically less stable than the ones already well ordered and packed in the interior. Large crystals, with their greater volume to surface area ratio, represent a lower energy state. Thus, many small crystals will attain a lower energy state if transformed into large crystals and this is what we see in Ostwald ripening.

3.6 Aqua regia (http://en.wikipedia.org/wiki/Aqua_regia)

Aqua regia (Latin for “royal water”) is a highly corrosive, fuming yellow liquid, formed by a fresh mixture of concentrated nitric acid (HNO_3) and concentrated hydrochloric acid (HCl), usually in a volumetric ratio of one to three. It is one of the few reagents able to dissolve gold and platinum. It was so named because it can dissolve the so-called royal, or noble metal, although tantalum, iridium, and a few other extremely passive metals are able to withstand it. Aqua regia is used in etching and in certain analytic procedures. Due to the formation of volatile nitrosyl chloride (NOCl) and chlorine (Cl_2), aqua regia will quickly lose its effectiveness. Therefore, it should be mixed immediately before use.

Aqua regia works to dissolve gold, even though neither constituent acid will do so alone, because, in combination, each acid performs a different task. Nitric acid is a powerful oxidizer, which actually dissolve a tiny amount of gold, forming gold ions (Au^{3+}). The hydrochloric acid provides a supply of chloride ions (Cl^-), which react with the gold to produce chloroaurate anions ($AuCl_4^-$), also in solution. The reaction with hydrochloric acid is an equilibrium reaction which favors formation of chloroaurate anions. This results in a removal of gold ions from solution and allows further oxidation of gold to take place, and so, the gold is dissolved. In addition, gold may be oxidized by the free chlorine present in aqua regia. The reactions are:

$$Au(s) + 3NO_3^-(aq) + 6H^+(aq) \rightarrow Au^{3+}(aq) + 3NO_2(g) + 3H_2O(l)$$

$$Au^{3+}(aq) + 4Cl^-(aq) \rightarrow AuCl_4^-(aq)$$

The oxidation reaction can also be written with nitric oxide as the product rather than nitrogen dioxide.

$$Au(s) + NO_3^-(aq) + 4H^+(aq) \rightarrow Au^{3+}(aq) + NO(g) + 2H_2O(l)$$

Upon mixing of concentrated hydochloric acid and concentrated nitric acid, chemical reactions will begin to occur. These reactions result in volatile products (nitrosyl chloride and chlorine) that result in the fuming nature of aqua regia. The

yellow color of the products also results in the characteristic color of aqua regia. As the volatile products escape from solution, the aqua regia will lose its potency.

$$HNO_3(aq) + 3HCl(aq) \rightarrow NOCl(g) + Cl_2(g) + 2H_2O(l)$$

Nitrosyl chloride can further decompose into nitric oxide and chlorine. This dissociation is equilibrium-limited. Therefore, the fumes over aqua regia contain nitrosyl chloride, nitric oxide, and chlorine.

$$2NOCl(g) \rightarrow 2NO(g) + Cl_2(g)$$

CHAPTER IV

EXPERIMENT

The experimental section in this work is separated into four parts: (i) preparation of titanium dioxide; (ii) deposition of gold on titanium dioxide; (iii) catalyst characterizations and (iv) photocatalytic reactions of ethylene. The details of the experiment are described as following:

4.1 Preparations of titanium dioxide

4.1.1 Chemicals

A list of chemicals used in the preparation is displayed in Table 4.1.

Table 4.1 The chemicals used in the preparation of titanium dioxide.

Chemicals	Supplier	Purity (%)
1. Titanium (IV) tert-butoxide (TNB,$Ti[O(CH_2)_3CH_3]_4$)	Aldrich	97
2. 1, 4-Butanediol (1, 4-BG, $HO(CH_2)_4OH$)	Aldrich	99
3. Titanium isopropoxide ($Ti[O(CH_2)_2CH_3]_4$)	Aldrich	97
4. Nitric acid (HNO_3)	APS	70
5. Ethanol (C_2H_5OH)	Carlo Erba	99.8

4.1.2 Equipments

4.1.2.1 Autoclave reactor

The body of the autoclave is made of stainless steel with the volume of 1,000 cm^3. It has 10 cm inside diameter. The temperature tolerance of the body is up to 350 ^oC. It is installed with the pressure gauge in the range of 0-140 bar and relief valve used to prevent runaway reaction. The iron jacket is used to reduce the volume of the autoclave to 300 cm^3 and the test tube is used to contain the reagent and solvent.

The picture of autoclave reactor is shown in Figure 4.1.

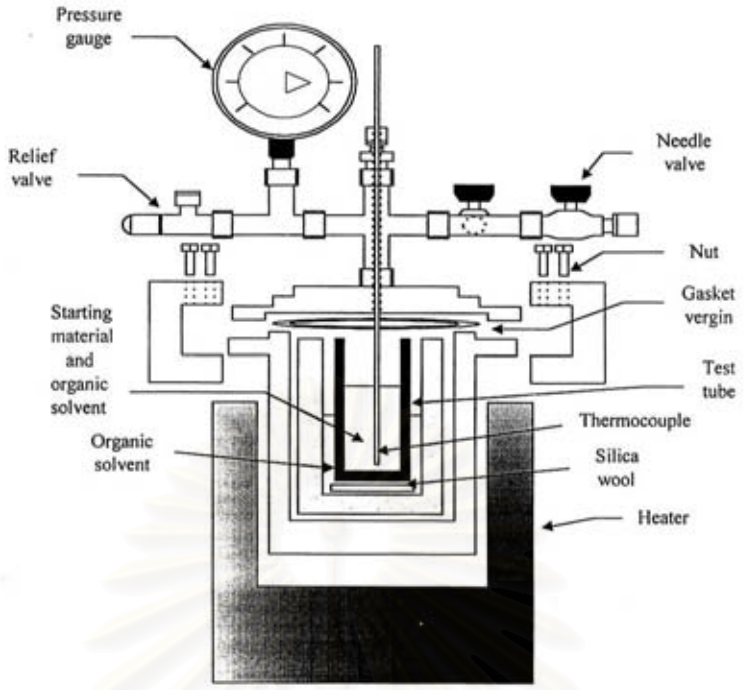

Figure 4.1 Autoclave reactor

4.1.2.2 Temperature program controller

A CHINO DB1000F temperature program controller was connected to a thermocouple with 0.5 mm diameter dipped into the reagent in the autoclave.

4.1.2.3 Electrical furnace (Heater)

Electrical furnace supplied the energy to heat the autoclave to the required temperature.

4.1.2.4 Gas controlling system

Nitrogen tank was set with a pressure regulator (1-150 bar) and needle valves were used to release gas from the autoclave.

The diagram of the equipments used in solvothermal method is shown in Figure 4.2.

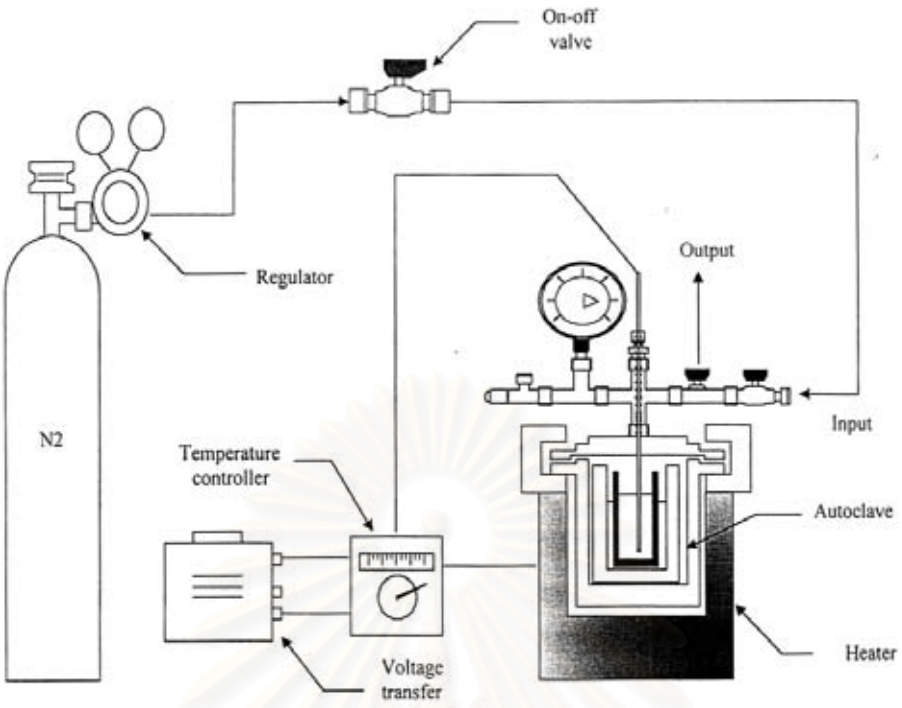

Figure 4.2 Diagram of the equipments used in solvothermal method.

4.1.3 Preparation

4.1.3.1 Solvothermal method (11 nm)

Titanium dioxide was prepared by using titanium (IV) tert-butoxide as starting material. First, 15 g of titanium (IV) tert-butoxide was mixed with 100 cm^3 of 1, 4-butanediol in the test tube and then set up in the autoclave. In the gap between the test tube and the inside wall of autoclave reactor, 30 cm^3 of 1, 4-butanediol was added. After the autoclave was completely purged with nitrogen, it was heated to 300 ^oC with the rate of 2.5 $^oCmin^{-1}$ and held at this temperature for two hours. The pressure in the reactor increased gradually with the increasing of the temperature. After the reaction, the autoclave was cooled to room temperature. The powder collected from the test tube was centrifuged five times with methanol, dried in the air at room temperature for six hours and dried in the oven at 110 ^oC overnight. The resulting powder was grounded to get the final titanium dioxide.

The amount of reagent and solvent used in this method is shown in Table 4.2

Table 4.2 The amount of reagent and solvent used in solvothermal method

Chemicals	Amount
In the test tube:	
1. Titanium (IV) tert-butoxide (TNB,$Ti[O(CH_2)_3CH_3]_4$)	15 g
2. 1, 4-Butanediol (1,4-BG,$HO(CH_2)_4OH$)	100 cm^3
In the gap:	
1. 1, 4-Butanediol (1,4-BG,$HO(CH_2)_4OH$)	30 cm^3

4.1.3.2 Sol-gel method (type I)

Titanium isopropoxide was used as a precursor. First, 7.22 cm^3 of 70% nitric acid was added to 1000 cm^3 of distilled water. While the acidic solution was stirred, 83.4 cm^3 of titanium isopropoxide was added slowly. The suspension was stirred continuously at room temperature for 3-4 days until clear sol was obtained. After that, the sol was dialyzed in a cellulose membrane with a molecular weight cutoff of 3500 (Spectrum Companies, Gardena, CA). The membrane containing sol was submerged in distilled water which was changed daily for 3-4 day until the pH value of the water raised to 3.5. To remove solvents, the dialyzed sol was poured into the plates, left in ambient atmosphere overnight and dried at 110°C in the oven. The resulting gel was then grounded and calcined at 250 ^oC for two hours to get the final titanium dioxide.

The amount of reagents used in this method is shown in Table 4.3.

Table 4.3 The amount of reagents used in sol-gel method (type I)

Chemicals	Amount (cm^3)
1. Titanium isopropoxide ($Ti[O(CH_2)_2CH_3]_4$)	83.4
2. Distilled water (H_2O)	1000
3. Nitric acid 70% (HNO_3)	7.22

4.1.3.3 Sol-gel method (type II)

Titanium isopropoxide was used as a precursor for this method. First, 20 cm^3 of absolute ethanol was mixed with 10 g of titanium isopropoxide. Then the mixture was added gradually into a solution of 100 cm^3 of distilled water and 20 cm^3 of absolute ethanol while being sonicated. After that, the mixture was continuously sonicated for two hours and centrifuged for five times with absolute ethanol. The wet powder was dried in air at room temperature overnight. The resulting powder was grounded and calcined at 450 ^oC for two hours to obtain the final product.

The amount of reagents used in this method is shown in Table 4.4.

Table 4.4 The amount of reagent and solvent used in sol-gel method (type II)

Chemicals	Amount
First beaker:	
1. Titanium isopropoxide ($Ti[O(CH_2)_2CH_3]_4$)	10 g
2. Absolute ethanol (C_2H_5OH)	20 cm^3
Second beaker:	
1. Distilled water (H_2O)	100 cm^3
2. Absolute ethanol (C_2H_5OH)	20 cm^3

4.2 Preparations of gold deposited titanium dioxide

4.2.1 Chemicals

The details of chemicals used in this section are shown in Table 4.5.

Table 4.5 The chemicals used in the preparation of gold deposited titanium dioxide.

Chemicals	Supplier	Purity (%)
1. Hydrogen tetrachloroaurate trihydrate ($HAuCl_4.3H_2O$)	Aldrich	99.9
2. Sodium hydroxide (NaOH)	EKA Chemicals	100
3. Hydrochloric acid (HCl)	J.T. Baker	38
4. Titanium dioxide (TiO_2- JRC-TIO1)	Dept. of Material Science, Shimane University	100

4.2.2 Preparation

The gold deposited titanium dioxide catalysts were prepared via deposition-precipitation method. First, the precursor for gold (hydrogen tetrachloroaurate trihydrate) in the amount of 0.0816 g (2 wt.% of the catalyst prepared) was dissolved in 100 cm^3 of distilled water. The initial pH value of the solution was 2.6. Then pH was raised to the desired value (6, 7, 9, and 10) using 0.1 M sodium hydroxide solution. When pH reached the desired value, 2 g of titanium dioxide prepared in section 4.1.3 was added to solution and cause the pH to drop slightly. The pH of the suspension was readjusted to the desired value again using the same method. After addition of titanium dioxide, the suspension was heated to 70 ^oC and held at that temperature for one hour. During the deposition, the pH was maintained by addition of 0.1 M sodium hydroxide solution or 0.1 M hydrochloric acid solution. After one hour, the suspension was cooled and centrifuged five times with distilled water. Then the suspension was vacuum-filtered and dried at 110 ^oC in the oven for two hours. The powder obtained was grouded to get the final catalyst.

The amount of reagents used in this section is shown in Table 4.6.

Table 4.6 The amount of reagents used in preparation of gold depositeded titanium dioxide.

Chemicals	Amount (for each pH)
1. Titanium dioxide (TiO_2):	
1) Solvothermal method (from section 4.1.3.1)	2 g
2) Sol-gel method type I (from section 4.1.3.2)	2 g
3) Sol-gel method type II (from section 4.1.3.3)	2 g
4) JRC-TIO1	2 g
2. Hydrogen tetrachloroaurate trihydrate ($HAuCl_4.3H_2O$)	0.0818 g (2 wt.%)
3. Distilled water (H_2O)	100 cm^3
4. Sodium hydroxide solution (0.1 M)	depended on condition
5. Hydrochloric acid solution (0.1 M)	depended on condition
Note: The pH used is 6, 7, 9 and 10 respectively	

4.3 Catalysts characterizations

4.3.1 X-ray diffraction spectroscopy (XRD)

The crystallinity and X-ray diffraction (XRD) patterns of the catalysts were performed by SIEMENS D5000 X-ray diffractometer connected with a personal computer using Diffract AT version 3.3 for a full control of the XRD analyzer. The experiments were carried out by using CuKα radiation with Ni filter and the operating conditions of the measurement were shown below.

2θ range of detection	:	20 – 80 ^{o}
Resolution	:	0.02 ^{o}
Number of Scan	:	15

The crystalline size was estimated from line broadening according to the Scherrer equation (see Appendix A) and α-Al_2O_3 was used as standard.

4.3.2 Transmission electron microscope (TEM)

The morphology and crystalline size of titanium dioxide and gold nanoparticles were observed by JEOL 2010 Transmission Electron Microscope (TEM) operated at 100 kV.

4.3.3 Surface area measurement

The single point BET surface area of the catalysts was measured by Micromeritics ChemiSorb 2750 using nitrogen as the adsorbate. The operating conditions were shown below.

Sample weight	:	0.2 g
Degas temperature	:	200 ^{o}C for as-synthesized sample

4.3.4 Electron spin resonance spectroscopy (ESR)

Ti^{3+} measurements were carried out at 77 K with a JES-RE2X ESR spectrometer. Recorded spectra were scanned and converted to a g value scale referred to a Mn^{2+} marker.

4.3.5 Inductively Coupled Plasma-Atomic Emission Spectroscopy (ICP-AES)

The amount of gold deposited on the surface of titanium dioxide was measured with a Optima 2100 DV spectrometer. 0.0125 g of catalyst was dissolved in aqua regia, mixture of concentrated hydrochloric acid and concentrated nitric acid in the ratio of 3:1 (3 cm^3:1 cm^3). The sample was diluted to the concentration of 5 ppm ($mg.l^{-1}$) from the catalyst which was assumed to have gold content of 2 %wt. in the volumetric flask which has the volume of 50 cm^3. The standard solutions were prepared from 1,000-ppm standard gold solution obtained from PerkinElmer. The standard gold solution was diluted to the concentration of 0.8 ppm and 10 ppm in the 25-cm^3 volumetric flask. 0.02 and 0.25 cm^3 of standard gold solution were mixed with aqua regia in the same ratio as used for preparation of samples and then diluted to desired volumes. For the blank, 3 cm^3 of concentrated hydrochloric acid and 1 cm^3 of concentrated nitric acid were mixed together and then diluted to 50 cm^3 in the volumetric flask.

The chemicals used in the preparation of samples for ICP-AES characterization are shown in the Table 4.7.

Table 4.7 Chemicals used in the preparation of samples for ICP-AES characterization.

Chemicals	Supplier	Purity (%)
1. Hydrochloric acid (HCl)	J.T. Baker	38
2. Nitric acid (HNO_3)	APS	70
3. Standard gold solution	PerkinElmer	1,000 ppm

4.4 Photocatalytic reaction of ethylene

4.3.1 Reactant

The reactant gas employed for this study was ethylene in air supplied by Thai Industrial Gas Limited. The gas mixture contained 0.1 %vol of ethylene in balance air. Total flow rate of gas in the experiments was 15 cm^3min^{-1}.

4.3.2 Equipments

4.3.2.1 Photoreactor

The photoreactor had two main components: an ultraviolet source and the tubular reactor. The reactor was made from a Pyrex glass tube with a diameter of 5 mm and a length of 27 cm. The stainless steel tube is 1.5″ in length and 3/8″ in diameter connected to the both ends of the reactor. Two sampling points were located on the left and right of catalyst bed. The catalyst was packed between two quartz wool layers fixed at the both ends of the reactor. The ultraviolet sources were black light blue fluorescent bulbs (8 Watts). Four light bulbs were located 1.5 cm away from the reactor in square configuration. The photoreactor was covered with two layers of aluminum foil to minimize radiation losses from the system.

The picture of the reactor was shown in Figure 4.3.

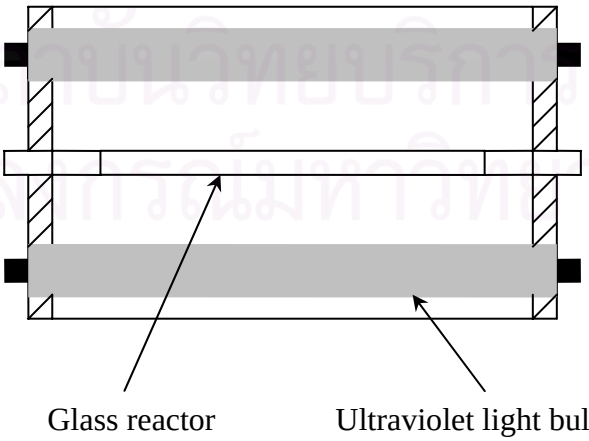

Figure 4.3 Photoreactor

4.3.2.2 Gas controlling system

Each feed line reactant was equipped with a pressure gauge and a ball valve. Flow rate of gas was adjusted and measured by metering valve and bubble flow meter, respectively.

4.3.3 Experimental procedure for determining the activity of the catalyst

The catalyst with the weight of 0.2 g was used for measuring photocatalytic activity. First, the catalyst was packed in the reactor between the layers of the quartz wool fixed at the both ends. Then the reactor was set in the system. Prior to each experiment, the catalyst was pretreated by air flow with the rate of 15 cm^3min^{-1} for 1 hour. While the flowing of air, the catalyst was illuminated by ultraviolet light sources in order to remove any organic compounds that might remain from previous experiments from the surface of the catalyst. After the pretreatment, the reactant, 0.1% (v/v) ethylene in air, was fed to the reactor at a flow rate of 15 cm^3min^{-1}. The temperature of the reactor under illumination, measured with a K-type thermocouple, was about 90°C. The flow rate of each gas was measured using a bubble flow meter.

The effluent gas was sampled to measure the concentration of ethylene using GC-14B gas chromatrograph (Shimadzu), equipped with a flame ionization detector. The operating conditions for the instrument were listed in Table 4.8. The composition of the effluent gas was measured every 20 minutes until steady state was achieved (as indicated by constant peak areas in the gas chromatograms).

Table 4.8 Operating conditions for gas chromatography

Gas chromatograph	SHIMADZU GC-14B
Detector	FID
Column	VZ10
Carrier gas	H_2 (99.999%)
Carrier gas flow (cm^3min^{-1})	30
Column temperature (^oC):	
Initial	70
Final	70
Injector temperature (^oC)	100
Detector temperature (^oC)	150
Current (mA)	-
Analyzed gas	Hydrocarbon (C_1-C_4)

CHAPTER V

RESULTS AND DISCUSSION

In this chapter, results and discussion are devided into two major parts: characterization of the catalysts and photocatalytic activities measurement using photooxidation of ethylene.

5.1 Characterization of catalysts

5.1.1 Characterization of bare TiO_2 catalysts

5.1.1.1 The phase structure and crystallite size

The phase structure of TiO_2 catalysts was determined using XRD technique. Four types of titanium dioxide prepared by different methods showed different XRD patterns.

The first catalyst was synthesized via a solvothermal method. The reaction of titanium (IV) tert-butoxide and 1, 4-butanediol at 300 ^{o}C under autogeneous pressure yielded nanocrystalline anatase titanium dioxide without the contamination of rutile, as indicated by nine peaks occurred at 2θ values of 25.3^{o}, 37.8^{o}, 48.1^{o}, 54.0^{o}, 55.2^{o}, 62.8^{o}, 68.0^{o}, 71.9^{o}, and 76.2^{o}. The second and third catalysts were prepared via sol-gel methods. The difference between these two catalysts was that the second one (sol-gel method type I) was prepared in nitric acid and water while the third one (sol-gel method type II) was prepared in ethanol and water. The phase structures of the catalyst prepared via the sol-gel method type I were mainly anatase with a small amount of brookite. The peak attributed to brookite phase occurred at the 2θ value of 30.9^{o}. The phase structure of the catalyst prepared via the sol-gel method type II was anatase only. The last catalyst was JRC-TIO1, a commercially available catalyst. The phase structures of this catalyst were mainly anatase with a small amount of rutile (1.46 %). The fraction of rutile in the catalyst was estimated using equation 5.1.

$$\%Rutile = \frac{1}{\left[(A/R)\times 0.884\right]+1}\times 100 \qquad (5.1)$$

Where A = peak area of anatase phase ($2\theta = 25.3^{o}$)

R = peak area of rutile phase ($2\theta = 27.5^{o}$).

The phase structures of all bare catalysts characterized by XRD are shown in Figure 5.1.

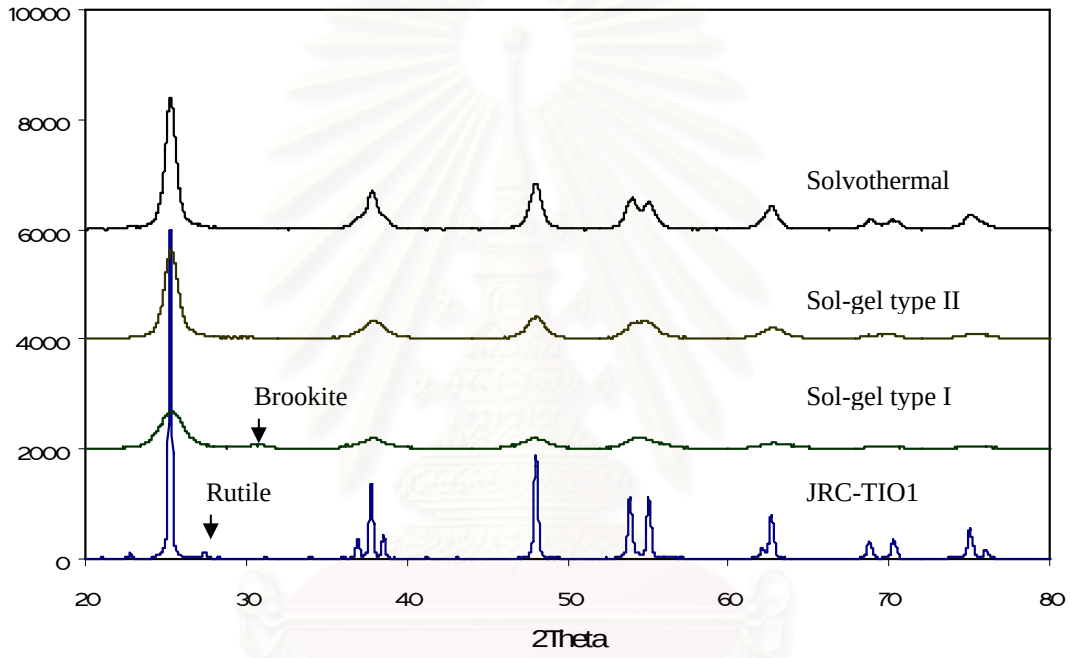

Figure 5.1 Phase structures of all bare catalysts.

The crystallite sizes of the catalysts were determined from the width at half-height of the (101) diffraction peak of anatase using the Scherrer equation. Example of crystallite size calculation using the Scherrer equation is illustrated in appendix B. The crystallite sizes of the catalysts calculated using the Scherrer equation are shown in Table 5.1.

Table 5.1 Crystallite sizes and specific surface areas of bare catalysts.

Catalysts	Crystallite size (nm)	Specific surface area (m^2g^{-1})
Solvothermal	10.9	79.5
Sol-gel type I	4.8	130.5
Sol-gel type II	8.4	82.0
JRC-TIO1	109.2	6.7

5.1.1.2 Specific surface area measurement

Specific surface areas of the catalysts are listed in Table 5.1. The catalyst prepared via the sol-gel method type I possessed largest specific surface area and the specific surface area of JRC-TIO1 catalyst was the smallest. This could be attributed to the crystallite size of the two catalysts.

5.1.1.3 Ti^{3+} measurement

The amounts of Ti^{3+} of the bare TiO_2 catalysts were measured by electron spin resonance spectroscopy (ESR). The results are shown in Table 5.2.

Table 5.2 The amount of Ti^{3+} of the bare TiO_2 catalysts (g^{-1})

Catalyst	Amount of Ti^{3+}
Solvothermal	30,021.08
Sol-gel type I	35,346.62
Sol-gel type II	8,066.15
JRC-TIO1	1,833.10

5.1.2 Characterization of gold deposited TiO_2 catalysts

5.1.2.1 Phase structure and crystallite size

The phase structure and crystallite size of gold deposited TiO_2 catalysts were determined by the same techniques employed for bare TiO_2 catalysts (see section 5.1.1). For titanium dioxide, the phase structures and crystallite sizes of all gold

deposited catalysts remained the same as those of bare catalysts except for the JRC-TIO1. The XRD patterns of gold deposited catalysts and bare catalysts are displayed in Figures 5.2 to 5.5. And the crystallite sizes of the catalysts are listed in Table 5.3.

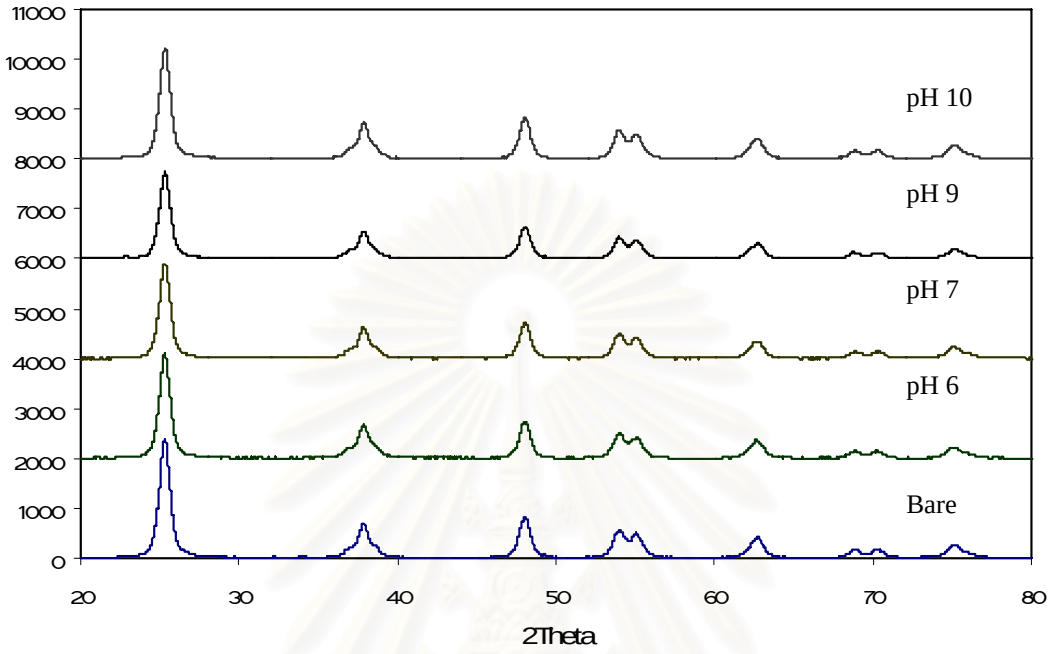

Figure 5.2 XRD Patterns of gold deposited TiO_2 and bare TiO_2, where TiO_2 was prepared via a solvothermal method.

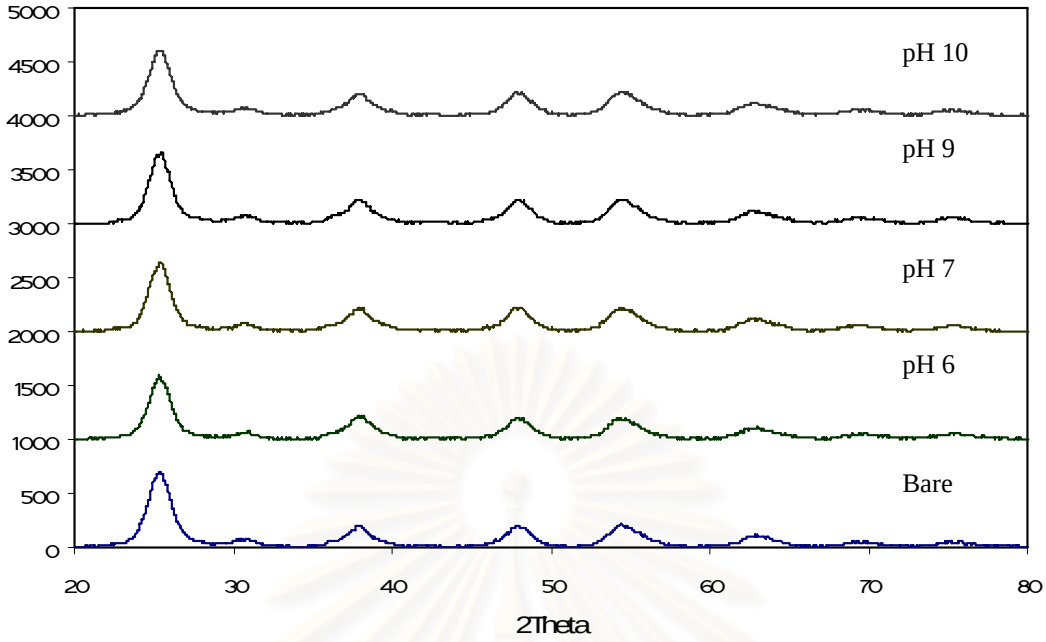

Figure 5.3 XRD Patterns of gold deposited TiO_2 and bare TiO_2, where TiO_2 was prepared via a sol-gel method type I.

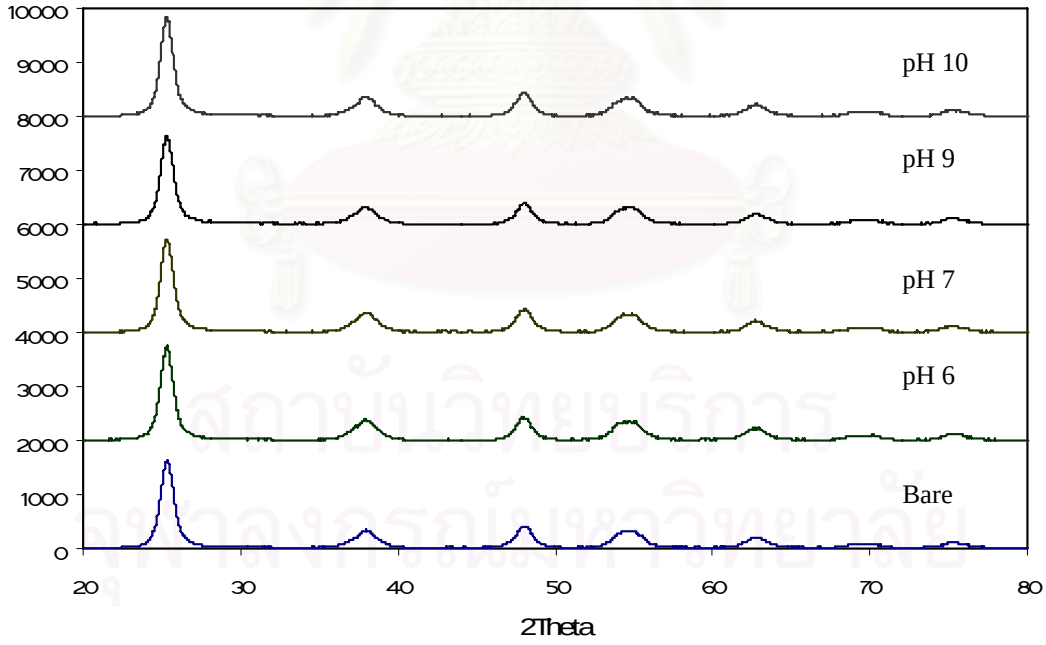

Figure 5.4 XRD Patterns of gold deposited TiO_2 and bare TiO_2, where TiO_2 was prepared via a sol-gel method type II.

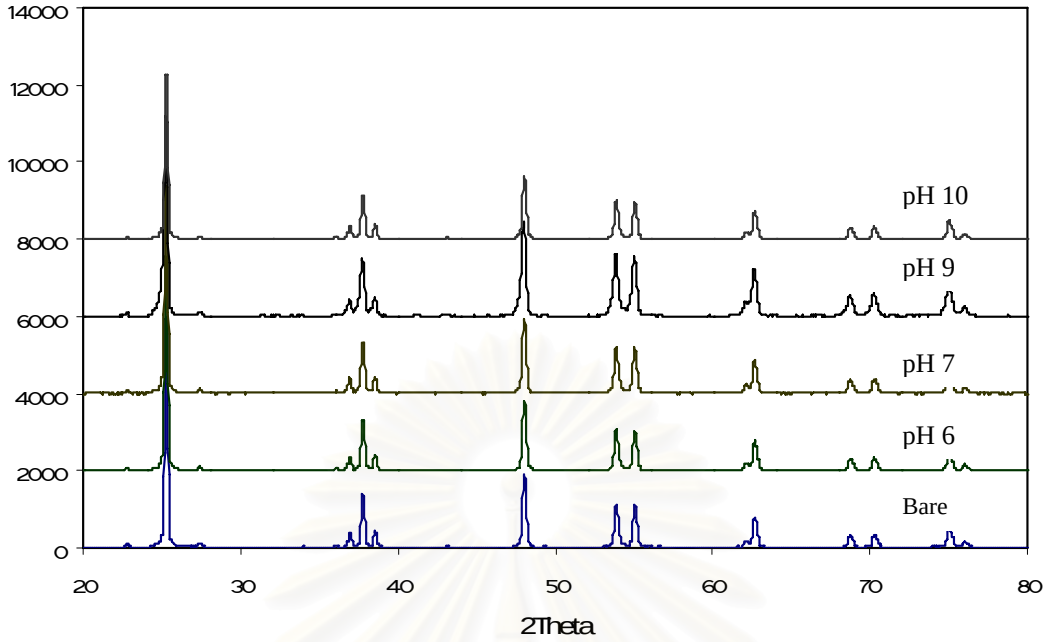

Figure 5.5 XRD Patterns of gold deposited TiO_2 and bare TiO_2, where TiO_2 was JRC-TIO1 catalyst.

Table 5.3 Crystallite sizes of titanium dioxide for gold deposited catalysts compared with bare catalysts (nm).

Condition	Solvothermal	Sol-gel type I	Sol-gel type II	JRC-TIO1
bare	10.9	4.8	8.4	109.2
pH 6	10.9	5.2	8.5	78.0
pH 7	10.9	5.3	8.6	81.5
pH 9	10.7	5.0	8.6	89.6
pH 10	10.7	4.8	8.8	94.3

For gold nanoparticles, no distinct diffraction of gold could be detected due to either small particle size or small amount of gold present. Therefore, transmission electron microscope (TEM) was employed to determine the particle sizes of gold nanoparticles. The TEM images of gold nanoparticles of all catalysts are displayed in Figures 5.6 to 5.21.

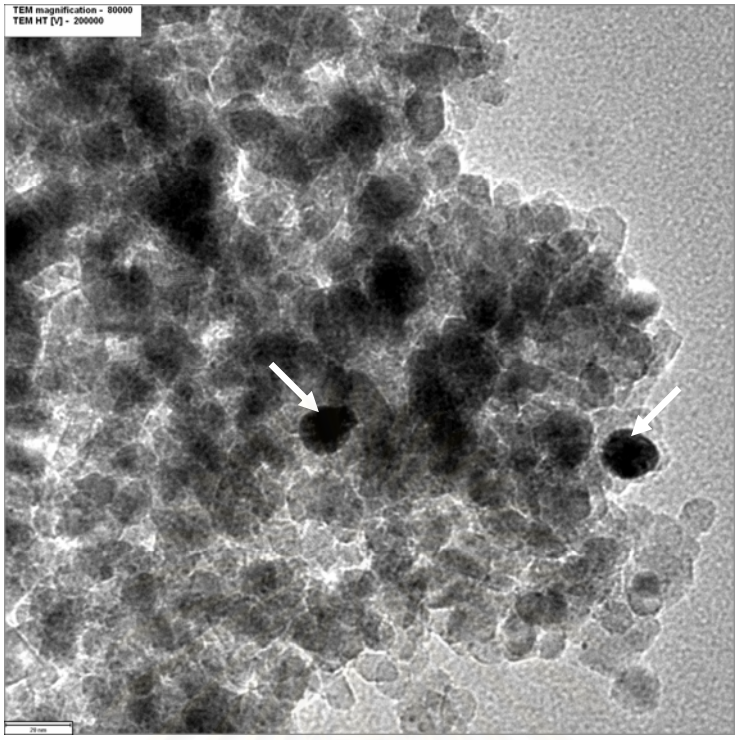

Figure 5.6 TEM image of catalyst prepared via a solvothermal method and gold deposition at pH 6. The scale bar is 20 nm. The arrows indicate some gold nanoparticles.

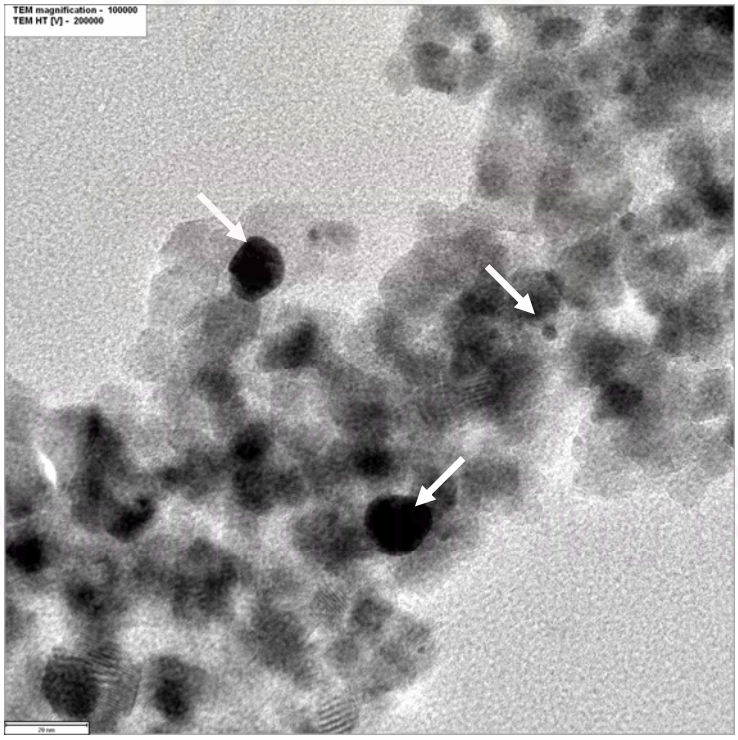

Figure 5.7 TEM image of catalyst prepared via a solvothermal method and gold deposition at pH 7. The scale bar is 20 nm. The arrows indicate some gold nanoparticles.

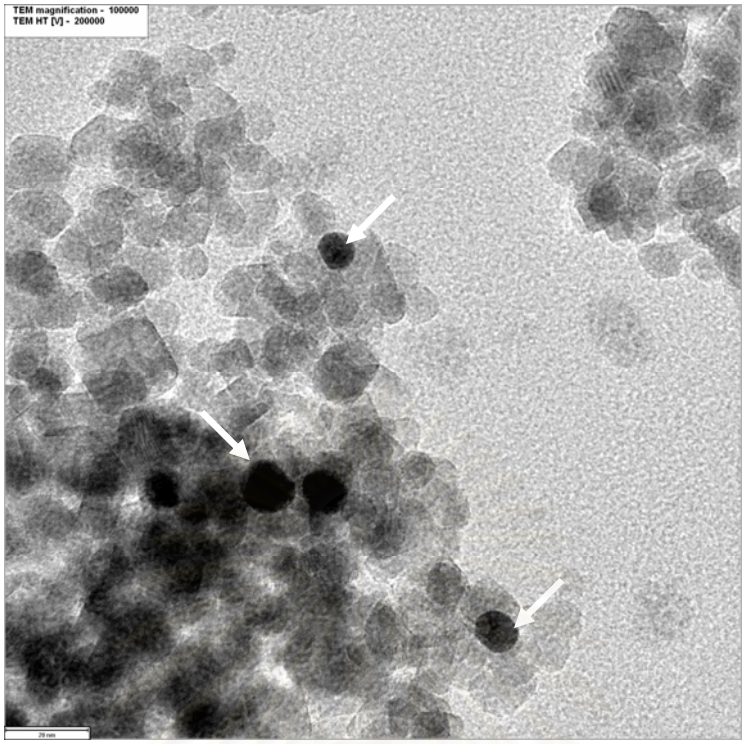

Figure 5.8 TEM image of catalyst prepared via a solvothermal method and gold deposition at pH 9. The scale bar is 20 nm. The arrows indicate some gold nanoparticles.

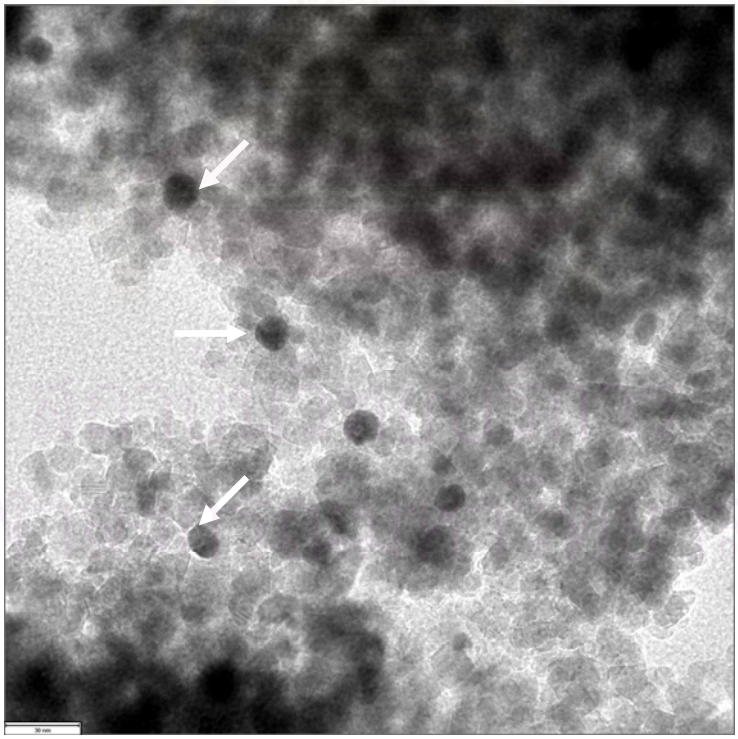

Figure 5.9 TEM image of catalyst prepared via a solvothermal method and gold deposition at pH 10. The scale bar is 30 nm. The arrows indicate some gold nanoparticles.

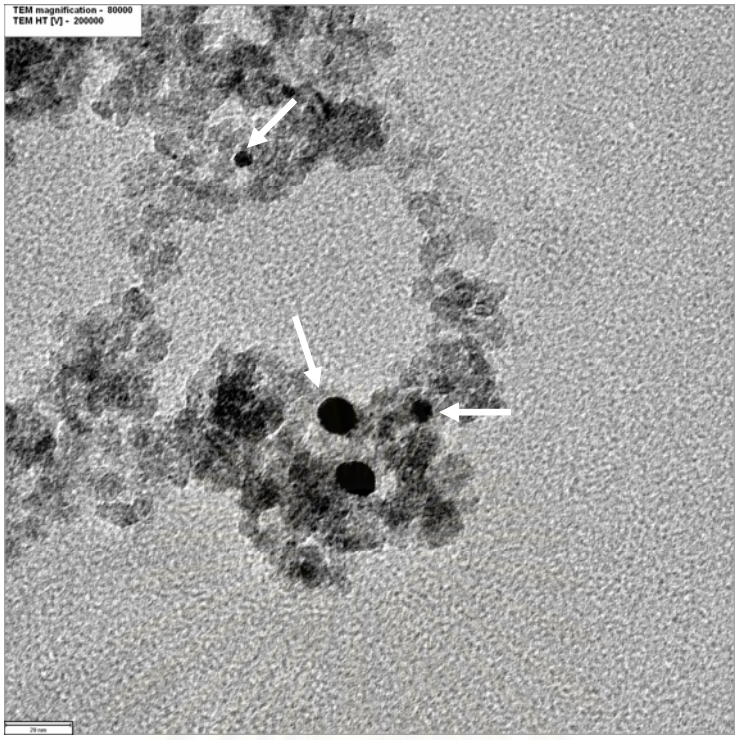

Figure 5.10 TEM image of catalyst prepared via a sol-gel method type I and gold deposition at pH 6. The scale bar is 20 nm. The arrows indicate some gold nanoparticles.

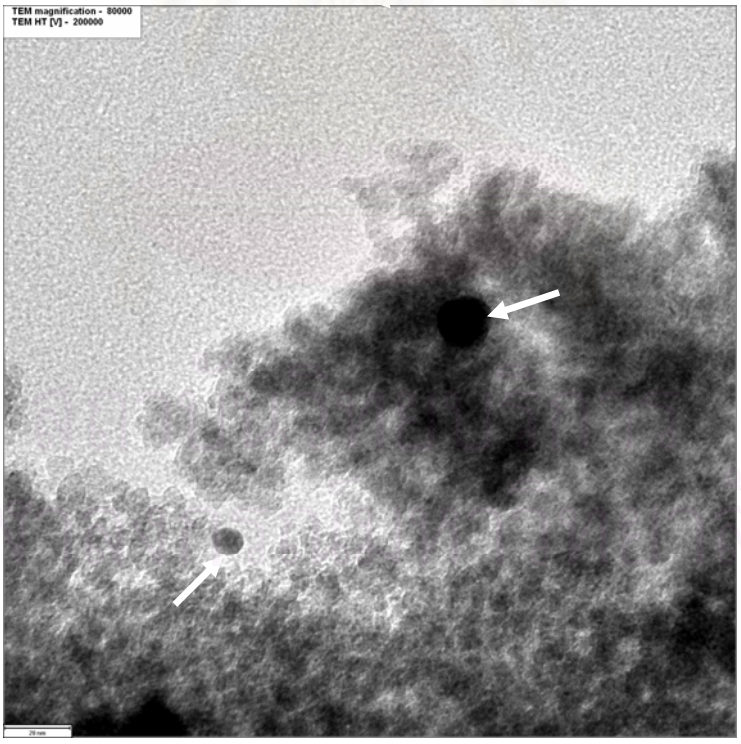

Figure 5.11 TEM image of catalyst prepared via a sol-gel method type I and gold deposition at pH 7. The scale bar is 20 nm. The arrows indicate some gold nanoparticles.

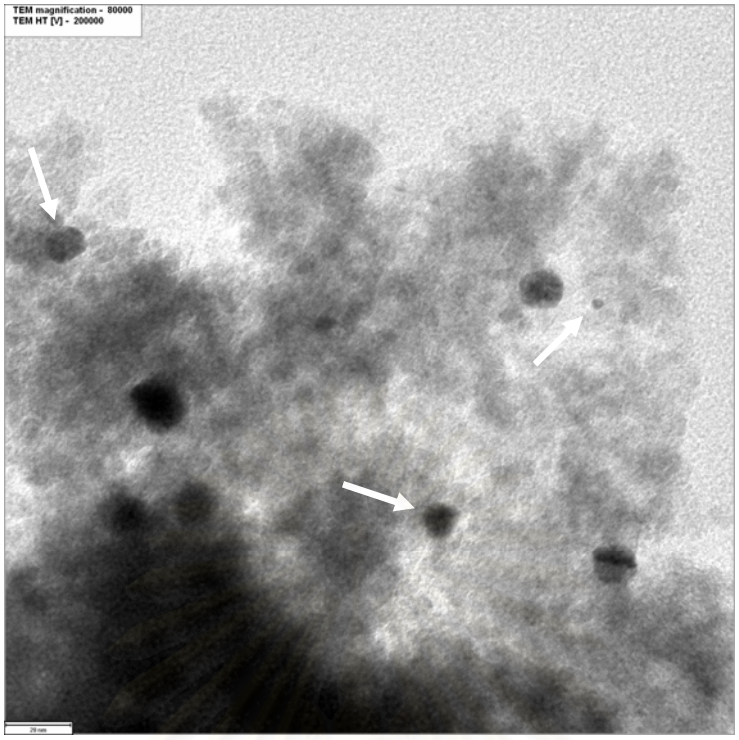

Figure 5.12 TEM image of catalyst prepared via a sol-gel method type I and gold deposition at pH 9. The scale bar is 20 nm. The arrows indicate some gold nanoparticles.

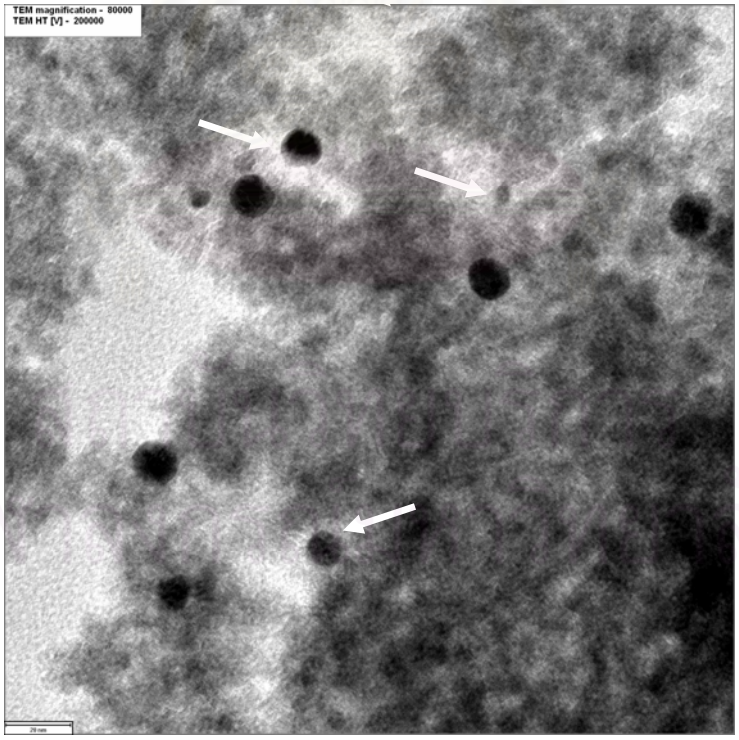

Figure 5.13 TEM image of catalyst prepared via a sol-gel method type I and gold deposition at pH 10. The scale bar is 20 nm. The arrows indicate some gold nanoparticles.

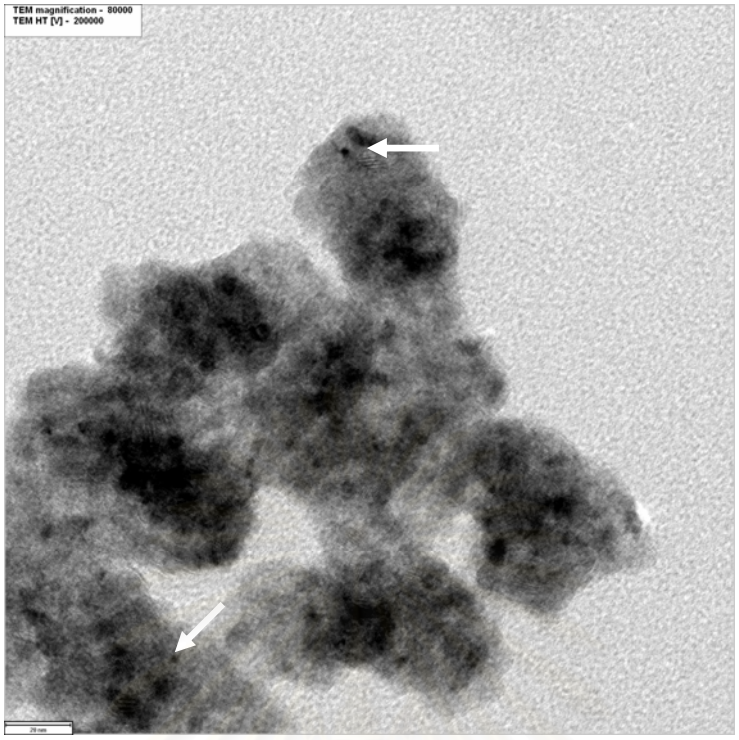

Figure 5.14 TEM image of catalyst prepared via a sol-gel method type II and gold deposition at pH 6. The scale bar is 20 nm. The arrows indicate some gold nanoparticles.

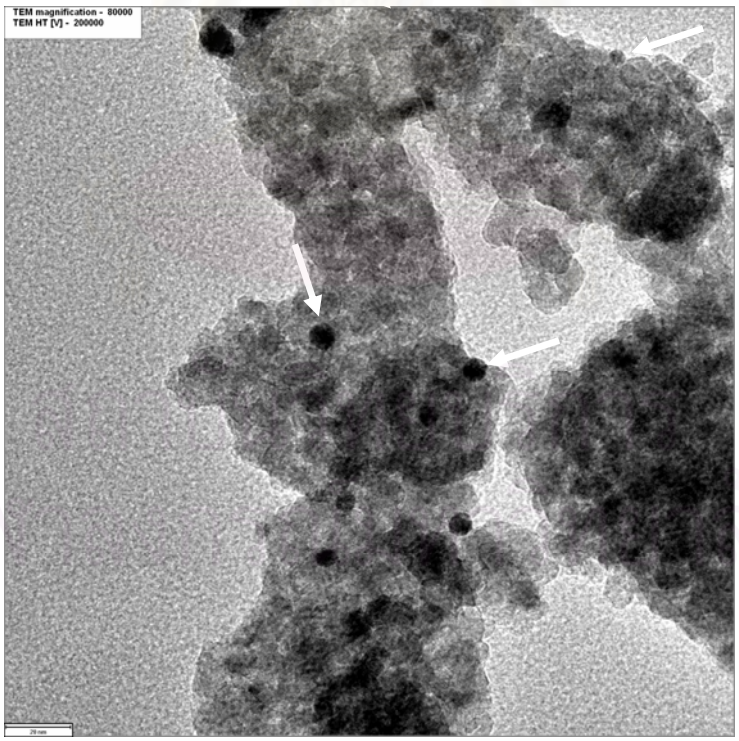

Figure 5.15 TEM image of catalyst prepared via a sol-gel method type II and gold deposition at pH 7. The scale bar is 20 nm. The arrows indicate some gold nanoparticles.

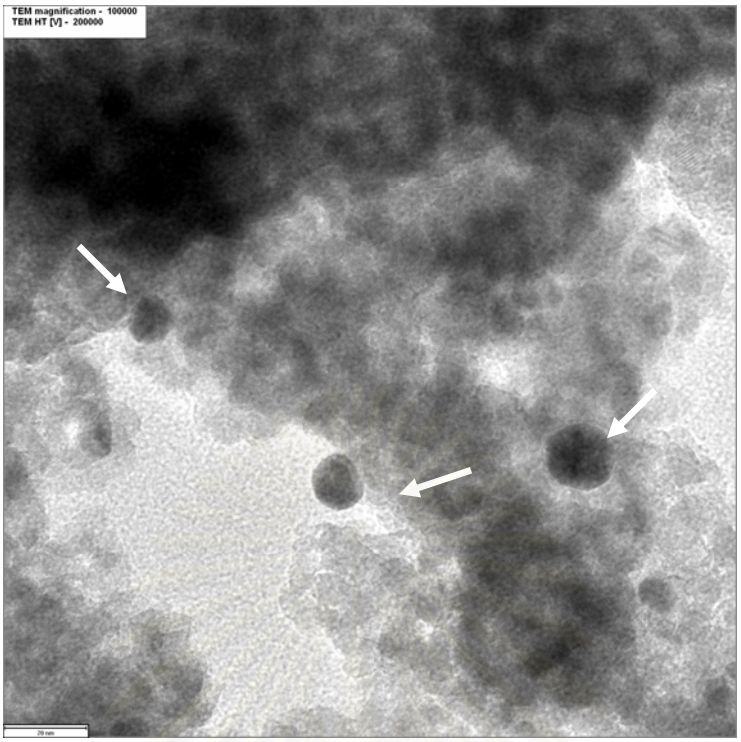

Figure 5.16 TEM image of catalyst prepared via a sol-gel method type II and gold deposition at pH 9. The scale bar is 20 nm. The arrows indicate some gold nanoparticles.

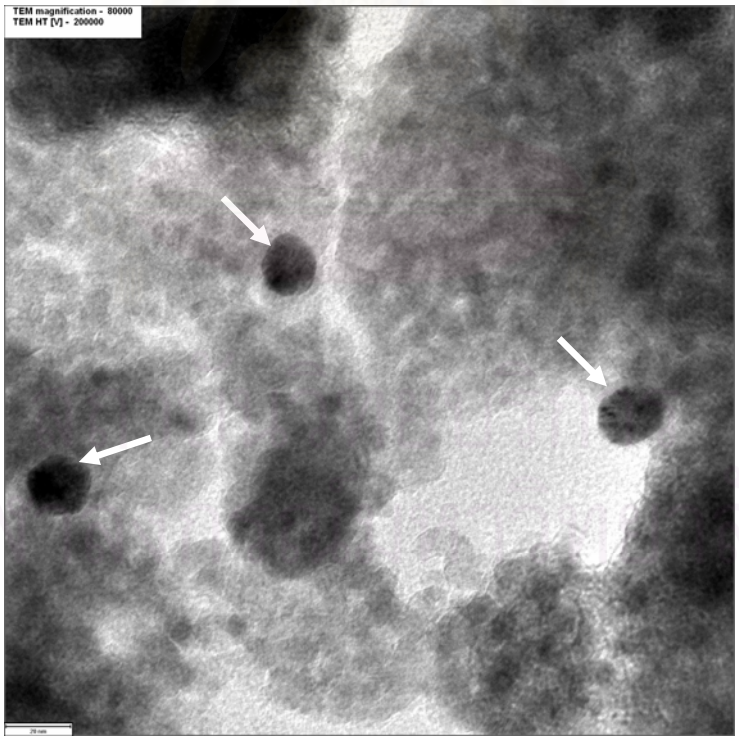

Figure 5.17 TEM image of catalyst prepared via a sol-gel method type II and gold deposition at pH 10. The scale bar is 20 nm. The arrows indicate some gold nanoparticles.

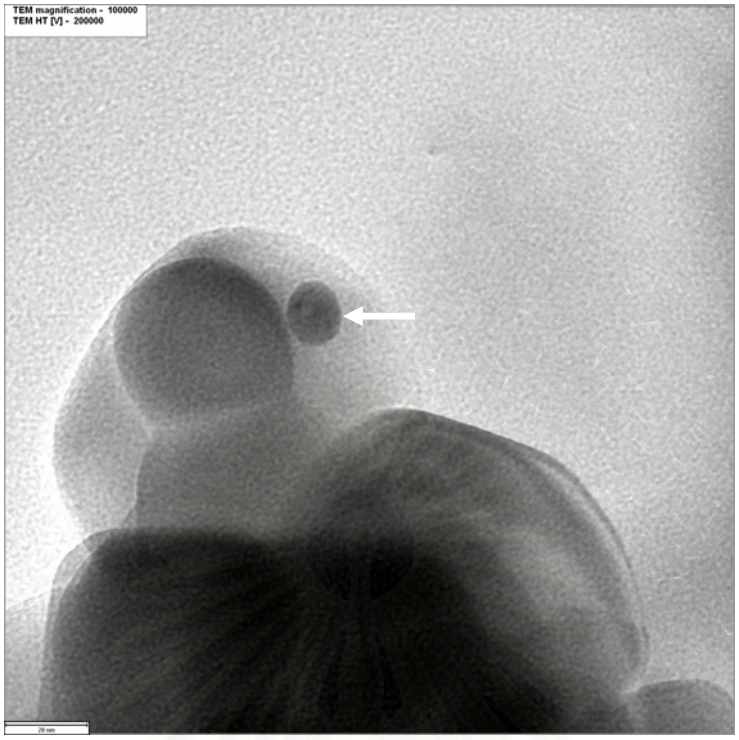

Figure 5.18 TEM image of catalyst prepared from JRC-TIO1 titanium dioxide and gold deposition at pH 6. The scale bar is 20 nm. The arrow indicates a gold nanoparticle.

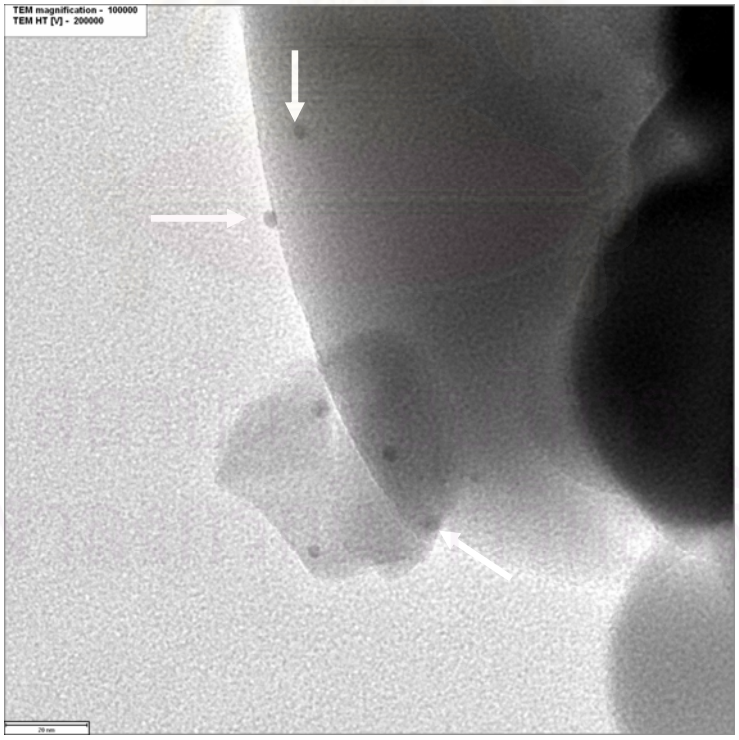

Figure 5.19 TEM image of catalyst prepared from JRC-TIO1 titanium dioxide and gold deposition at pH 7. The scale bar is 20 nm. The arrows indicate some gold nanoparticles.

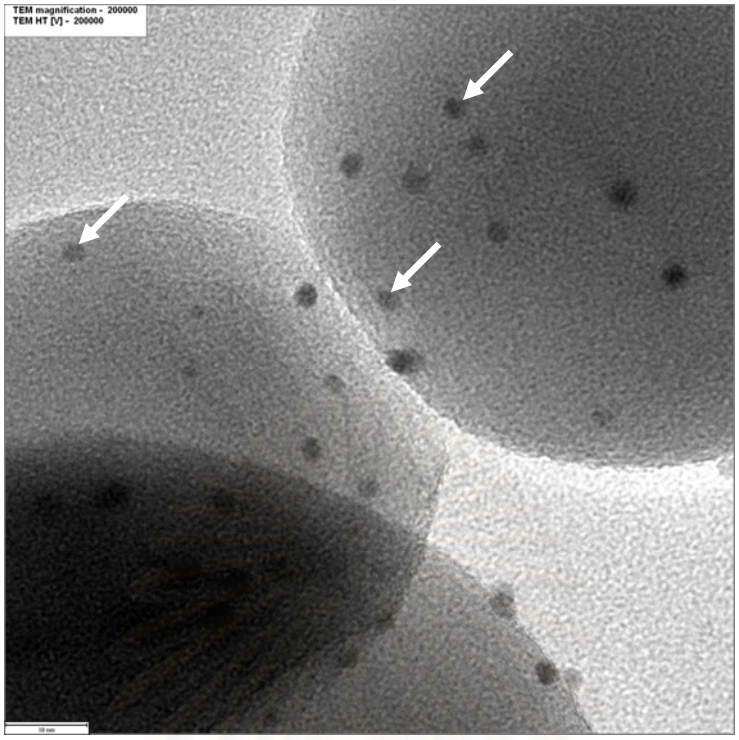

Figure 5.20 TEM image of catalyst prepared from JRC-TIO1 titanium dioxide and gold deposition at pH 9. The scale bar is 10 nm. The arrows indicate some gold nanoparticles.

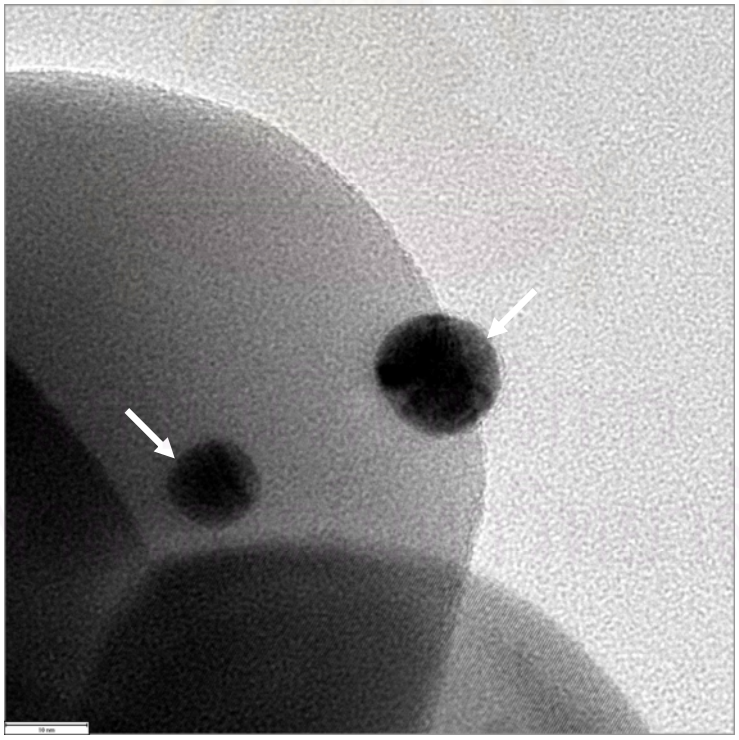

Figure 5.21 TEM image of catalyst prepared from JRC-TIO1 titanium dioxide and gold deposition at pH 10. The scale bar is 10 nm. The arrows indicate some gold nanoparticles.

From TEM images, the average particles sizes of gold nanoparticles were determined from calculating the average of the size of all gold particles present in the images (see Appendix F). The results are shown in Table 5.4.

Table 5.4 The average particle sizes of gold nanoparticles of gold deposited TiO_2 catalysts (nm).

pH	Solvothermal	Sol-gel type I	Sol-gel type II	JRC-TIO1
6	9.8	7.8	5.8	13.1
7	10.3	15.8	10.3	5.8
8	11.6	12.5	13.7	3.3
10	15.1	12.7	21.6	14.6

From Table 5.4, all catalysts except for JRC-TIO1 titanium dioxide with gold deposition at pH 9 have the average particle sizes of gold nanoparticles larger than 5 nm.

5.1.2.2 Specific surface area measurement

The Specific surface areas of all gold deposited catalysts compared with bare catalysts are shown in Table 5.5.

Table 5.5 Specific surface areas of gold deposited TiO2 catalysts compared with bare catalysts (m^2g^{-1}).

Condition	Solvothermal	Sol-gel type I	Sol-gel type II	JRC-TIO1
bare	79.5	130.5	82.0	6.7
pH 6	81.1	139.2	82.8	7.0
pH 7	80.5	135.3	82.9	7.2
pH 9	83.2	137.0	83.3	6.3
pH 10	82.9	139.9	80.6	6.3

From Table 5.5, the specific surface areas of all gold deposited catalysts remained the same as those of bare catalysts. Deposition of gold nanoparticles on the surface of titanium dioxide did not alter the surface area of the catalysts significantly.

5.1.2.3 Ti^{3+} measurement

The amounts of Ti^{3+} of the gold deposited TiO_2 catalysts were measured by Electron spin resonance spectroscopy (ESR). The results compared with bare catalysts are shown in Table 5.6.

Table 5.6 The amount of Ti^{3+} of the gold deposited catalysts compared with bare catalysts (g^{-1})

Condition	Solvothermal	Sol-gel type I	Sol-gel type II	JRC-TIO1
bare	30,021.08	35,346.62	8,066.15	1,833.10
pH 6	3,657.12	2,024.53	3,557.98	1,801.08
pH 7	3,829.14	2,571.98	3,838.13	1,995.56
pH 9	4,354.63	2,661.89	3,635.02	2,467.66
pH 10	3,597.88	3,099.04	3,413.23	2,475.36

From Table 5.6, the amount of Ti^{3+} of titanium dioxide catalysts that were synthesized via solvothermal method, sol-gel method type I and sol-gel method type II decreased with the presence of gold nanoparticles and this decrease did not depend on the pH value. However, the amount of Ti^{3+} of JRC-TIO1 titanium dioxide increased with the presence of gold nanoparticles and the amount of Ti^{3+} increased as pH increased.

The results of ESR measurement are shown in Figures 5.22 to 5.25.

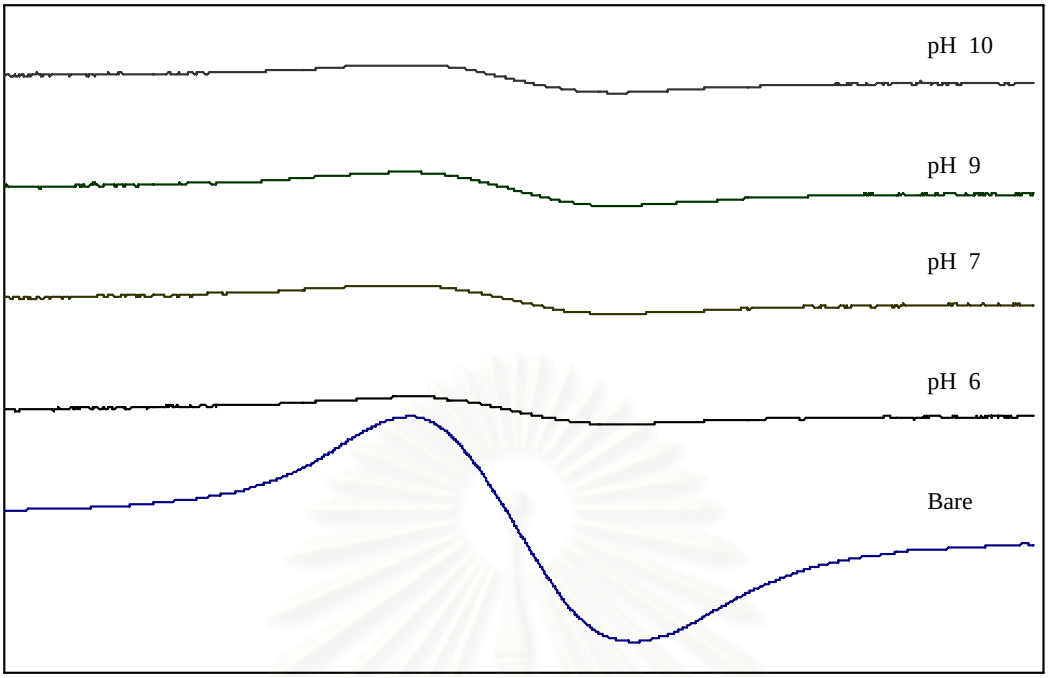

Figure 5.22 ESR results of gold deposited TiO_2 and bare TiO_2, where TiO_2 was prepared via a solvothermal method.

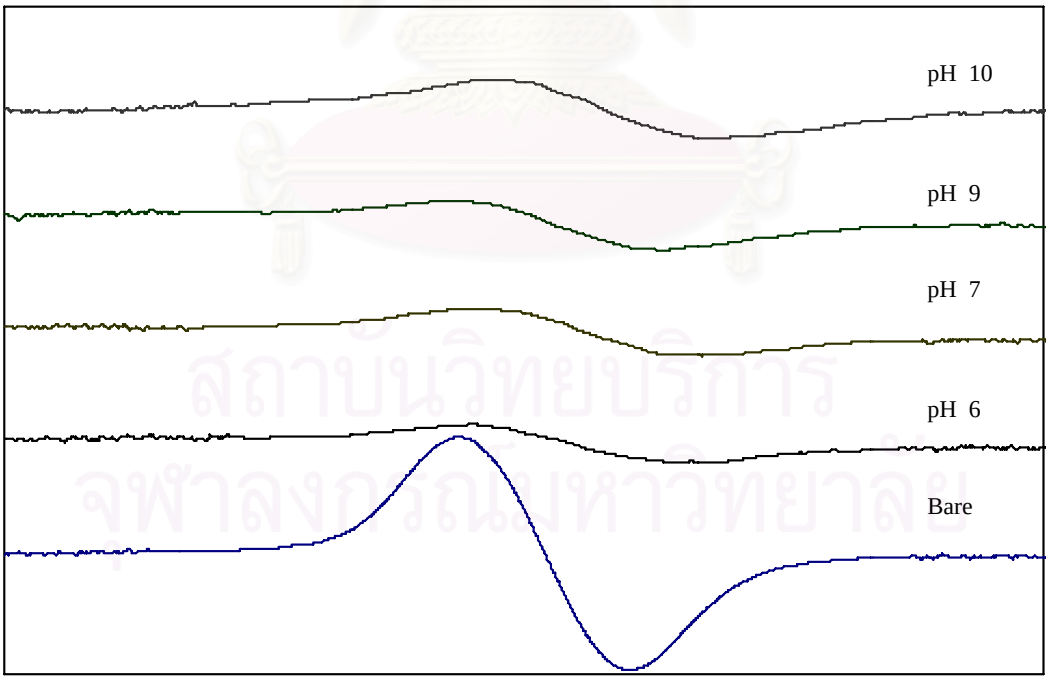

Figure 5.23 ESR results of gold deposited TiO_2 and bare TiO_2, where TiO_2 was prepared via a sol-gel method type I.

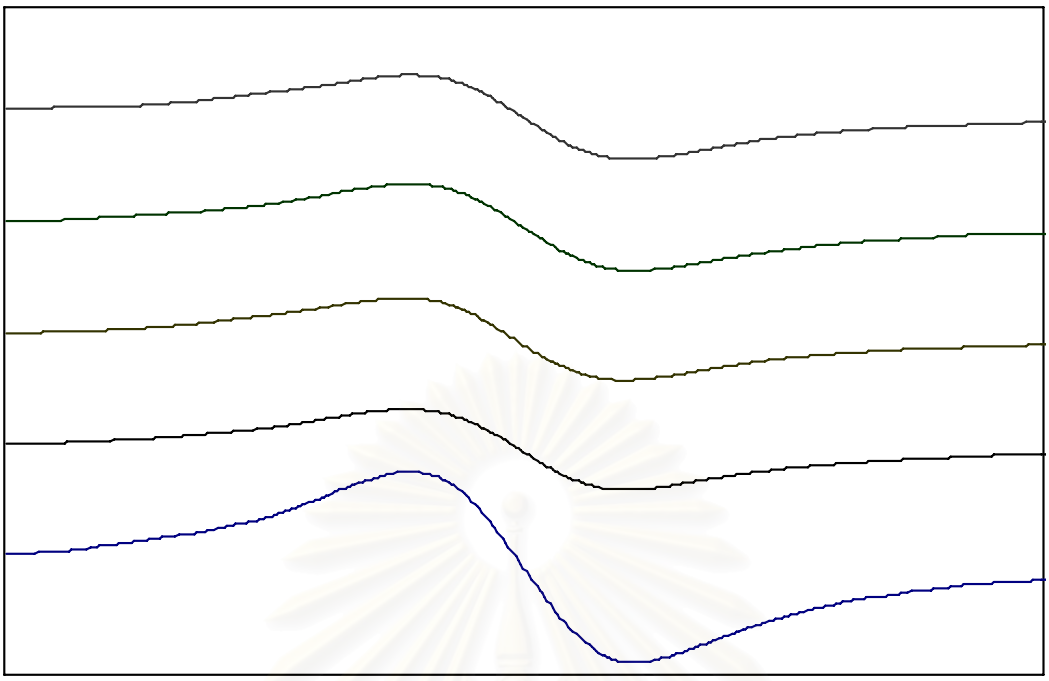

Figure 5.24 ESR results of gold deposited TiO_2 and bare TiO_2, where TiO_2 was prepared via a sol-gel method type II.

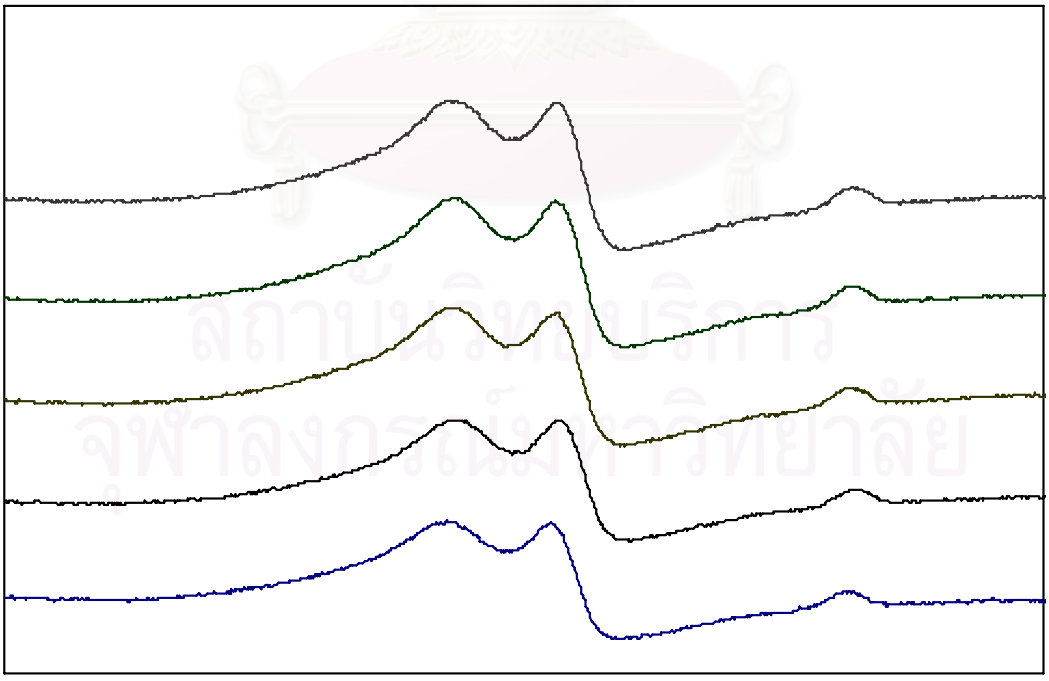

Figure 5.25 ESR results of gold deposited TiO_2 and bare TiO_2, where TiO_2 was JRC-TIO1 catalyst.

5.1.2.4 The amount of gold deposited on titanium dioxide

The amount of gold deposited on the surfaces of titanium dioxides was measured by inductively coupled plasma-atomic emission spectroscopy (ICP- AES) The results are shown in Table 5.7.

Table 5.7 The amount of gold deposited on the surfaces of each catalyst (*10^{-2} mg).

Condition	Solvothermal	Sol-gel type I	Sol-gel type II	JRC-TIO1
pH 6	22.740	19.030	20.310	4.180
pH 7	16.905	14.445	13.720	1.500
pH 9	4.545	7.440	2.935	0.370
pH 10	2.935	4.390	0.475	0.330

From Table 5.7, the gold uptake of TiO_2 that was synthesized via a solvothermal method was the highest and that of JRC-TIO1 was the lowest. For all catalysts, the gold uptakes were highest at a pH value of 6 and decreased as pH rose. This was attributed to a change of the charge on the surface of TiO_2. The surface of TiO_2 became increasingly negative as pH exceeded the isoelectric point (pH ~ 4) and resulted in an electrostatic repulsion of gold-containing anion. The gold-containing anion from the hydrolysis of the $[AuCl_4]^-$ ion in the solution is presented in Equations 5.2 to 5.7 (Nechayev and Zvonareva, 1983).

$$[AuCl_4]^- + H_2O \leftrightarrow AuCl_3(H_2O) + Cl^- \quad (5.2)$$

$$AuCl_3(H_2O) \leftrightarrow [AuCl_3(OH)]^- + H^+ \quad (5.3)$$

$$[AuCl_3(OH)]^- + H_2O \leftrightarrow AuCl_2(H_2O)(OH) + Cl^- \quad (5.4)$$

$$AuCl_2(H_2O)(OH) \leftrightarrow [AuCl_2(OH)_2]^- + H^+ \quad (5.5)$$

$$[AuCl_2(OH)_2]^- + H_2O \leftrightarrow [AuCl(OH)_3]^- + Cl^- + H^+ \quad (5.6)$$

$$[AuCl(OH)_3]^- + H_2O \leftrightarrow [Au(OH)_4]^- + Cl^- + H^+ \quad (5.7)$$

The relative concentrations of these species as a function of pH are shown in Figure 5.26.

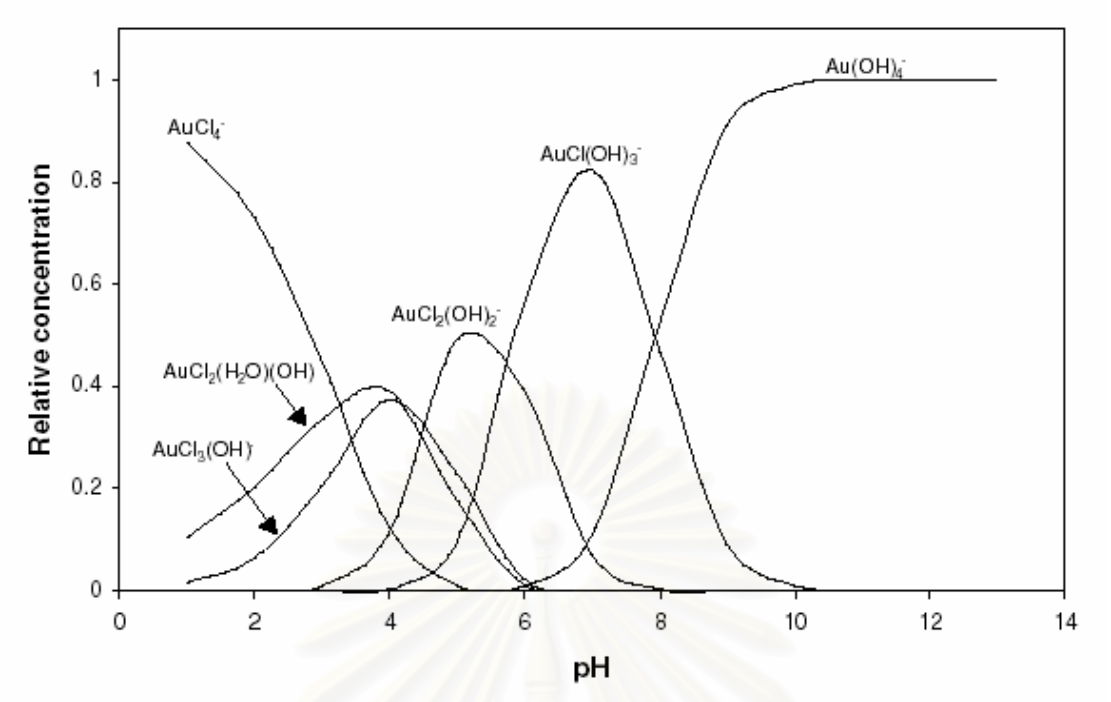

Figure 5.26 Relative equilibrium concentrations of gold complexes as a function of pH (Nechayev and Nikolenko, 1986).

5.2 Photocatalytic activity measurement for the catalysts

The reaction used to test photoactivity of the catalysts was the photooxidation of ethylene. Conversions of ethylene at steady state of all catalysts are shown in Figure 5.27.

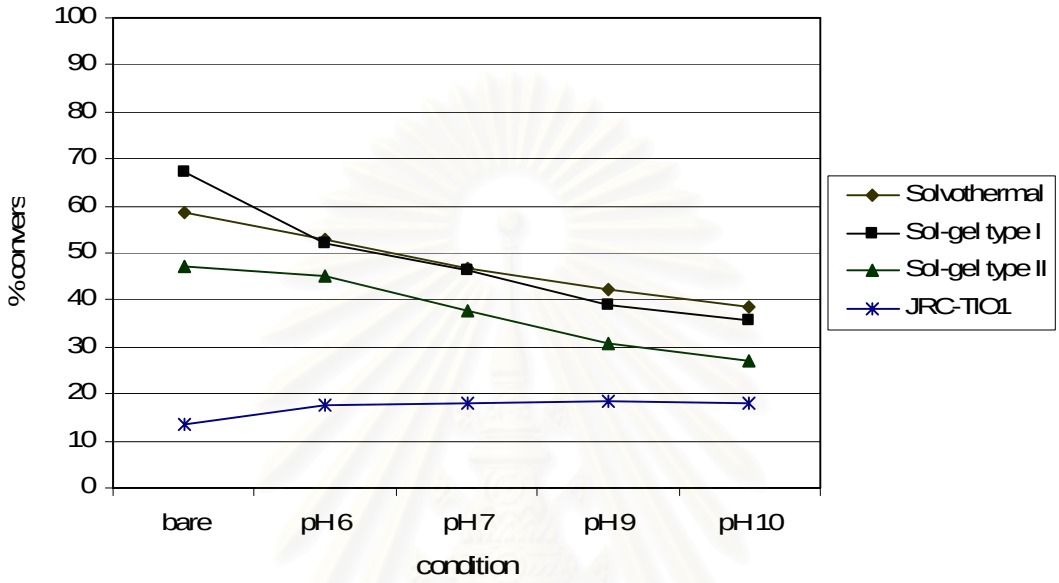

Figure 5.27 Conversions of ethylene at steady state of all catalysts.

5.2.1 Photocatalytic activities of bare TiO_2 catalysts

From Figure 5.27, bare JRC-TIO1 catalyst (JRCB) yielded the lowest conversion of ethylene (13.45%). The catalysts prepared via sol-gel method type II (SG2B) and solvothermal method (STB) yielded conversions of ethylene at 47.25 and 58.49 %, respectively. The catalyst prepared via sol-gel method type I (SG1B) yielded the highest conversion of ethylene at 67.19%. Ethylene conversions of JRCB and SG1B catalysts were results of crystallite sizes and specific surface areas. The JRCB catalyst had the largest crystallite size (109.2 nm) and smallest specific surface area (6.7 m^2g^{-1}) and the SG1B catalyst possessed the smallest crystallite size (4.8 nm) and largest specific surface area (130.5 m^2g^{-1}). However, crystallite size and surface area could not be used to explain ethylene conversion of SG2B and STB catalysts. These two catalysts possessed similar specific surface area (SG2B – 82.0 m^2g^{-1} and STB – 79.5 m^2g^{-1}) but the the SG2B catalyst had smaller crystallite size than that of the STB

catalyst (SG2B – 8.4 nm and STB – 10.9 nm). However, the amount of Ti^{3+} on the surface of the STB catalyst is higher than that of the SG2B catalyst. As a result, the ethylene conversion of the STB catalyst was higher than that of the SG2B catalyst.

5.2.2 Photocatalytic activity of gold deposited TiO_2 catalysts

Titanium dioxide that was synthesized via sol-gel methods type I and II and solvothermal method exhibited lower conversion of ethylene when they were deposited with gold nanoparticles. On the other hand, ethylene conversion for JRC-TIO1 increased when they were deposited with gold nanoparticles.

As seen in Tables 5.3 and 5.5, the crystallite sizes of titanium dioxide and specific surface areas of the catalysts did not change significantly when they were deposited with gold nanoparticles. However, the amount of Ti^{3+} of the first group decreased when they were deposited with gold nanoparticles while that of the second group increased. This could explain the opposite trends in ethylene conversion of the two groups.

The changes in photoactivity of gold deposited TiO_2 catalysts compared to bare TiO_2 catalysts are displayed in Table 5.8.

Table 5.8 The changes in photoactivity (depicted by conversion of ethylene) of gold deposited TiO_2 catalysts compared to bare TiO_2 catalysts.

Condition	ST	Change (%)	SG1	Change (%)	SG2	Change (%)	JRC	Change (%)
bare	58.49	-	67.19	-	47.25	-	13.45	-
pH 6	53.02	-9.35	51.87	-22.80	44.97	-4.83	17.71	+31.67
pH 7	46.82	-19.95	46.32	-31.06	37.82	-19.96	17.89	+33.01
pH 9	42.07	-28.07	39.05	-41.88	30.57	-35.30	18.64	+38.59
pH 10	38.61	-33.99	35.77	-46.76	27.14	-42.56	17.87	+32.86

Where ST = Solvothermal method

SG1 = Sol-gel method type I

SG2 = Sol-gel method type II

JRC = JRC-TIO1

\- = decreasing

\+ = increasing

5.2.3 Effect of pH on photocatalytic activity of gold deposited TiO_2 catalysts

According to section 5.2.2, the catalysts are separated into two groups. The photoactivity of the first group decreased with the presence of gold nanoparticles and the acticity of the second group increased with the presence of gold nanoparticles.

5.2.3.1 Effect of pH on photoactivity of gold deposited TiO_2 catalysts in the first group

The catalysts in the first group consisted of titanium dioxide that was synthesized via a solvothermal method,a sol-gel method type I and a sol-gel method type II. The crystallite sizes of titanium dioxide in this group are small and their photocatalytic activities decreased as the pH used during gold deposition increased. The highest conversion occurred at a pH value of 6 and the lowest occurred at a pH value of 10. ESR results indicated that the presence of gold nanoparticles decreased photoactivities of the catalysts in this group because it decreased the amount of Ti^{3+} on the surface of these catalysts. However, the decrease in the amounts of Ti^{3+} of these catalysts could not explain the gradual decrease in photocatalytic activities of the catalysts that were deposited with gold nanoparticles.

From Table 5.4, the average particle sizes of gold nanoparticles on the surfaces of titanium dioxide at every pH value were larger than 5 nm and therefore were considered to be catalytically inactive. However, the ratios of active gold nanoparticles (smaller than 5 nm) at each pH value were different. For each catalyst, the ratios of active gold nanoparticles are the highest at a pH value of 6 and the lowest at a pH value of 10. Although the amounts of Ti^{3+} were similar for each type of catalyst, the difference in the amount of active gold nanoparticles also affected the photoactivities of the catalysts. Nevertheless, the photoactivities of the gold deposited

TiO2 catalysts were still lower than that of the bare TiO_2 catalysts because inactive gold nanoparticles acted as recombination centers. Furthermore, the ICP-AES results indicated that the percentage of gold deposited on the surfaces of the catalysts decreased with an increase in pH. This also contributed to the decrease in the photoactivity of the catalysts at higher pH.

The ratios of active gold nanoparticles for the catalysts in this group (which were synthesized via a solvothermal method, a sol-gel method type I and a sol-gel method type II) are shown in Table 5.9 and the particle size distributions for the catalysts in this group are displayed in Figures 5.28 to 5.39.

Table 5.9 Percentage of active gold nanoparticles (%) of all gold deposited TiO_2 catalysts at various pH values.

pH	Solvothermal	Sol-gel type I	Sol-gel type II	JRC-TIO1
6	47.1	15.1	43.4	3.6
7	51.3	10.7	14.0	48.1
9	2.7	8.7	2.5	97.0
10	0.0	2.7	0.0	0.0

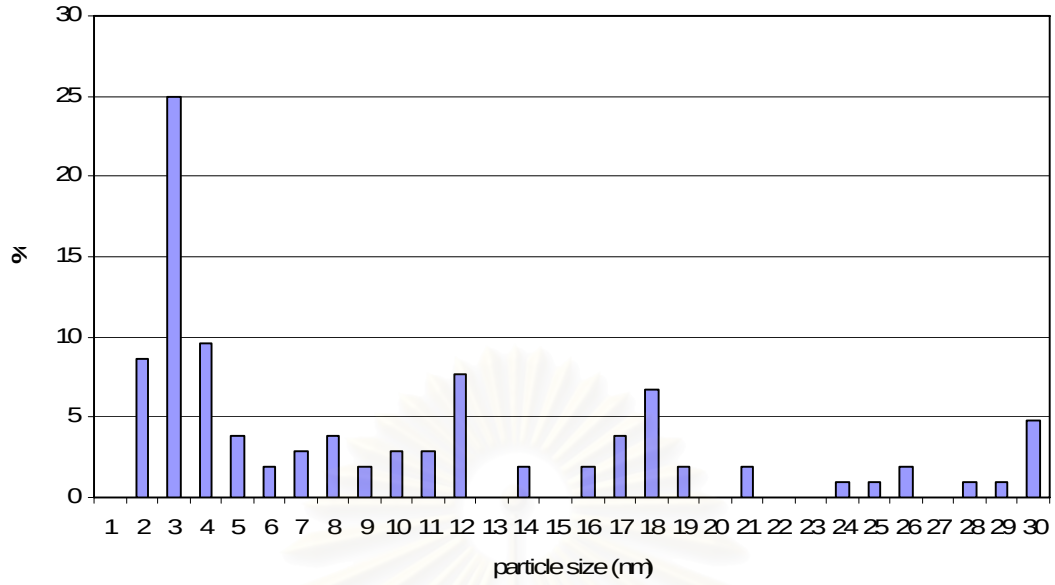

Figure 5.28 Particle size distribution of gold nanoparticles for TiO_2 prepared via a solvothermal method and gold deposition at pH 6.

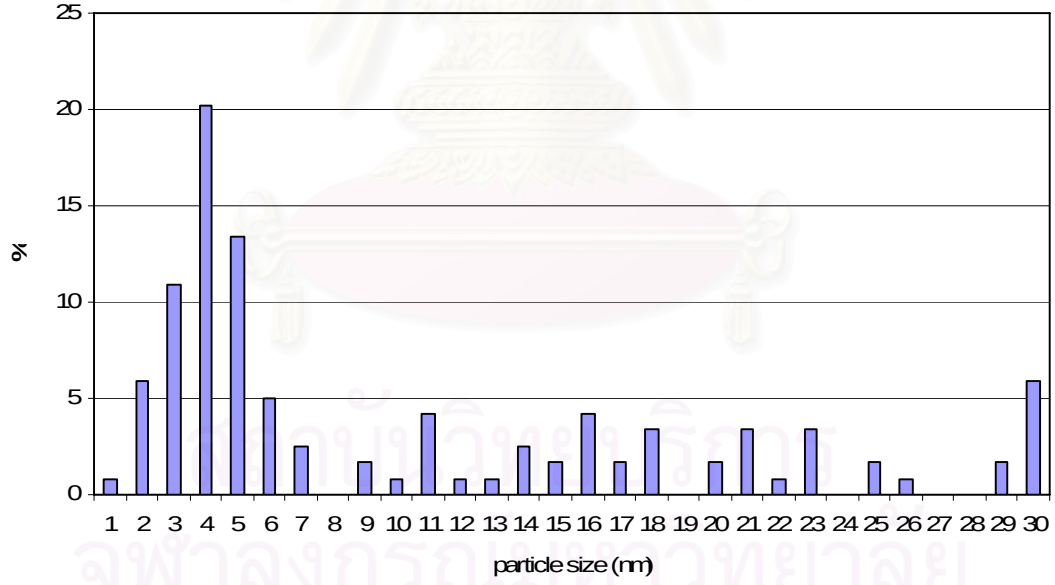

Figure 5.29 Particle size distribution of gold nanoparticles for TiO_2 prepared via a solvothermal method and gold deposition at pH 7.

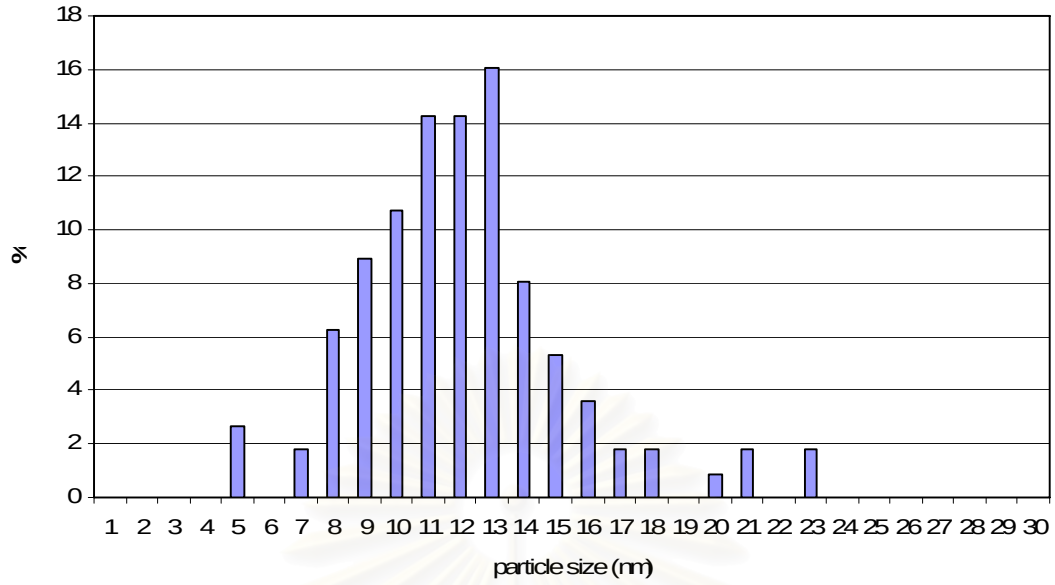

Figure 5.30 Particle size distribution of gold nanoparticles for TiO_2 prepared via a solvothermal method and gold deposition at pH 9.

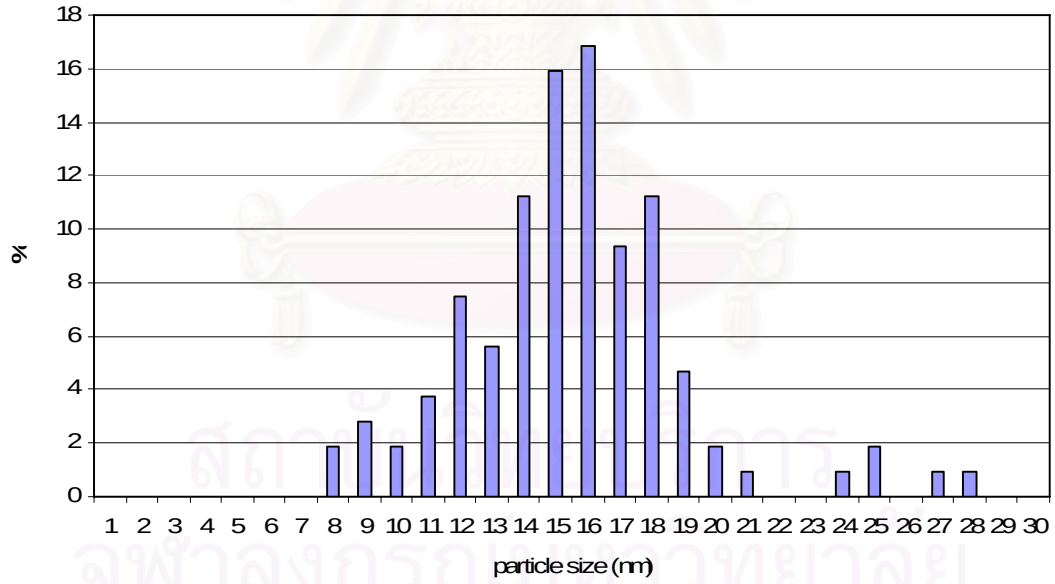

Figure 5.31 Particle size distribution of gold nanoparticles for TiO_2 prepared via a solvothermal method and gold deposition at pH 10.

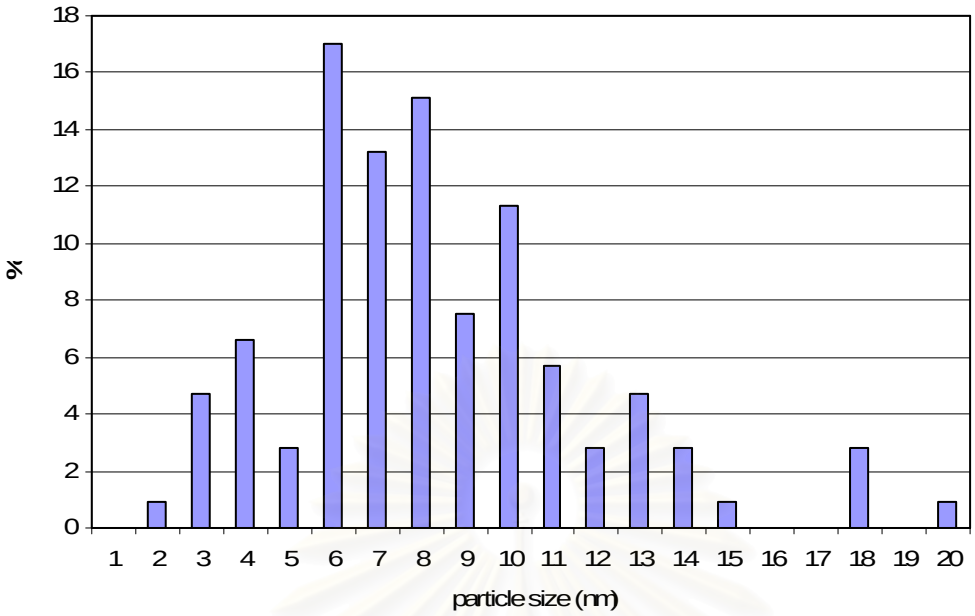

Figure 5.32 Particle size distribution of gold nanoparticles for TiO_2 prepared via a sol-gel method type I and gold deposition at pH 6.

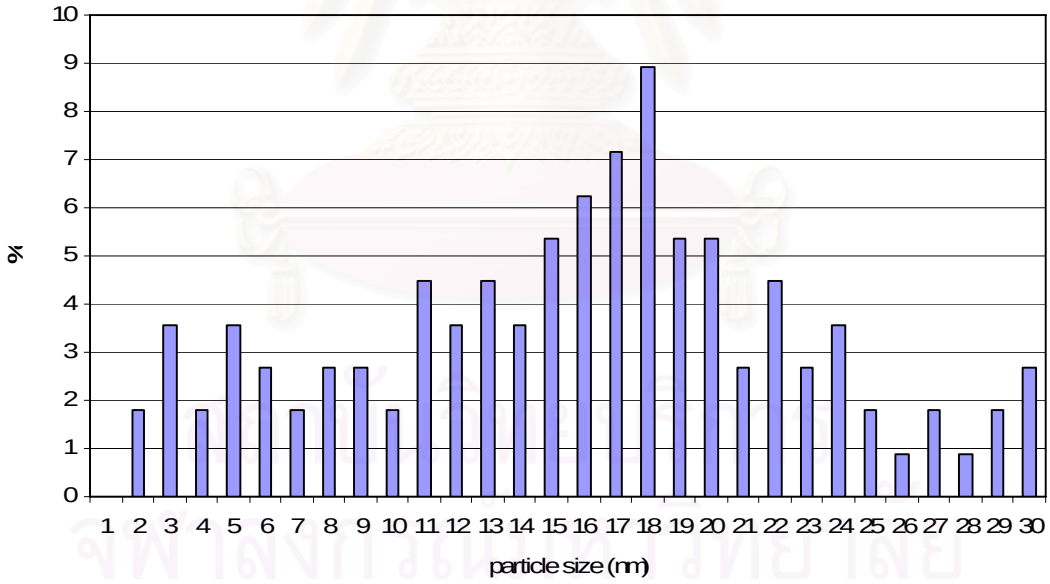

Figure 5.33 Particle size distribution of gold nanoparticles for TiO_2 prepared via a sol-gel method type I and gold deposition at pH 7.

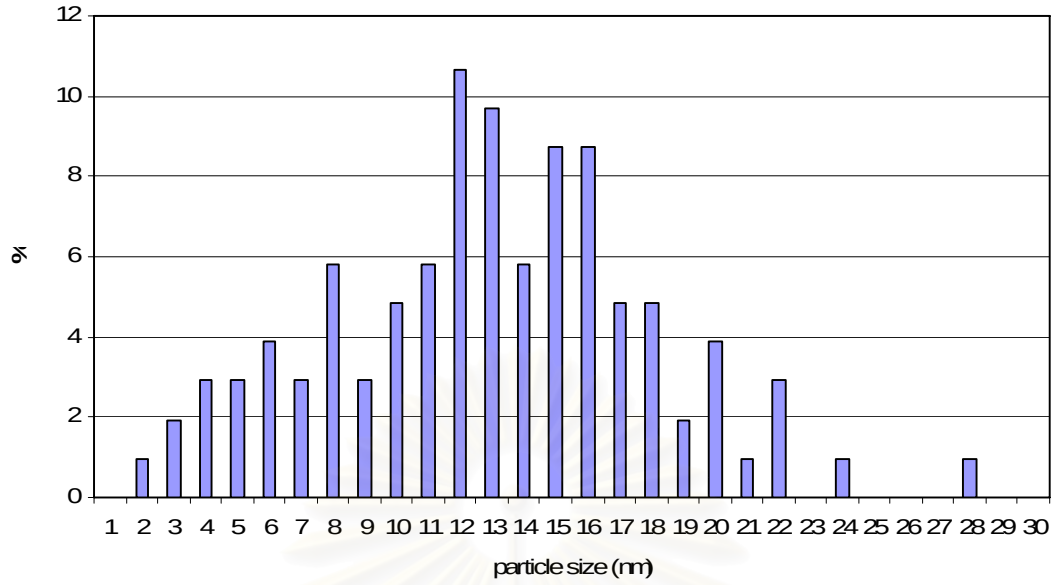

Figure 5.34 Particle size distribution of gold nanoparticles for TiO_2 prepared via a sol-gel method type I and gold deposition at pH 9.

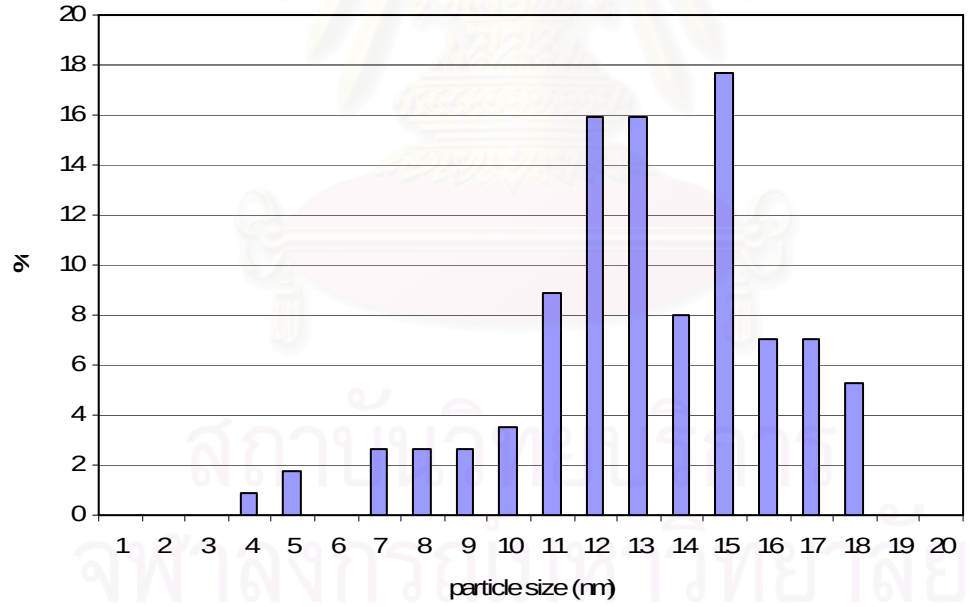

Figure 5.35 Particle size distribution of gold nanoparticles for TiO_2 prepared via a sol-gel method type I and gold deposition at pH 10.

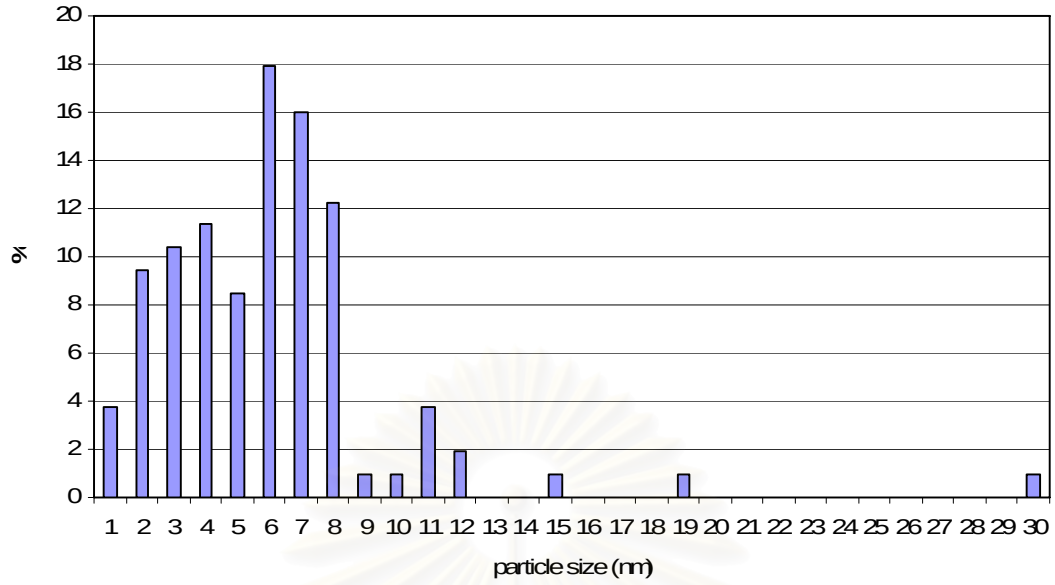

Figure 5.36 Particle size distribution of gold nanoparticles for TiO_2 prepared via a sol-gel method type II and gold deposition at pH 6.

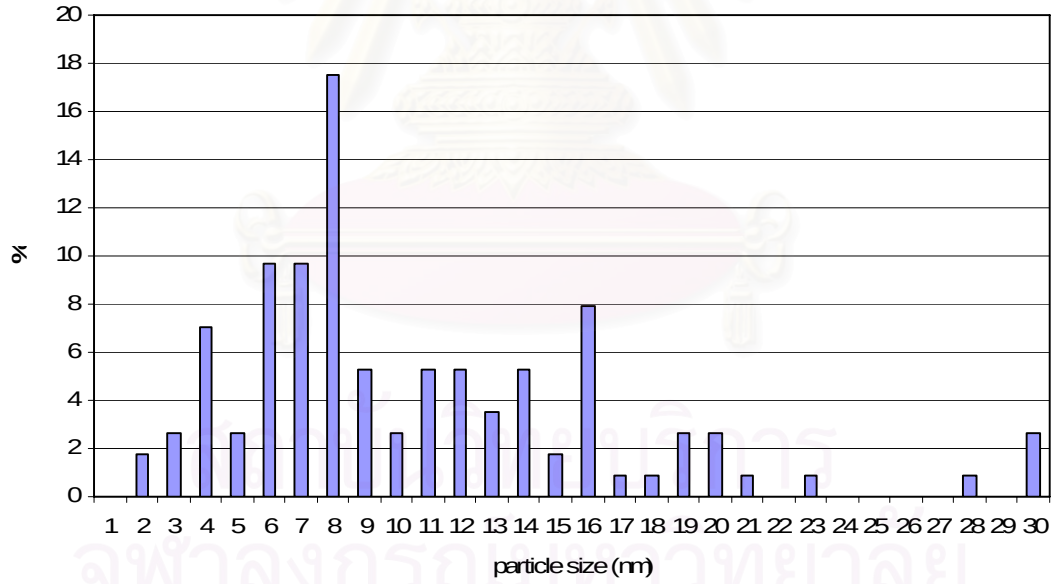

Figure 5.37 Particle size distribution of gold nanoparticles for TiO_2 prepared via a sol-gel method type II and gold deposition at pH 7.

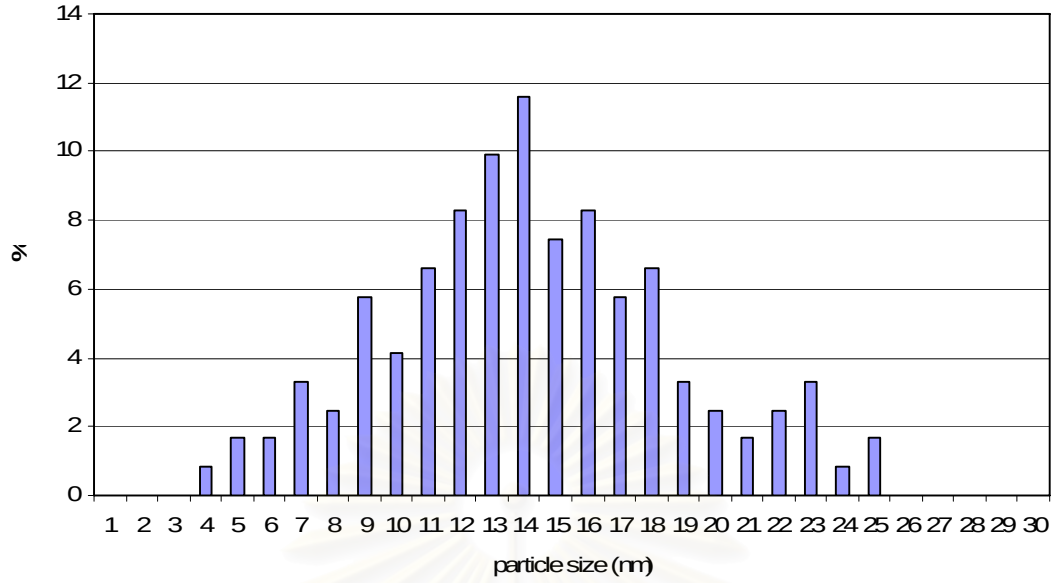

Figure 5.38 Particle size distribution of gold nanoparticles for TiO_2 prepared via a sol-gel method type II and gold deposition at pH 9.

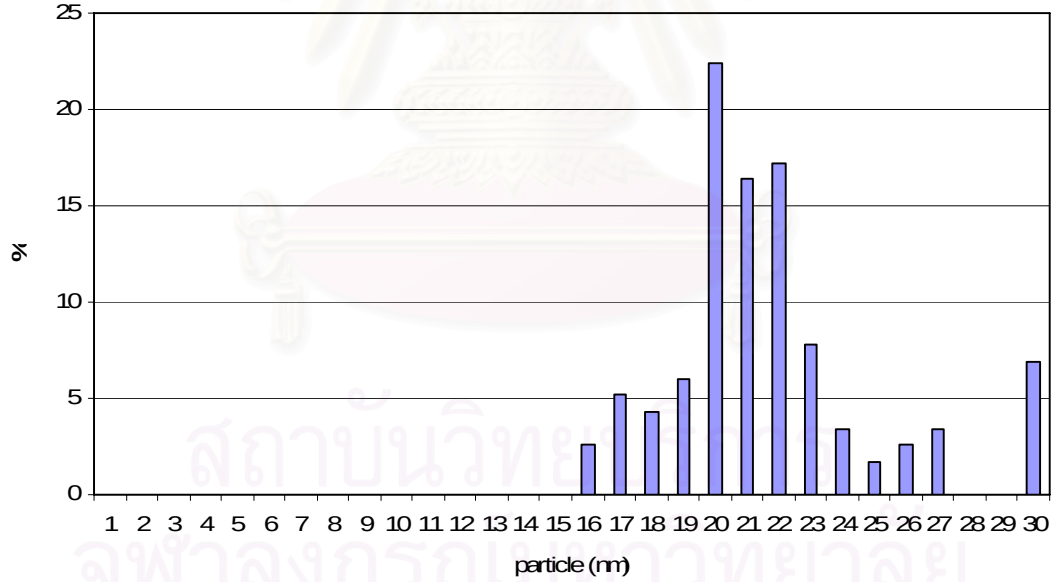

Figure 5.39 Particle size distribution of gold nanoparticles for TiO_2 prepared via a sol-gel method type II and gold deposition at pH 10.

5.2.3.2 Effect of pH on photocatalytic activity of JRC-TIO1 titanium dioxide

The crystallite sizes of JRC-TIO1 titanium dioxide were large and their ethylene conversions increased when they were deposited with gold nanoarticles. The highest conversion occurred at a pH value of 9 and the lowest occurred at a pH value of 6. ESR results indicated that the presence of gold nanoparticles increased photoactivity of the catalysts because it increased the amount of Ti^{3+} on the surface of these catalysts. From Table 5.6, the amount of Ti^{3+} of the catalysts could explain a trend from the bare one to those that were deposited with gold nanoparticles. The amount of Ti^{3+} increased from the catalyst which was deposited with gold at a pH value of 6 to the highest at a pH value of 10. The amount of Ti^{3+} of catalysts which were deposited with gold at a pH value of 9 and 10 were similar.

From Table 5.4, the average particle size of gold nanoparticles deposited at a pH value of 9 was smaller than 5 nm. This could be attributed to be catalytically active and made this catalyst to have the highest conversion of ethylene. At other pH values, the average particle size of gold nanoparticles was larger than 5 nm. This could be attributed to be catalytically inactive.

The ratios of active gold nanoparticles for the catalysts in this group is shown in Table 5.8 and the particle size distributions of gold nanoparticles for the catalysts in this group are displayed in Figures 5.40 to 5.43.

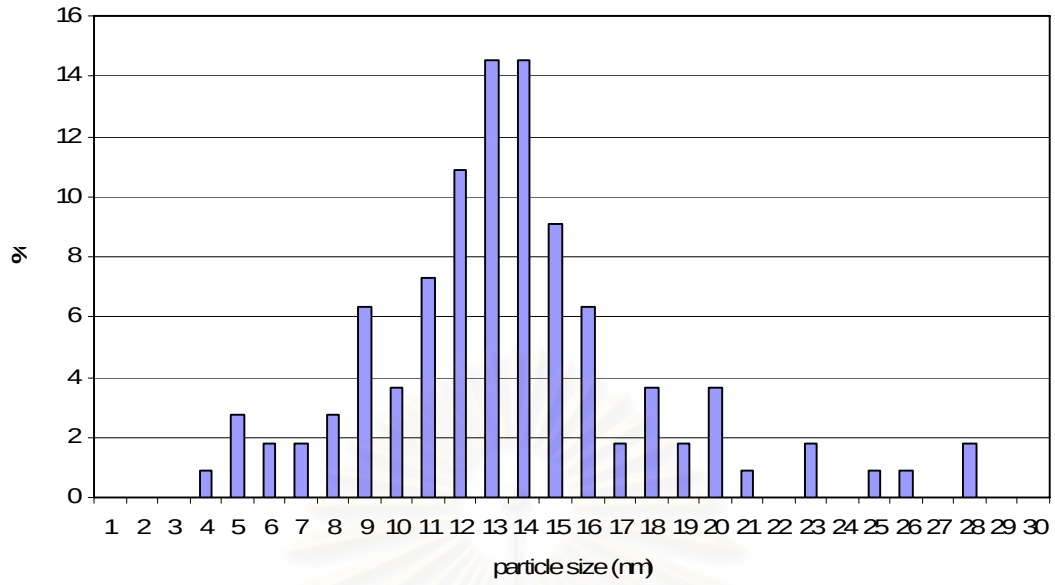

Figure 5.40 Particle size distribution of gold nanoparticles for TiO_2 prepared from JRC-TIO1 titanium dioxide and gold deposition at pH 6.

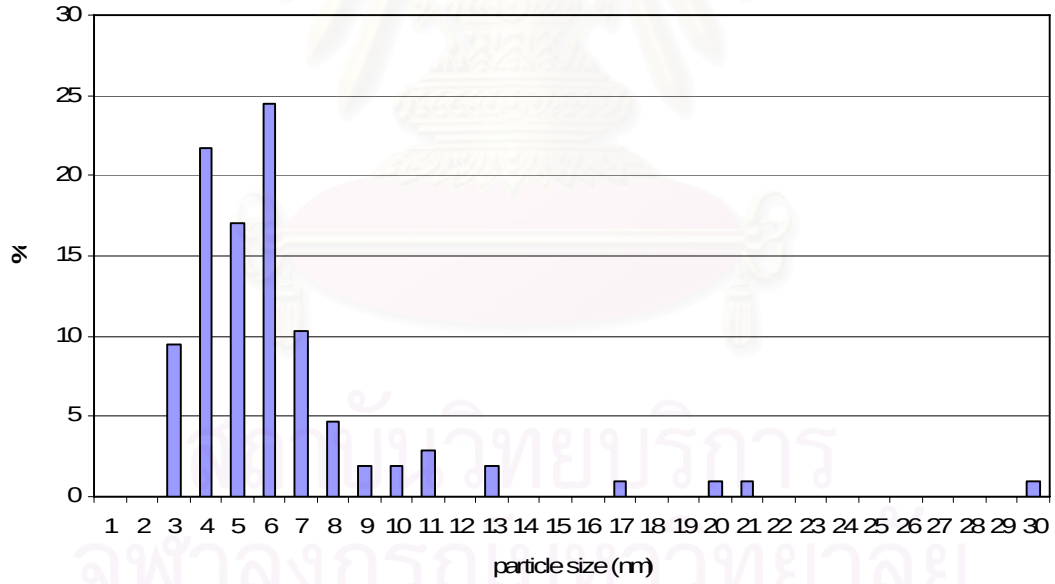

Figure 5.41 Particle size distribution of gold nanoparticles for TiO_2 prepared from JRC-TIO1 titanium dioxide and gold deposition at pH 7.

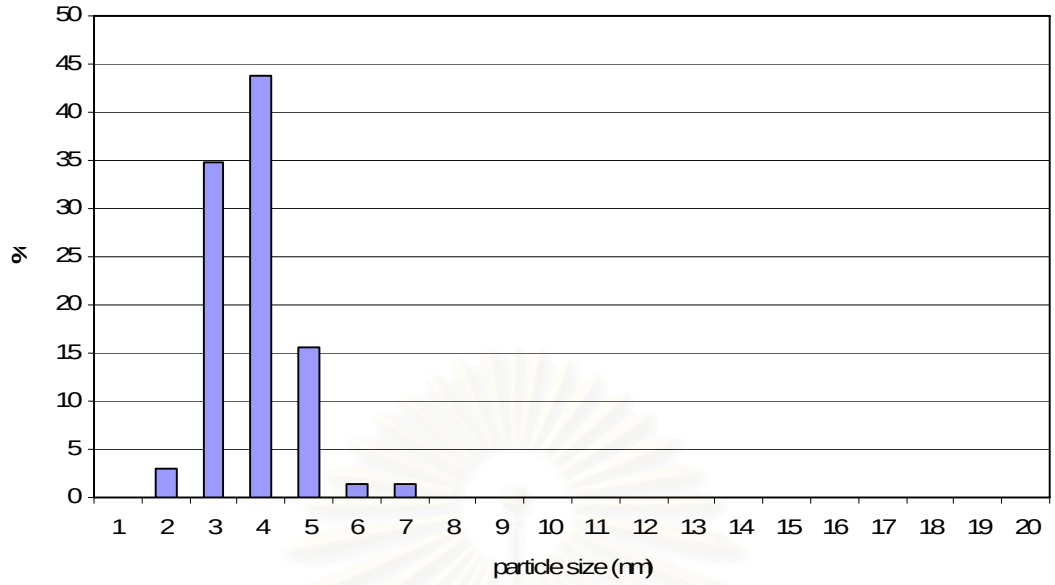

Figure 5.42 Particle size distribution of gold nanoparticles for TiO_2 prepared from JRC-TIO1 titanium dioxide and gold deposition at pH 9.

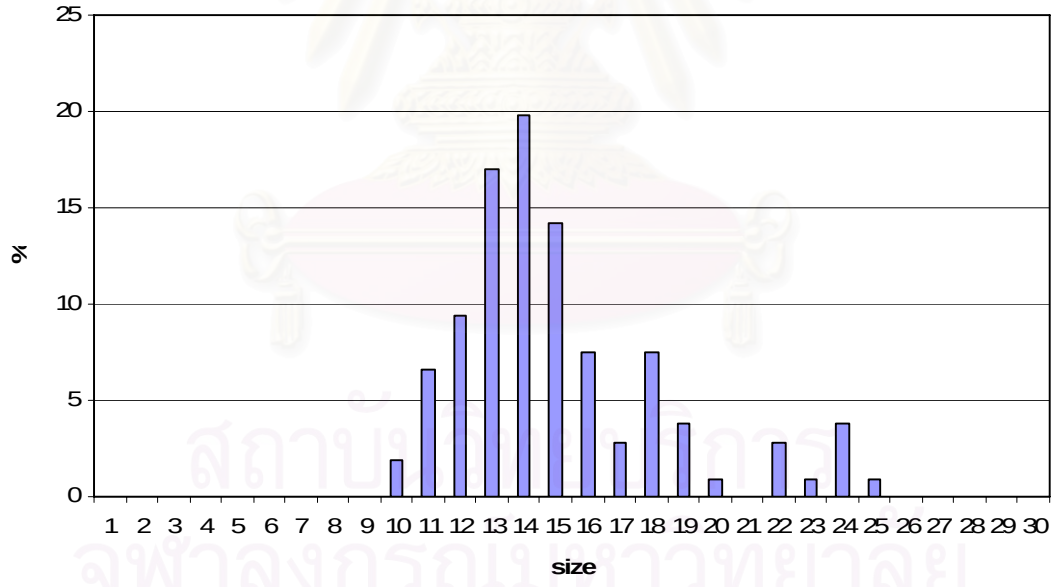

Figure 5.43 Particle size distribution of gold nanoparticles for TiO_2 prepared from JRC-TIO1 titanium dioxide and gold deposition at pH 10.

When compared between the first group and the second group, the photoactivity of the first group was higher than that of the second group at all pH values. Although the photoactivity of the first group decreased with the increase of pH

while that of the second group increased, the photoactivity of it was still higher. This was from the amount of gold deposited on the surface of it. Although the percentage of active gold nanoparticles on the surface of the second group was higher, the amount of gold deposited on the surface of it was lower. Therefore, the photoactivity of the second group was lower.

CHAPTER VI

CONCLUSIONS AND RECOMMENDATION

6.1 Conclusions

The conclusions of this research are the following:

1. Gold nanoparticles have the positive effect on photoactivity of the titanium dioxide which has large crystalline size and has the negative effect on those which have small crystalline size. This is because the presence of gold nanoparticles increases the amount of Ti^{3+} of titanium dioxide which has large crystalline size but it is opposite with that which has small crystalline size.
2. For small-crystalline-size titanium dioxide which is deposited with gold nanoparticles, when the pH increases, the photoactivity decreases. This is affected from the amount of deposited and active gold nanoparticles on the surface of titanium dioxide that decreases with increasing of the pH.
3. For large-crystalline-size titanium dioxide which is deposited with gold nanoparticles, the highest photoactivity occurs at the pH value of 9 according to the increasing of the amount of Ti^{3+} and the most number of active gold nanoparticles formed at this condition.
4. Gold nanoparticles tend be smaller at low pH (pH 6) for small-crystalline-size titanium dioxide and tend to be smaller at higher pH (pH 7 and 9) for large-crystalline-size titanium dioxide.

6.2 Recommendation for the future studies

From the previous conclusions, the following recommendations for the future studies are proposed.

1. Study of the effect of amount of gold doped on titanium dioxide at various pH values and crystalline sizes.

2. Study of the effect of pH used during the preparation in the acidic range (less than 6).

REFERENCES

Alberici, R.M., and Jardim, W.F. Applied Catalysis B: Environmental 14 (1997): 55-68.

Arabatzis, I.M.; Stergiopoulos, T.; Andreeva, D.; Kitova, S.; Neophytides, S.G. and Falaras, P. J. Catal. 220 (2003): 127-135.

Augugliaro, V.; Coluccia, S.; Loddo, V.; Marchese, L.; Martra, G.; Palmisano, L. And Schiavello, M. Applied Catalysis B: Environmental 20 (1999): 15-27.

Balasubramanian, G.; Dionysios, D.D.; Suidan, M.T. Baudin, I. and Laine, J.-M. Applied Catalysis B: Environmental 47 (2004): 73-84.

Bibby, D.M., and Dale, M.P. Nature (London) 317 (1985): 157-158.

Bond, G.C., and Thompson, D.T. Catal. Rev.-Sci. Eng. 41 (1999): 319-388.

Calza, P.; Minero, C., and Pelizzetti, E. Environ. Sci. Techol. 31 (1997): 2198-2203.

Dagan, G., and Tomkiewicz, M. J. Non-Cryst. Solids 175, 2-3 (1994): 294-302.

Debeila, M.A.; Raphulu, M.C.; Mokoena, E.; Avalos, M.; Petranovskii, V.; Coville, N.J., and Scurrell, M.S. Material Science and Engineering A 396 (2005): 61-69.

Demicheli, M.C.; Hoang, L.C.; Ménézo, J.C.; Barbier, J. and Pinabiau-Carlier, M. Appl. Catal. A 97 (1993): 11-17.

Diebold, U. Surface Science Reports 48 (2003): 53-229.

Dutta, P.K.; Ginwalla, A.; Hogg, B.; Patton, B.R.; Chwieroth, B.; Liang, Z.; Gouma, P.; Mills, M. and Akbar, S. J. Phys. Chem. B.103 (1999): 4412-4422.

Farkas, G.; Chin, S.L.; Galarneau, P. and Yergeau, F. Optics Communications 48 (1983): 275-278.

Fox, M.A., and Dulay, M.T. Chem. Rev. 93 (1993): 341-357.

Fu, X., Clark, L., Zeltner, W., and Anderson , A. J. Photochem. Photobiol. A: Chem. 97 (1996): 181-186.

Fujishima, A.; Hashimoto, K., and Watanabe, T. TiO_2 Photocatalysis Fundamental and Applications. 1st ed. Tokyo: BKC, 1999.

Gąsior, M.; Grzybowska, B.; Samson, K.; Ruszel, M. and Haber, J. Catal. Today 91-92 (2004): 131-135.

Haruta, M.; Yamada, N.; Kobayashi, T., and Ijima, S. J. Catal. 115 (1989): 301-309.

Haruta, M. Catal. Today 36 (1997): 153-166.

Hayashi, T.; Tanaka, K., and Haruta, M. J. Catal. 178 (1998): 566-575.

Hoffmann, M.R.; Martin, S.T.; Choi, W., and Bahnemann, D.W. Chem. Rev. 95 (1995): 69-96.

Howe, R.F., and Gratzel, M. J. Phys. Chem. 89 (1985): 4495.

Howe, R.F., and Gratzel, M. J. Phys. Chem. 91 (1987): 3906.

Inoue, M.; Otsu, H.; Kominami, H., and Inui, T. J. Am.Ceram. Soc. 74 (1991): 1452-1454.

Inoue, M.; Kominami, H., and Inui, T. J. Am. Ceram. Soc. 79, 9 (1992): 2597-2598.

Iwamoto, S.; Saito, K.; Inoue, M., and Kagawa, K. Nano. Lett. 1, 8 (2001): 417-421.

Jung, K.; Park, S., and Anpo, M. J. Photochem. Photobiol.A: Chem. 170 (2004): 247-252.

Kamat, P.V. Chem. Rev. 93 (1993): 267-300.

Kang, M.; Lee, S.Y.; Chung, C.H.; Cho, S.M.; Han, G.Y.; Kim, B.W., and Yoon, K.J. J. Photochem. Photobiol. A: Chem. 144 (2001): 185-191.

Kang, Y.M. and Wan, B.Z. Catal. Today 35 (1997): 379-392.

Kim, C.-S.; Moon, B.K.; Park, J.-H.; Choi, B.-C., and Seo, H.-J. J. Cryst. Growth 257 (2003): 309-315.

Kolenko, Y.V.; Churagulov, B.R.; Kunst, M.; Mazerolles, L. and Colbeau-Justin, C. Applied Catalysis B: Environmental 54 (2004): 51-58.

Kominami, H.; Kato, J.; Takada, Y.; Doushi, Y., and Ohtani, B. Catal. Lett. 46 (1997): 235-240.

Kominami, H.; Kohno, M.; Takada, Y.; Inoue, M., and Inui, T. Ind. Eng. Chem. Res. 38 (1999): 3925-3931.

Kontos, A.I.; Arabatzis, I.M.; Tsoukleris, D.S.; Kontos, A.G.; Bernard, M.C.; Petrakis, D.E., and Falaras, P. Catal. Today 101 (2005): 275-281.

Li, F.B., and Li, X.Z. Appl. Catal. A: General 228 (2002): 15-27.

Linsebigler, A.L.; Lu, G., and Yates, Jr. J. T. Chem. Rev. 95 (1995): 735-758.

Litter, M.L. Applied Catalysis B:Environmental, 23 (1999): 89-114.

Mills, A., and Wang, J. J. Photochem. Photobiol. A: Chem. 118 (1997): 53.

Montoya, I.A.; Viveros, T.; Dominguez, J.M.; Canales, L.A., and Schifer, I. Catal. Lett. 15 (1992): 207-217.

Nakano, K.; Obuchi, E.; Takagi, S.; Yamamoto, R.; Tanizaki, T.; Taketomi, M.; Eguchi, M.; Ichida, K.; Suzuki, M. and Hashimoto, A. Separation and Purification technology 34 (2004): 67-72.

Nakaoka, Y., and Nosaka, Y. J. Photochem. Photobiol. A: Chem. 110 (1997): 299-305.

Nam, W., and Han, G. Korea J. chem. Eng. 20 (2003): 1149-1153.

Nechayev, Y.A. and Nikolenko, N.V. Geochem. Intl. 23 (1986): 32.

Nechayev, Y.A. and Zvonareva, G.V. Geokhimiya 6 (1983): 919 [In Russian].

Nkosi, B.; Adams, M.D.; Coville, N.J. and Hutchings, G.J. J. Catal. 128 (1991): 378-386.

Othmer, K. Encyclopedia of chemical technology. Vol.6. 4 th ed. New York: A Wiley-Interscience Publication, John Wiley&Son, 1991.

Sakthivel, S.; Shankar, M.V.; Palanichamy, M.; Arabindoo, B; Bahnemann, D.W., and Murugesan, V. Water Research 38 (2004): 3001-3008.

Sakurai, H., and Haruta, M. Appl. Catal. A 127 (1995): 93.

Sakurai, H., and Haruta, M. Catal. Today. 29 (1996): 361-365.

Sonawane, R.S.; Hedge, S.G., and Dongare, M.K. Mater. Chem. Phys. 77 (2002): 744-750.

Sopyan, I.; Watanabe, M.; Murasawa, S.; Hashimoto, K. and Fujishima, A. J. Photochem. Photobiol.A: Chem. 98 (1996): 79-86.

Sornnarong Thienkaew. Synthesis of large-Surface Area Silica Modified Titanium (IV) Oxide Ultra Fine Particles. Master's thesis, Department of Chemical Engineering, Graduated School, Chulalongkorn University, 2000.

Su, C.; Hong, B.Y., and Tseng, C.M. Catal. Today 96 (2004): 119-126.

Torimoto, T.; Fox III, R.J., and Fox, M.A. J. Electrochem. Soc. 143 (1996): 3712-3717.

Ueda, A.; Oshima, T., and Haruta, M. Appl. Catal. B. 12 (1997): 81-93.

Ueda, M., and Haruta, M. Appl. Catal. B. 18 (1998): 115-121.

Wang, C.; Deng, Z.-X.; Zhang, G.; Fan, S., and Li, Y. Powder Technology 125 (2002): 39-44.

Xu, Y.; Yao, K.; Zhou, X., and Cao, Q. Sens. Actuators B 13-14 (1993): 492-494.

Yanagisawa, K.; Ioku, K., and Yamasaki, N. J. Am. Ceram. Soc. 8,5 (1997): 1303-1306.

Zaharescu, M.; Crisan, M.; Simionescu, L.; Crisan, D., and Gartner, M. J. Sol-Gel Sci. 8, 1-3 (1997):249-253.

APPENDICES

APPENDIX A

CALCULATION OF THE CRYSTALLITE SIZE

Calculation of the crystallite size by Debye-Scherrer equation

The crystallite size was calculated from the width at half-height of the diffraction peak of XRD pattern using the Debye-Scherrer equation.

From Scherrer equation:

$$D = \frac{K\lambda}{\beta \cos \theta} \qquad \text{(A.1)}$$

where D = Crystallite size, Å

K = Crystallite-shape factor = 0.9

λ = X-ray wavelength, 1.5418 Å for CuKα

θ = Observed peak angle, degree

β = X-ray diffraction broadening, radian

The X-ray diffraction broadening (β) is the pure width of a powder diffraction, free of all broadening due to the experimental equipment. Standard α-alumina is used to observe the instrumental broadening since its crystallite size is larger than 2000 Å. The X-ray diffraction broadening (β) can be obtained by using Warren's formula.

From Warren's formula:

$$\beta^2 = B_M^2 - B_S^2 \qquad \text{(A.2)}$$

$$\beta = \sqrt{B_M^2 - B_S^2}$$

Where B_M = The measured peak width in radians at half peak height.

B_S = The corresponding width of a standard material.

Example: Calculation of the crystallite size of titania

The half-height width of 101 diffraction peak = 0.93125^{o}

= 0.01625 radian

The corresponding half-height width of peak of α-alumina = 0.004 radian

The pure width = $\sqrt{B_M^2 - B_S^2}$

= $\sqrt{0.01625^2 - 0.004^2}$

= 0.01577 radian

β = 0.01577radian

2θ = 25.56^{o}

θ = 12.78^{o}

λ = 1.5418 Å

The crystallite size = $\frac{0.9x\,1.5418}{0.01577\ \cos 12.78}$ = 90.15Å

= 9 nm

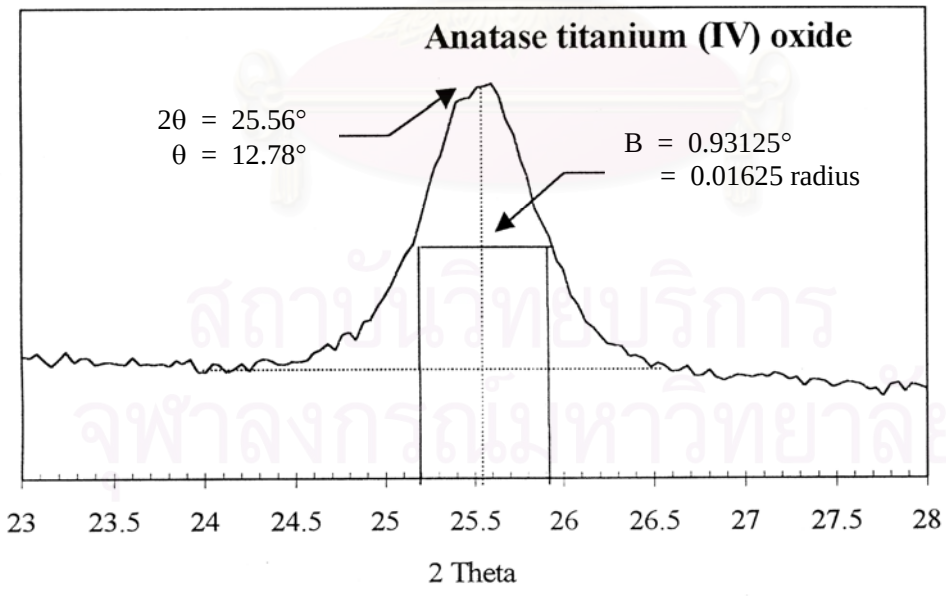

Figure A.1 The 101 diffraction peak of titania for calculation of the crystallite size

B

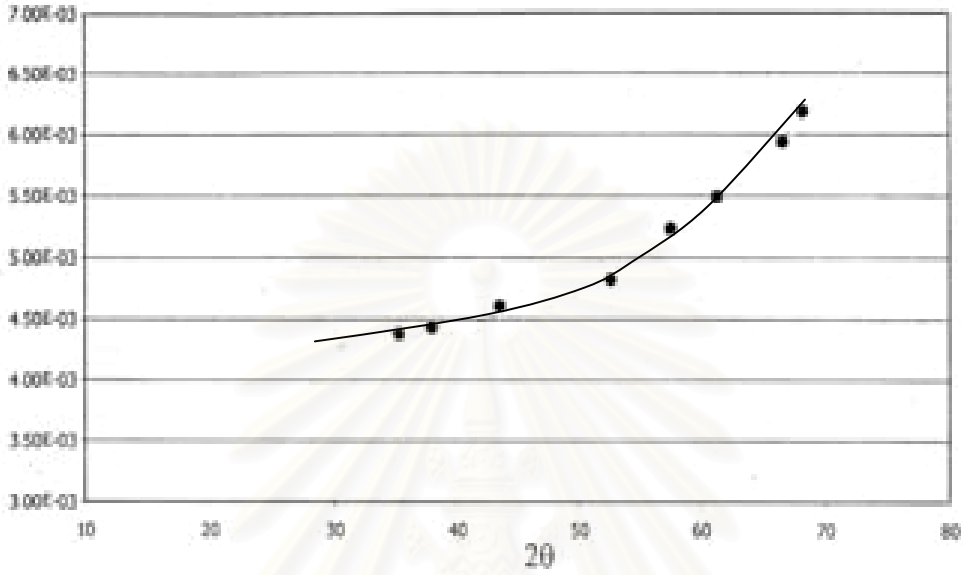

Figure A.2 The plot indicating the value of line broadening due to the equipment. The data were obtained by using α-alumina as standard.

APPENDIX B

THE OPERATING CONDITIONS OF GAS CHROMATOGRAPHY

The composition of hydrocarbons in the product stream was analyzed by a Shimadzu GC14B gas chromatograph equipped with a flame ionization detector. The operating conditions for each instrument are shown in the Table B.1.

Table B.1 The operating condition for gas chromatograph.

Gas Chromagraph	SHIMADZU GC-14B
Detector	FID
Column	VZ10
Carrier gas	H_2 (99.999%)
Carrier gas flow (ml/min)	30 cc/min
Column temperature	
- initial (^oC)	70
- final (^oC)	70
Injector temperature (^oC)	100
Detector temperature (^oC)	150
Current (mA)	-
Analysed gas	Hydrocarbon C_1-C_4

The calibration curve for calculation of composition of ethylene in reactor effluent was obtained and was shown in Figure B.1.

The VZ10 column were used with a gas chromatography equipped with a flame ionization detector to analyze the concentration of products including of ethylene.

Mole of ethylene as y-axis and area determined from gas chromatography as x-axis were plotted. The calibration curve of ethylene was illustrated in the following figure.

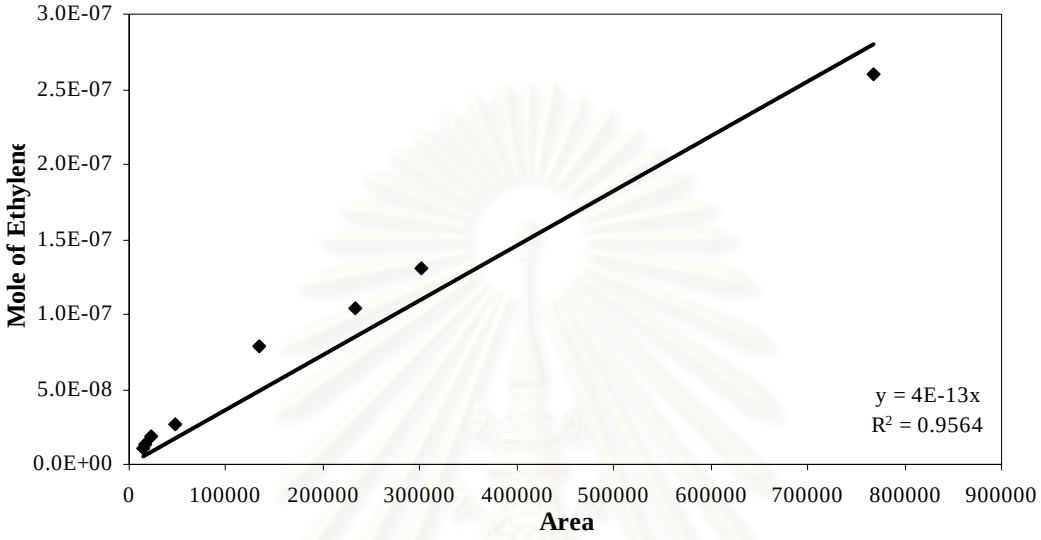

Figure B.1 The calibration curve of ethylene.

APPENDIX C

CALCULATION OF BET SURFACE AREA BY THE SINGLE POINT METHOD

From Brunauer-Emmett-Teller (BET) equation:

$$\frac{X}{V(1-X)} = \frac{1}{VmC} + \frac{(C-1)X}{VmC} \qquad (C.1)$$

Where: X = relative partial pressure of N_2, P/P_o

P_o = saturated vapor pressure of N_2 (or adsorbed gas) at the experimental temperature

P = equilibrium vapor pressure of N_2

V = volume of gas adsorbed at a pressure P; ml at the NTP/ g of sample

V_m = volume of gas adsorbed at monolayer, ml. at the NTP / g of sample

C = constant

Assume $C \rightarrow \infty$, then

$$\frac{X}{V(1-X)} = \frac{X}{Vm} \qquad (C.2)$$

$$Vm = V(1-P/P_o)$$

From the gas law,

$$\frac{P_bV}{273} = \frac{P_tV}{T} \qquad (C.3)$$

Where: V = constant volume

P_b = pressure at 0 ^oC

P_t = pressure at t ^oC

T = 273.15 + t, K

P_t = 1 atm and thus, P_b = (273.15 / T)

Partial pressure of Nitrogen:

$$P = \frac{[\text{Flow of } (He+N_2) - \text{Flow of He }]}{\text{Flow of } (He+N_2)} \quad (C.4)$$

$$= 0.3 \text{ atm}$$

N_2 saturated vapor pressure, P_o = 1.1 atm

$$p = P / P_o = P / 1.1 = 0.3/1.1 = 0.2727$$

How to measure V

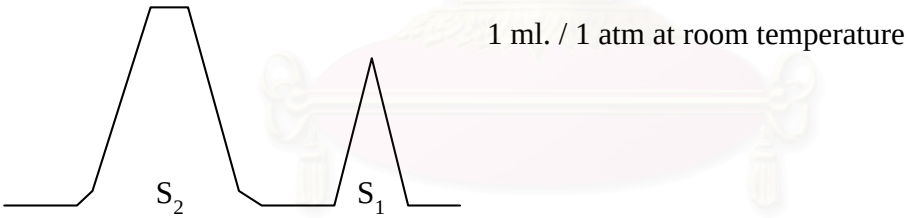

$$V = \frac{S_2}{S_1} \times \frac{1}{W} \times \frac{273.15}{T} \text{ ml. / g of catalyst} \quad (C.5)$$

Where, S_1 = Nitrogen 1 ml/1 atm of room temperature area

S_2 = Desorption of nitrogen area

W = Weight of the sample (g)

T = Room temperature (K)

Therefore,

$$Vm = \frac{S_2}{S_1} \times \frac{1}{W} \times \frac{273.15}{T} \quad X\ (1\text{-}p)$$

$$Vm = \frac{S_2}{S_1} \times \frac{1}{W} \times \frac{273.15}{T} \quad x\ 0.7273 \qquad (C.6)$$

Surface area of catalyst:

$$S = \frac{N\sigma V_m}{M}$$

Where, N = Avogadro number = 6.02×10^{23}

σ = area occupied by one molecule of adsorbed nitrogen = 16.2×10^{-20}

M = volume of one mole nitrogen = 22410 cm^3/mol

Then,

$$S = 4.352\ Vm$$

$$S = \frac{S_2}{S_1} \times \frac{1}{W} \times \frac{273.15}{T} \quad x\ 0.7273\ x\ 4.352$$

$$S = \frac{S_2}{S_1} \times \frac{1}{W} \times \frac{273.15}{T} \quad x\ 3.1582 \qquad (C.7)$$

APPENDIX D

CALCULATION OF THE AMOUNT OF GOLD USED IN THE PREPARATION OF CATALYSTS

The amount of gold used in each batch of experiment was calculated as following:

In each batch of this thesis, gold was deposited with the ratio of 2 %wt. This meant that there was titanium dioxide 98 g and gold 2 g in catalyst 100 g. In each batch of the experiment we used 2 g of titanium dioxide. Hence,

Titanium dioxide 98 g, gold was used 2 g

Titanium dioxide 2 g, gold was used = $\frac{2 \times 2}{98}$ = 0.0408 g

Molecular and atomic weight of hydrogentetrachloroaurate trihydrate ($HAuCl_4.3H_2O$) and gold are 393.83 and 196.97, respectively. Hence,

Gold 196.67 g was obtained from precursor 393.83 g

Gold 0.0408 g was obtained from precursor = $\frac{0.0408 \times 393.83}{196.67}$ = 0.0817 g

However, the purity of the precursor is 99.9 %. Hence,

Precursor 99.9 g was obtained from material 100 g

Precursor 0.0817 g was obtained from material = $\frac{0.0817 \times 100}{99.9}$ = 0.0818 g

Thus, the amount of material used in each batch of experiment = 0.0818 g

APPENDIX E

CALCULATION OF PREPARATION AND RESULT OF ICP-AES

Calculation of ICP-AES preparation

1. Preparation of samples

The amount of each catalyst used for characterization was calculated as following:

The amount of gold from the sample, which was prepared to the concentration of 5 ppm or 5 $mg.l^{-1}$ in the 50-cm^3 volumetric flask was;

In the volume 1,000 cm^3, the content of gold was 0.005 g

In the volume 50 cm^3, the content of gold was $= \frac{50 \times 0.005}{1{,}000} = 0.00025$ g

From the assumption that all gold content was deposited on the surface of titanium dioxide during the preparation of the catalyst, therefore the content of gold in 100 g of catalyst was 2 g and the amount of catalyst used for characterization was;

Gold 2 g was obtained from catalyst 100 g

Gold 0.00025 g was obtained from catalyst $= \frac{0.00025 \times 100}{2} =$ 0.0125 g

Thus the amount of each catalyst used for characterization was 0.0125 g.

2. Preparation of standard solutions

The standard solutions were prepared from 1,000-ppm standard gold solution. The standard gold solution was diluted to the concentration of 0.8 ppm and 10 ppm in

the 25-cm^3 volumetric flask. The amount of standard gold solution used in the experiment was calculated as following:

The amounts of gold in the solutions were;

0.8-ppm standard solution:

In the volume 1,000 cm^3, the content of gold was 0.0008 g

In the volume 25 cm^3, the content of gold was $= \frac{25 \times 0.0008}{1{,}000} = 0.00002$ g

10-ppm standard solution:

In the volume 1,000 cm^3, the content of gold was 0.01 g

In the volume 25 cm^3, the content of gold was $= \frac{25 \times 0.01}{1{,}000} = 0.00025$ g

The amounts of standard gold solution used in the experiment were;

0.8-ppm standard solution:

Gold 1 g was obtained from standard gold solution 1,000 cm^3

Gold 0.00002 g was obtained from standard gold solution $= \frac{0.00002 \times 1{,}000}{1}$

$= 0.02$ cm^3

10-ppm standard solution:

Gold 1 g was obtained from standard gold solution 1,000 cm^3

Gold 0.00025 g was obtained from standard gold solution $= \frac{0.00025 \times 1{,}000}{1}$

$= 0.25$ cm^3

Thus the amounts of standard gold solution used to prepare 0.8 and 10-ppm standard solution were 0.02 and 0.25 cm^3, respectively.

Calculation of ICP-AES results

The results from ICP-AES characterization were calculated into percentage of gold deposited on the surface of catalysts. The example of calculation is as following:

For titanium dioxide synthesized via solvothermal method and deposited gold at pH value of 6, the initial weight of catalyst was 0.013 g and the gold content obtained from ICP-AES was 4.548 ppm. Therefore the percentage of gold deposited on the surface of catalyst was;

Expected value (2 %wt. gold or 100 % deposited):

The amount of gold in the catalyst was;

In catalyst 100 g, there is gold 2 g

In catalyst 0.013 g, there is gold = $\frac{0.013 \times 2}{100}$ = 0.00026 g

= 0.26 mg

The concentration of gold in the solution was;

In 50 cm^3 of solution, the concentration of gold was 0.26 mg

In 1,000 cm^3 of solution, the concentration of gold was = $\frac{1{,}000 \times 0.26}{50}$

= 5.2 mg

= 5.2 ppm

The concentration of gold obtained from ICP-AES was 4.548. Hence;

The percentage of gold deposited on the surface of catalyst was = $\frac{4.548 \times 100}{5.2}$

= 87.46 %

APPENDIX F

PARTICLE SIZE DISTRIBUTION OF GOLD NANOPARTICLES AND CALCULATION OF TEM RESULTS

Particle size distribution of gold nanoparticles

The particle size distributions of gold nanoparticles of all gold deposited catalysts are shown in Table G.1-G.4.

Table G.1 Particle size distribution of gold nanoparticles of the solvothermal group (nm).

No.	pH 6	pH 7	pH 9	pH 10
1	8.9	30.5	11.4	14.3
2	7.6	36.2	12.1	14.6
3	20.3	48.3	11.4	17.8
4	24.1	2.5	7.3	14.6
5	16.5	3.2	10.2	14.0
6	14.0	4.1	10.2	19.0
7	44.4	4.4	10.2	18.1
8	16.5	2.2	14.3	10.5
9	16.5	2.5	12.1	8.9
10	8.9	21.0	11.1	14.0
11	25.4	3.2	14.0	11.7
12	20.3	1.9	12.7	13.0
13	17.8	3.2	7.6	16.5
14	17.1	40.0	13.0	14.9
15	11.4	4.4	4.4	8.6
16	2.5	3.2	8.3	15.2
17	4.2	3.8	12.7	14.6
18	2.8	2.2	13.3	15.2
19	2.2	3.2	15.2	17.5
20	2.3	3.2	10.5	15.9
21	1.7	10.2	12.1	15.2
22	1.9	3.5	19.0	7.6
23	2.2	3.2	10.8	15.2
24	2.9	1.9	12.1	15.1
25	2.5	3.5	11.4	13.2
26	2.6	5.1	10.2	17.9

No.	pH 6	pH 7	pH 9	pH 10
27	3.2	3.8	12.1	15.8
28	2.6	32.4	11.4	16.8
29	27.0	3.2	11.4	13.7
30	2.7	4.8	14.0	14.7
31	3.8	2.9	9.5	15.8
32	2.2	3.8	12.7	14.3
33	2.4	3.5	9.5	13.0
34	2.7	4.1	11.4	7.9
35	1.6	28.6	11.4	26.3
36	1.6	4.4	17.8	15.8
37	15.2	14.6	22.2	12.6
38	2.2	9.5	10.8	12.6
39	3.8	5.7	4.4	14.7
40	3.5	13.3	21.0	11.6
41	2.8	6.3	8.9	27.4
42	3.9	8.9	11.4	14.7
43	3.0	3.2	8.9	11.6
44	2.3	14.0	11.4	16.8
45	3.5	21.0	13.3	16.8
46	9.5	15.9	14.6	16.8
47	24.0	25.4	8.3	14.7
48	12.0	19.0	10.8	18.9
49	9.2	14.6	9.5	17.9
50	6.4	24.8	11.4	17.9
51	11.2	10.2	12.7	15.8
52	25.2	4.1	9.5	11.6
53	1.6	2.5	14.6	15.8
54	17.6	17.1	11.4	17.9
55	17.6	15.9	10.8	12.6
56	2.0	20.6	10.8	8.9
57	2.8	15.9	12.1	10.2
58	2.0	3.8	12.7	23.2
59	1.6	4.4	12.7	14.9
60	2.3	5.1	7.0	15.9
61	2.5	5.1	8.9	16.8
62	2.8	8.9	11.1	14.9
63	11.1	14.0	12.7	15.2
64	18.4	3.8	9.5	13.7
65	17.9	6.3	9.8	11.4
66	5.8	3.2	11.4	11.4
67	37.4	4.1	10.8	9.8

No.	pH 6	pH 7	pH 9	pH 10
68	17.9	2.5	11.4	14.3
69	28.9	2.5	12.1	15.2
70	10.5	5.1	10.8	18.1
71	4.5	17.1	10.2	17.2
72	2.6	2.5	10.2	14.3
73	18.4	10.8	9.5	19.2
74	15.3	24.1	9.5	12.7
75	2.9	22.2	12.7	17.2
76	3.2	10.8	12.1	15.9
77	2.4	15.2	10.2	18.4
78	33.6	15.2	12.7	14.9
79	10.8	22.2	13.3	10.8
80	17.8	1.0	22.2	17.8
81	29.2	2.2	14.3	15.2
82	1.9	6.3	10.8	16.5
83	2.5	3.8	9.8	14.3
84	35.2	28.6	8.6	13.7
85	11.1	2.5	4.8	13.7
86	6.3	2.5	15.2	11.4
87	7.9	4.4	6.9	12.1
88	11.1	3.2	7.6	13.7
89	11.1	22.2	8.6	18.4
90	10.5	12.7	9.8	24.8
91	2.8	4.4	12.7	14.3
92	2.3	1.9	8.6	17.8
93	7.6	1.9	7.9	13.7
94	4.2	21.6	7.3	11.4
95	3.2	16.5	15.2	16.5
96	7.6	22.2	16.5	20.4
97	9.2	4.4	13.7	10.8
98	5.8	4.1	14.3	17.8
99	3.2	2.9	13.7	15.2
100	11.1	17.8	11.4	13.7
101	6.4	41.3	7.3	24.4
102	14.0	3.2	8.6	16.5
103	16.5	3.2	15.2	12.7
104	4.2	1.9	9.5	16.5
105		1.6	16.5	17.2
106		1.9	8.6	15.9
107		3.2	13.3	9.8
108		5.1	9.8	

No.	pH 6	pH 7	pH 9	pH 10
109		4.4	7.3	
110		17.8	17.8	
111		16.5	14.9	
112		4.1	20.4	
113		34.9		
114		11.4		
115		10.8		
116		21.0		
117		20.0		
118		3.2		
119		4.4		
Average	9.8	10.3	11.6	15.1
Max	44.4	48.3	22.2	27.4
Min	1.6	1.0	4.4	7.6

Table G.2 Particle size distribution of gold nanoparticles of the sol-gel type I group (nm).

No.	pH 6	pH 7	pH 9	pH 10
1	4.8	25.6	21.6	10.3
2	7.9	20.0	12.0	10.3
3	6.2	18.0	13.2	13.7
4	6.2	16.8	20.0	7.7
5	8.2	17.6	13.6	10.3
6	7.2	10.4	11.2	10.3
7	9.2	20.0	14.4	8.6
8	11.3	16.0	20.8	4.3
9	7.2	17.6	7.2	13.7
10	7.2	24.0	3.6	9.4
11	8.2	16.0	10.4	12.0
12	5.6	17.6	14.4	16.3
13	5.1	10.4	19.2	12.9
14	3.1	24.0	12.8	15.4
15	6.7	18.4	14.4	12.0
16	9.2	20.0	21.6	12.0
17	12.3	14.4	21.6	14.6
18	6.2	8.0	15.6	12.9
19	7.2	4.4	17.6	17.1
20	5.1	17.6	18.4	17.1
21	7.2	3.2	24.0	3.4
22	7.2	17.6	15.2	12.0

No.	pH 6	pH 7	pH 9	pH 10
23	6.9	20.0	17.2	6.9
24	9.4	21.6	15.2	14.6
25	13.7	16.8	12.0	10.3
26	8.6	19.2	13.6	12.0
27	10.3	18.4	14.8	12.0
28	7.1	18.4	2.1	17.1
29	8.4	16.0	3.2	14.6
30	9.0	11.2	8.5	15.0
31	7.7	14.4	8.5	17.1
32	9.0	24.0	8.5	16.1
33	9.7	44.0	9.5	13.9
34	11.0	18.0	9.5	7.2
35	6.5	21.2	20.0	12.0
36	7.1	21.6	14.4	9.6
37	2.9	18.4	12.8	16.0
38	7.1	12.0	9.6	12.8
39	2.9	17.6	15.2	10.4
40	5.7	14.4	12.4	14.4
41	12.9	16.8	11.2	11.6
42	5.7	16.8	15.5	10.4
43	14.3	12.8	11.8	12.8
44	5.7	16.8	16.6	16.8
45	5.7	3.9	17.1	14.4
46	6.4	5.2	16.1	12.8
47	5.7	11.6	12.9	15.2
48	3.6	14.2	4.3	6.8
49	10.0	16.8	8.0	12.8
50	4.5	5.2	5.6	16.4
51	8.2	2.6	16.8	12.8
52	5.5	10.3	16.8	11.2
53	9.1	15.5	18.4	13.6
54	5.5	2.6	7.2	14.4
55	5.2	20.6	7.6	12.0
56	12.9	20.6	14.8	12.8
57	13.5	15.5	10.4	12.8
58	6.5	23.2	5.6	16.8
59	9.4	16.1	14.4	15.2
60	6.3	13.9	14.4	15.6
61	3.1	13.9	5.6	12.0
62	5.0	10.2	6.4	12.8
63	6.5	5.4	4.0	12.8

No.	pH 6	pH 7	pH 9	pH 10
64	7.7	21.6	20.0	8.8
65	5.8	16.8	4.8	9.6
66	6.5	1.6	17.6	12.0
67	5.2	4.8	16.8	14.4
68	5.2	2.4	11.2	14.8
69	6.5	15.2	6.4	11.6
70	3.2	15.2	12.8	13.2
71	1.3	12.0	10.4	14.4
72	11.0	17.1	12.8	14.4
73	2.6	12.4	12.0	12.8
74	5.8	55.2	12.8	14.4
75	10.3	17.6	7.2	12.8
76	7.7	1.6	6.0	14.4
77	11.0	13.6	12.8	13.6
78	5.2	22.4	11.2	14.4
79	11.6	8.9	15.2	4.5
80	12.3	26.4	4.8	11.2
81	3.2	21.6	9.6	12.8
82	17.1	2.2	10.4	14.4
83	7.7	18.4	2.4	10.4
84	3.4	28.9	9.6	11.2
85	2.6	8.9	16.0	12.8
86	17.1	22.4	12.0	13.6
87	12.0	13.6	11.2	14.4
88	8.6	22.4	16.0	14.4
89	17.1	6.3	14.4	17.1
90	20.6	12.4	6.4	6.3
91	8.6	4.8	8.0	7.7
92	9.4	4.4	16.0	8.8
93	5.2	28.9	10.4	10.4
94	5.7	24.8	11.6	11.2
95	13.7	9.4	13.6	12.8
96	12.3	7.7	13.6	13.6
97	10.3	14.4	13.6	14.4
98	2.6	27.4	12.8	15.4
99	3.2	9.1	12.8	16.8
100	8.6	40.2	17.6	11.2
101	9.4	18.4	10.4	12.8
102	9.1	12.7	1.1	14.4
103	7.7	24.1	27.6	15.4
104	6.5	8.4		16.8

No.	pH 6	pH 7	pH 9	pH 10
105	6.5	10.2		9.1
106	7.7	14.4		10.4
107		12.7		11.2
108		7.7		12.8
109		19.2		13.6
110		20.3		14.4
111		26.4		15.4
112		6.3		16.8
113				17.1
Average	7.8	15.8	12.5	12.7
Max	20.6	55.2	27.6	17.1
Min	1.3	1.6	1.1	3.4

Table G.3 Particle size distribution of gold nanoparticles of the sol-gel type II group (nm).

No.	pH 6	pH 7	pH 9	pH 10
1	3.2	5.1	13.3	20.4
2	5.6	14.2	17.9	20.8
3	2.4	5.8	13.7	17.2
4	4.8	2.1	4.6	20.4
5	3.2	5.3	9.4	21.2
6	2.8	2.6	16.6	56.0
7	2.4	1.1	11.4	20.4
8	6.4	6.3	19.0	19.2
9	5.6	20.0	10.5	26.4
10	5.6	6.4	15.2	25.2
11	2.0	12.8	24.1	20.8
12	2.8	8.0	14.6	21.6
13	3.2	7.2	24.8	21.2
14	4.8	3.2	12.7	39.6
15	4.0	6.0	15.2	30.0
16	3.8	8.8	13.3	38.4
17	7.0	3.2	10.8	20.0
18	2.5	3.2	14.0	19.6
19	4.4	9.6	11.7	22.4
20	2.4	3.2	12.7	24.0
21	3.2	3.2	14.0	22.4
22	2.4	3.6	22.2	23.2
23	10.8	6.4	16.2	26.4
24	7.0	15.2	13.7	22.4

No.	pH 6	pH 7	pH 9	pH 10
25	7.0	4.8	15.9	19.2
26	5.7	6.4	18.4	20.4
27	3.8	4.8	12.4	22.4
28	4.4	7.2	14.9	22.4
29	3.5	20.0	22.2	21.6
30	1.3	6.4	14.6	19.2
31	6.4	13.6	17.1	21.2
32	2.8	7.6	15.2	18.4
33	5.6	13.6	22.2	17.2
34	6.0	16.0	14.0	20.4
35	5.2	10.4	22.9	15.9
36	3.2	15.2	13.3	19.6
37	6.4	12.0	11.4	21.6
38	4.0	5.2	17.9	19.6
39	6.4	15.2	13.2	24.4
40	6.4	6.4	12.8	22.4
41	6.4	14.4	10.4	20.8
42	6.4	10.4	14.3	19.2
43	5.6	9.6	12.3	19.6
44	7.2	8.0	15.2	20.8
45	6.0	5.6	13.8	34.6
46	4.4	7.2	14.9	19.2
47	5.2	7.2	16.6	21.6
48	7.2	6.4	12.8	25.4
49	6.4	3.6	11.7	17.2
50	29.6	4.4	12.8	19.2
51	5.6	5.6	9.4	20.8
52	5.6	48.0	8.9	21.2
53	5.2	6.4	6.2	18.4
54	7.7	8.8	15.2	19.6
55	5.2	7.2	14.3	21.2
56	5.5	7.2	12.3	22.4
57	2.6	8.0	13.2	32.4
58	10.3	8.0	17.6	19.6
59	6.5	6.4	10.8	20.4
60	18.7	7.2	18.4	26.4
61	9.0	6.4	4.4	19.2
62	10.3	10.4	16.6	21.6
63	10.3	4.0	16.6	16.2
64	7.7	5.6	11.7	21.2
65	5.2	8.0	12.3	20.8

No.	pH 6	pH 7	pH 9	pH 10
66	5.8	11.2	14.3	19.6
67	7.1	2.0	10.8	17.2
68	4.5	5.6	7.2	25.4
69	1.3	8.0	18.4	21.2
70	3.2	18.4	8.9	21.6
71	6.4	5.6	9.4	33.2
72	1.6	2.4	15.8	19.2
73	3.6	15.2	5.4	18.9
74	2.8	11.2	5.1	21.2
75	2.4	12.0	17.9	26.4
76	1.6	8.4	13.2	20.4
77	5.6	12.8	20.4	21.6
78	4.8	7.2	3.5	23.2
79	7.2	9.6	8.9	23.2
80	6.4	15.2	11.7	19.2
81	1.2	20.8	11.4	19.6
82	1.6	16.8	21.6	21.2
83	4.4	13.6	17.6	21.6
84	8.0	28.0	10.8	16.8
85	8.0	13.6	11.4	20.4
86	14.8	7.6	6.5	21.6
87	7.2	7.2	20.4	18.4
88	5.6	8.4	19.2	20.8
89	8.0	22.4	11.7	19.6
90	8.0	18.4	15.8	21.6
91	1.6	17.2	8.9	19.2
92	6.4	8.8	19.2	33.2
93	8.8	15.2	17.6	20.4
94	11.2	29.6	6.5	19.6
95	6.8	13.6	7.2	16.8
96	1.6	12.0	7.2	22.4
97	6.8	12.8	12.3	18.9
98	8.0	12.8	13.8	17.2
99	8.0	29.6	10.4	15.9
100	11.2	16.0	15.8	19.6
101	4.5	20.0	21.3	24.4
102	1.9	16.0	12.3	19.2
103		13.6	8.9	21.2
104		11.2	18.4	18.4
105		10.4	16.6	16.5
106		10.4	9.4	16.5

No.	pH 6	pH 7	pH 9	pH 10
107		6.4	17.6	15.9
108		7.2	15.8	19.2
109		10.4	21.6	19.2
110		18.4	14.3	20.8
111		7.2	16.6	18.4
112		5.6	6.2	22.4
113		7.2	9.4	20.8
114		8.8	11.7	16.2
115			8.6	20.4
116			12.8	19.6
117			13.2	
118			14.9	
119			8.6	
120			10.8	
121			23.2	
Average	5.8	10.3	13.7	21.6
Max	29.6	48.0	24.8	56.0
Min	1.2	1.1	3.5	15.9

Table G.4 Particle size distribution of gold nanoparticles of the JRC-TIO1 group (nm).

No.	pH 6	pH 7	pH 9	pH 10
1	14.4	7.3	3.5	15.2
2	7.2	3.2	4.1	17.5
3	16.0	4.1	2.9	16.8
4	11.2	4.1	3.8	13.7
5	4.3	4.4	4.4	15.9
6	17.0	12.7	3.2	13.3
7	12.8	7.3	1.9	14.0
8	12.8	4.4	6.3	13.3
9	4.3	2.9	4.1	16.2
10	4.3	10.2	2.2	17.5
11	10.6	10.8	2.2	21.3
12	13.2	7.0	2.9	19.0
13	18.4	4.4	2.9	17.1
14	19.0	6.3	3.2	12.7
15	12.7	4.4	3.2	24.4
16	20.6	6.3	2.2	13.3
17	25.4	3.8	2.2	14.3
18	10.6	4.4	4.8	14.3

No.	pH 6	pH 7	pH 9	pH 10
19	13.8	5.7	2.5	14.9
20	17.0	3.8	2.5	16.8
21	12.7	7.0	2.9	17.8
22	7.4	4.4	2.9	12.7
23	18.0	4.4	4.8	13.3
24	10.6	3.8	2.2	12.7
25	12.7	5.4	2.5	14.3
26	19.0	5.1	3.2	14.9
27	19.0	5.1	3.2	11.4
28	14.0	4.4	3.5	12.7
29	14.4	3.5	4.1	10.2
30	17.8	2.9	2.2	13.7
31	17.9	9.5	3.5	18.4
32	13.6	5.4	3.2	13.3
33	19.0	19.0	2.9	14.3
34	13.5	6.3	1.6	23.2
35	22.2	7.0	3.2	12.1
36	12.7	8.9	4.4	17.5
37	11.4	12.7	2.9	15.9
38	8.6	7.9	2.2	12.1
39	5.4	5.4	3.2	13.7
40	13.3	8.6	4.8	14.9
41	16.2	3.2	3.7	11.7
42	14.4	34.9	2.2	13.3
43	10.6	21.0	4.1	13.3
44	12.7	4.4	3.2	15.2
45	15.9	5.7	3.2	18.4
46	14.4	2.9	3.5	14.9
47	11.7	3.8	3.5	12.1
48	6.9	3.2	2.9	10.2
49	9.8	5.4	2.5	13.3
50	27.4	5.1	3.2	11.4
51	13.3	10.2	3.8	14.3
52	8.9	3.8	3.2	11.4
53	12.1	3.8	2.5	12.1
54	14.4	3.8	4.8	17.1
55	7.4	3.2	2.9	13.3
56	11.4	7.0	2.9	21.6
57	17.8	4.4	2.9	10.2
58	10.2	7.0	3.5	23.2
59	9.8	6.3	3.5	14.9

No.	pH 6	pH 7	pH 9	pH 10
60	13.7	6.0	2.2	15.9
61	15.9	9.5	3.2	13.7
62	12.1	5.1	2.9	10.8
63	14.9	2.5	3.2	12.7
64	8.9	7.6	3.8	12.7
65	11.7	2.5	3.2	14.3
66	13.3	4.8	2.5	21.6
67	12.1	5.1	2.5	17.5
68	11.4	3.8	3.2	18.4
69	14.4	4.4	2.9	12.1
70	13.3	3.2	3.8	13.7
71	6.9	6.3	4.4	11.7
72	3.8	5.1	3.2	23.2
73	8.9	3.2	2.9	23.2
74	13.3	2.5	3.8	14.9
75	10.8	2.5	4.1	9.8
76	11.4	3.8	3.2	13.3
77	12.7	5.1	3.0	15.2
78	14.9	5.1	3.2	11.7
79	11.4	3.8	3.5	22.4
80	9.5	3.8	5.7	12.7
81	15.2	5.1	1.4	13.7
82	8.6	5.1	1.9	12.1
83	12.7	3.5	2.9	12.7
84	13.7	2.9	2.7	12.1
85	13.7	3.2	4.0	9.8
86	11.7	5.7	2.7	11.7
87	14.9	5.1	3.3	15.2
88	10.6	3.8	3.7	13.7
89	15.9	5.1	4.6	14.3
90	8.6	5.1	3.2	14.3
91	14.4	7.9	3.2	10.2
92	12.1	2.5	3.5	12.1
93	13.7	4.4	3.2	11.7
94	27.4	5.1	3.2	13.3
95	9.8	4.4	2.5	17.1
96	22.4	5.1	3.7	18.4
97	12.7	5.1	3.3	13.7
98	15.2	4.4	2.9	10.8
99	11.4	5.1	2.9	10.8
100	11.4	5.4	3.5	15.9

No.	pH 6	pH 7	pH 9	pH 10
101	13.3	5.1	2.9	12.1
102	10.6	16.5	4.4	11.4
103	24.8	3.2	2.5	11.4
104	5.4	4.1	4.1	13.3
105	12.7	3.2	2.2	12.7
106	15.2	2.5	4.4	14.3
107	13.3		6.7	
108	8.6		3.2	
109	12.7		3.8	
110	11.7		3.2	
111			4.8	
112			3.2	
113			2.5	
114			3.2	
115			2.5	
116			2.9	
117			2.5	
118			3.8	
119			2.9	
120			2.2	
121			3.2	
122			4.4	
123			2.7	
124			5.4	
125			3.5	
126			4.1	
127			3.5	
128			2.5	
129			3.3	
130			3.8	
131			4.4	
132			4.1	
133			3.8	
134			3.5	
135			3.2	
Average	13.1	5.8	3.3	14.6
Max	27.4	34.9	6.7	24.4
Min	3.8	2.5	1.4	9.8

Calculation of TEM results

Average particle size of gold nanoparticles

The average particle size of gold nanoparticles of each catalyst was calculated from the equation:

$$d_{ave} = \frac{\sum_{i}^{n} d_i}{n} \qquad \text{(F.1)}$$

Where d_i = the diameter of each gold nanoparticle (nm)

n = the number of gold nanoparticles appeared in the TEM images of each catalyst (more than 100 particles for each catalyst)

Ratio of active gold nanoparticles

The ratio of active gold nanoparticles (%) of each catalyst was calculated from the equation:

$$r_{active} = \frac{n_j}{n_i} \times 100 \qquad \text{(F.2)}$$

Where r_{active} = ratio of active gold nanoparticles

n_j = the number of active gold nanoparticles of each catalyst (diameter less than 5 nm)

n_i = the number of gold nanoparticles appeared in the TEM images of each catalyst (more than 100 particles for each catalyst)

APPENDIX G

CALCULATION OF Ti^{3+}

The amount of Ti^{3+} of each catalyst was calculated as following:

$$Ti^{3+} = R \times \left(\frac{h}{w \times s} \right) \qquad \text{(G.1)}$$

Where R = ratio of ratio of the peak height of the bare catalyst (to compare the results which came from different amplitudes. For the same amplitude, R was equal to 1). R was calculated from equation (G.2).

h = the peak height from ESR result.

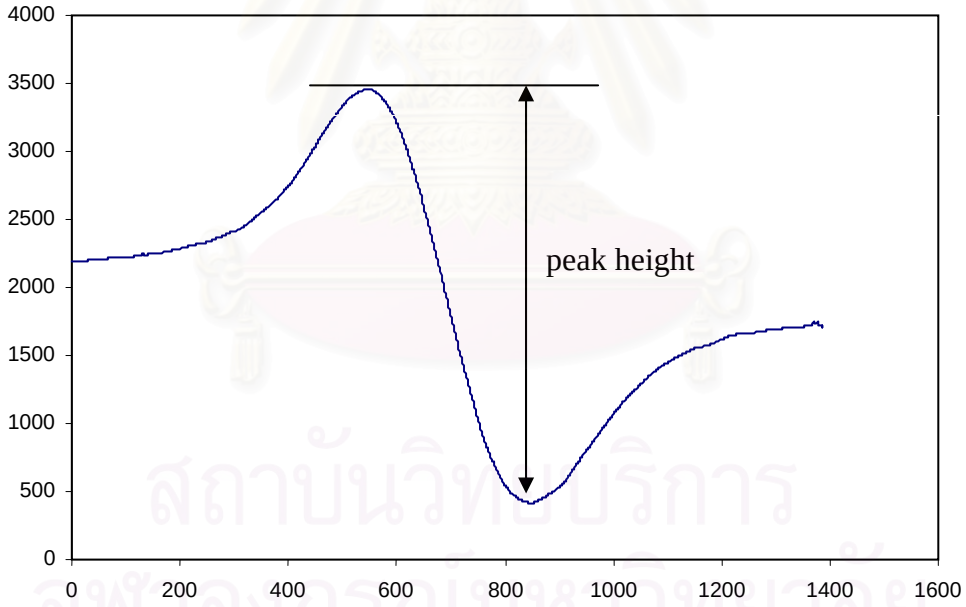

w = weight of catalyst used in measurement (g).

s = BET surface area of the catalyst ($m^2.g^{-1}$).

The ratio of ratio of the peak height of the bare catalyst was calculated from the equation:

$$R = \frac{r_a}{r_b} \qquad \text{(G.2)}$$

Where

$$r_a = \frac{h_a}{\left(\frac{h_{Mn1a} + h_{Mn2a}}{2}\right)} \qquad \text{(G.3)}$$

$$r_b = \frac{h_b}{\left(\frac{h_{Mn1b} + h_{Mn2b}}{2}\right)} \qquad \text{(G.4)}$$

R = ratio of ratio of the peak height of bare catalyst

r_a, r_b = ratio of the peak height of bare catalyst *a* and *b*, respectively

h_a, h_b = peak height of bare catalyst *a* and *b*, respectively

h_{Mn1a}, h_{Mn2a} = peak heights of both peaks of the Manganese internal standard of bare catalyst *a*, respectively

h_{Mn1b}, h_{Mn2b} = peak heights of both peaks of the Manganese internal standard of bare catalyst *b*, respectively

VITA

Mr. Peerapon Buakaew was born in Phatthalung, Thailand on December 2, 1981. He graduated high school from Triam Udom Suksa School, Bangkok on 2000 and received his Bachelor Degree of Chemical Engineering from the Faculty of Engineering, Chulalongkorn University in 2004.